

ENERGY AND PASSIVITY BASED CONTROL FOR BIPEDS AND ASSISTIVE  
WALKING DEVICES

by

Mark R. Yeatman

APPROVED BY SUPERVISORY COMMITTEE:

---

Robert Gregg, Chair

---

Mark Spong, Co-Chair

---

Steve Yurkovich

---

Tyler Summers

Copyright © 2020

Mark R. Yeatman

All rights reserved

*This thesis is dedicated to all of the people  
who have helped me get to where I am.  
Chief among these are my parents: Deborah, Russ, George.  
But we are all of us connected.*

ENERGY AND PASSIVITY BASED CONTROL FOR BIPEDS AND ASSISTIVE  
WALKING DEVICES

by

MARK R. YEATMAN, BS

DISSERTATION

Presented to the Faculty of  
The University of Texas at Dallas  
in Partial Fulfillment  
of the Requirements  
for the Degree of

DOCTOR OF PHILOSOPHY IN  
MECHANICAL ENGINEERING

THE UNIVERSITY OF TEXAS AT DALLAS

December 2020

## ACKNOWLEDGMENTS

I thank my advisor, Bobby Gregg, for his guidance, advice, and friendship. He has always trusted me, and given me the freedom and license to pursue my ideas. Others have remarked that in science we stand on the shoulders of giants, and in my journey I have found that to be unequivocally true. The list of these people could go on for pages (and in fact does in the references section). A special thanks to my significant other, Sutton Wheelis, and the various members of the Locolab for their support. I could not have succeeded without you.

Portions of this work were supported by NSF Awards 1652514 / 1949869, and by the National Institute of Child Health & Human Development of the NIH under Award Numbers DP2HD080349 and R01HD094772.

November 2020

ENERGY AND PASSIVITY BASED CONTROL FOR BIPEDS AND ASSISTIVE  
WALKING DEVICES

Mark R. Yeatman, PhD  
The University of Texas at Dallas, 2020

Supervising Professor: Robert Gregg, Chair

Locomotion is inherently an energy regulation challenge; ground impacts deplete the mechanical energy of the walking system with every step. When a person's leg is amputated, one of the conventional medical devices used to help them recover their mobility is a passive prosthesis. However, this device is incapable of doing positive work on the human body to counteract energy depletion and restore the user's mechanical energy. Powered prostheses have been developed and researched to address this, but recent control methods have focused on tracking joint trajectories or impedance while ignoring the fundamental kinetic aspect of human locomotion. The prevailing goal of this work is to construct a control method for a powered lower-limb prosthesis that explicitly and directly enhances the kinetics of the combined human-prosthesis system to assist human locomotion. The method proposed to accomplish this utilizes energy and passivity based control techniques to modify the dynamics of the prosthesis. This dissertation develops control theory related to these techniques for autonomous bipedal robots so that they can then be translated onto the target prosthesis system. Specifically, it shows how to use energy shaping and regulation to change characteristics of a walking gait, like walking speed, via switching of a small set of physically meaningful parameters. Experimental results that demonstrate proof-of-concept on a powered knee-ankle prosthetic leg are presented.

## TABLE OF CONTENTS

ACKNOWLEDGMENTS . . . . .	v
ABSTRACT . . . . .	vi
LIST OF FIGURES . . . . .	viii
LIST OF TABLES . . . . .	ix
CHAPTER 1 INTRODUCTION AND MOTIVATION . . . . .	1
1.1 State of the Art in Powered Lower-Limb Prostheses . . . . .	1
1.2 Energy Shaping and Regulation Control as an Alternative Approach . . . . .	3
1.3 Organization of the Dissertation . . . . .	3
CHAPTER 2 MODELING BIPED LOCOMOTION . . . . .	5
2.1 Lagrangian Mechanical Systems with Holonomic Constraints . . . . .	6
2.2 Rigid Impact Dynamics . . . . .	9
2.3 Hybrid Biped Dynamics and Orbital Stability . . . . .	10
2.4 Passivity . . . . .	12
CHAPTER 3 ENERGY SHAPING AND REGULATION CONTROL . . . . .	14
3.1 Energy Shaping . . . . .	15
3.2 Energy Regulation . . . . .	18
3.2.1 Regulation of a Work-Based Energy Function . . . . .	20
3.3 Application to Hybrid Locomotive Systems . . . . .	21
3.4 A Hopping Robot Example . . . . .	23
3.4.1 Hopper Dynamics . . . . .	23
3.4.2 Hopper Control . . . . .	25
3.4.3 An Impact-to-Impact Energy Update Law . . . . .	26
CHAPTER 4 APPLICATION ON BIPED ROBOTS . . . . .	28
4.1 The Spring Loaded Inverted Pendulum . . . . .	28
4.1.1 Control . . . . .	31
4.1.2 Simulations . . . . .	33
4.2 The Compass Gait Biped . . . . .	37
4.2.1 Control . . . . .	40

4.2.2	Simulations . . . . .	42
4.3	The RABBIT Model . . . . .	46
4.3.1	Control . . . . .	48
4.3.2	Simulation . . . . .	52
4.4	The Flat Foot Biped . . . . .	54
4.4.1	Centralized Simulations . . . . .	57
4.4.2	Decentralized Model . . . . .	64
4.4.3	Decentralized Energy Regulation . . . . .	68
4.4.4	Decentralized Simulations . . . . .	70
4.4.5	Model Parameter Error . . . . .	74
CHAPTER 5	APPLICATION ON A POWERED PROSTHETIC LEG . . . . .	77
5.1	Model and Hardware . . . . .	77
5.2	Control . . . . .	78
5.3	Experiments . . . . .	87
CHAPTER 6	CONCLUSIONS . . . . .	92
REFERENCES	. . . . .	95
BIOGRAPHICAL SKETCH	. . . . .	103
CURRICULUM VITAE		



## LIST OF FIGURES

3.1	Block diagram of the hierarchy for energy shaping and energy regulation control.	16
4.1	Diagram of the spring loaded inverted pendulum. . . . .	29
4.2	Sample walking trajectory of the SLIP model, average walking speeds of $1.1\text{ms}^{-1}$ . $m = 70\text{kg}, k = 12250\text{Nm}^{-1}, L_o = 0.94\text{m}$ . . . . .	31
4.3	The ground reaction force of one “foot” along the sample trajectory, starting at touchdown. . . . .	32
4.4	Speed-Energy-Stiffness surface for the SLIP model under the regulation control. The minimum speed achieved was $2.82\frac{m}{s}$ , the maximum $7.95\frac{m}{s}$ . . . . .	35
4.5	Sample trajectory of transition from $6\frac{m}{s}$ to $3\frac{m}{s}$ under the regulation control. The stiffness and reference energy were switched at the horizontal dashed line. . . . .	35
4.6	Speed-Energy-Stiffness surface for the SLIP model under the oscillator control. The minimum speed achieved was $3.65\frac{m}{s}$ , the maximum $8.05\frac{m}{s}$ . . . . .	36
4.7	Contact Angle-Energy-Stiffness surface for the SLIP model under regulation control.	36
4.8	Contact Angle-Energy-Stiffness surface for the SLIP model under the oscillator control. . . . .	37
4.9	Diagram of the compass gait biped. . . . .	38
4.10	Projected phase portrait of a passive limit cycle. The trajectory starts at the starred points. $m_h = 10\text{kg}, m_s = 5\text{kg}, a = 0.5\text{m}, b = 0.5\text{m}$ . . . . .	40
4.11	Length ratio versus average speed for physical and virtual dynamics. $\beta$ is the physical length ratio, $\tilde{\beta}$ is the virtual length ratio, $u_t^{\text{vel}}$ converges to a desired walking speed, $u_t^{\text{nat}}$ converges to the energy equilibrium induced by the discrete dynamics. Data points that bifurcated or were unstable are not displayed. . . . .	43
4.12	Energy versus length ratio for the adaptive energy regulation controllers. Data points that bifurcated or were unstable are not displayed. . . . .	44
4.13	Time integral of torque squared versus average speed for physical and virtual dynamics length ratio changes. Data points that bifurcated or were unstable are not displayed. . . . .	44
4.14	The slope period-1 passive limit cycle versus the stairs period-2 passive limit cycle.	45
4.15	Transition from passive period-2 limit cycle to an energy regulated period-1 limit cycle. The energy regulation control is turned on after 4 steps, at the green vertical line. . . . .	45
4.16	Diagram of the Rabbit biped, a 5 Link robot with a torso and knees. The virtual spring between the hip and the ground is shown in purple. . . . .	46

4.17	Diagram of the embedded virtual pendulum and swing foot trajectory. . . . .	51
4.18	Simulation of the RABBIT biped with embedding of the energy regulated SLIP model versus the true SLIP model. . . . .	53
4.19	Energy over the Rabbit-SLIP embedded limit cycle. . . . .	54
4.20	Diagram of an 8-DOF flat foot humanoid biped with overlaid coordinate system. . . . .	55
4.21	Generalized energy (E) of the PD controlled (inner-loop) biped system while traversing the limit cycle. There are three constant energy levels with discrete jumps between them. . . . .	59
4.22	Centralized storage function for the perturbed system with PBC and without PBC, over 5 steps. The transition between steps is marked by a large decrease in storage, caused by heel impact. . . . .	60
4.23	Torque over time for the centralized controller $U$ for the first three steps. . . . .	62
4.24	Maximum absolute value of the eigenvalues of the linearization of the Poincaré map as the gain $k$ is varied from 0 to 10. . . . .	62
4.25	Diagram of a decentralized model of the human-prosthesis system. . . . .	65
4.26	Generalized energy of all three systems while traversing the limit cycle. There is a break in the y-axis of the graph to accommodate the difference in average magnitude of the energy trajectories. . . . .	71
4.27	System storage function across PBC implementations. . . . .	73
4.28	System storage function for a decentralized PBC with perfect model parameters versus a decentralized PBC with random $+ - 30\%$ error in the model parameters. . . . .	75
4.29	Robustness of decentralized control vs model parameter error norm with $k = 1$ . . . . .	76
5.1	A picture of the experimental setup with UTD Leg 2. . . . .	79
5.2	Virtual spring between the center of pressure and a surrogate for the center of mass. . . . .	81
5.3	Diagram of relation of COP to constraint forces for the flat foot contact condition. . . . .	82
5.4	Knee and ankle positions versus time of the prosthesis and reference biological data from [1]. The blue highlighted area is stance, the yellow is swing. . . . .	88
5.5	A smoothing spline fit to the COP-virtual spring contact point over normalized stance time. The COP is measured relative to the heel, with the positive direction being the way the user is facing. . . . .	89
5.6	Net torques. . . . .	90
5.7	Spring torques. . . . .	91
5.8	Energy oscillator torques. . . . .	91

## LIST OF TABLES

4.1	Rabbit Model Simulation Parameters . . . . .	53
4.2	Flat Foot Model Simulation Parameters . . . . .	58
4.3	Reciprocal of the gait sensitivity norm calculated across controllers and scaling gains . . . . .	74

## CHAPTER 1

### INTRODUCTION AND MOTIVATION

Locomotion is inherently an energy regulation challenge; ground impacts deplete the mechanical energy of the walking system with every step. When a person’s leg is amputated, one of the conventional medical devices used to help them recover their mobility is a passive prosthesis. However, this device is incapable of doing positive work on the human body to counteract energy depletion and restore the user’s mechanical energy. This leads to lower walking speeds, higher metabolic costs, and gait abnormalities [2]. Powered prostheses have been developed and researched to address this, but recent control methods have focused on tracking joint trajectories or impedance while ignoring the fundamental kinetic aspect of human locomotion. *The prevailing goal of this work is to construct control methods for a powered lower-limb prosthesis that explicitly and directly enhance the kinetics of the combined human-prosthesis system to assist human locomotion.*

#### 1.1 State of the Art in Powered Lower-Limb Prostheses

A prosthesis is a mechanical structure that replaces the functionality of a missing limb segment. These devices can be classified into passive versus powered devices. Most commercially available lower-limb prostheses fall into the passive category, in that they cannot generate net positive work [3]. The history of passive devices is long; it begins pre-20th century with wooden structures like peg-legs and the Hanger Limb [4], a knee-ankle prosthesis made from barrel staves after the American Civil War. The design focus for modern passive prosthetic legs is weight and friction minimization, to reduce socket interaction forces against the wearer’s skin and muscle fatigue from moving the device. This has largely been accomplished by improvements in material selection (e.g., using aluminum and carbon fiber). Powered devices are inherently heavier and bulkier than passive devices due to the addition

of actuation components. Older designs of powered devices used heavy, high friction power transmission components [5] that were not back-driveable. Recent work has created a lighter, more compact, back-driveable, knee-ankle prosthetic leg [6]. This back-driveability is particularly important in regard to control, because it is much simpler to use impedance and energy based control methods on this style of device [7].

While powered devices are still confined to research spaces, they have been demonstrated to have the potential to provide better patient outcomes than conventional passive devices [2]. The first landmark research into the control of powered knee-ankle limb comes from Goldfarb [8] in the early 1990s, which outlines a five mode finite state controller that switches based on where the user is in their gait cycle. Each one of these states uses a different rule to generate joint torques (e.g., lock the knee during stance, then command a set torque during early swing, then damp the joints during late swing). Research into impedance based rules followed [9], with some focusing on biomimetically emulating human leg impedance [10]. An effort to reduce the number of different rules in the overall control emerged in recent years with [11]. Inspired by research into autonomous bipeds [12], [11] uses an Inertial Measurement Unit on the users hip to generate a phase variable that provides a single, continuous measurement of gait cycle progression. This phase variable parameterizes joint trajectories derived from human motion capture data, and are played back as the user walks using a high gain Position-Derivative controller. However, if the user wishes change tasks by changing their walking speed or walking up a slope, the desired joint trajectories must also be changed. This is partially addressed in [13], which generates multi-dimensional trajectory surfaces parameterized by phase and task variables. However, the research into the control of prosthetic legs largely focuses on simply placing the leg in front of the user and supporting them during stance. This paradigm ignores the primary advantage of powered devices over passive devices, positive work generation, which emerges as a byproduct of trajectory error rather than as an explicit output of the control law.

## 1.2 Energy Shaping and Regulation Control as an Alternative Approach

A paradigm shift from a desired kinematic behavior to a desired kinetic behavior of energy regulation and/or force output could allow us to frame positive work generation as an explicit output of the prosthesis system. I believe the best control framework to achieve this is that of *energy shaping* [14] (although the phrase is a bit of misnomer). The general idea is to define a target system for the closed-loop dynamics that can be described by an energy function or Hamiltonian. Feedback control is used to make up for the difference in the open-loop energy function and the target energy function, *matching* the closed-loop energy to the target energy (so perhaps a better label would have been “dynamics matching”). This energy difference could allow us to explicitly generate positive work on the human-prosthesis system. In the field of biped locomotion, energy shaping has been applied to generate walking gaits by various changes to the kinetic and potential energy functions [15, 16]. Research in the application of this technique to exoskeletons has recently emerged in [17, 18], but the powered prosthetic leg application remains open. A complimentary idea to energy shaping is energy regulation, although the two ideas are sometimes lumped together [15, 19]. Here, the idea is to drive the closed-loop energy of the system to a reference value associated with a passive or “natural” limit cycle. This leaves the mechanical energy function unaltered, but prescribes that it take a desired value. This allows energy to an explicit output of the system, increases limit cycle robustness [15, 20], and can help counteract energy losses from unmodeled dynamics.

## 1.3 Organization of the Dissertation

This dissertation expands upon research in orbital stabilization of hybrid biped locomotion by considering ways to dynamically change gaits during online operation through switches in a very small set of control parameters in simple walking systems. It also investigates methods

to leverage these ideas on complex biped models and a powered knee-ankle prosthesis. In Chapter 2, background information necessary to model biped locomotion and stable walking motion is given, along with the notion of passivity. Next in Chapter 3, the mathematical details of energy shaping and regulation control are shown, and the ability to regulate a time varying work based energy function in the passivity based framework is demonstrated. The following Chapter 4 covers the control application on simulations of several biped models, ranging from simple to complex. I show how the concepts of energy shaping and regulation can be used in conjunction to allow online gait changes through parameter switching, that the exact reference energy associated with a limit cycle does not need to be known prior to online operation, and that the simple biped models can be exactly embedded into higher order models to facilitate locomotion. Chapter 5 covers the control application on a physical prosthetic leg, how a virtual spring with energy regulation can be embedded, and offers a proof-of-concept experimental implementation. The final Chapter 6 summarizes all the results of the dissertation and has directions for future work.

## CHAPTER 2

### MODELING BIPED LOCOMOTION

Understanding how a system works requires a model of its behavior. Models of biped walking range from simple models like the inverted pendulum [21] to extremely complicated musculoskeletal models like [22] that simulate the mechanical properties of a human body. In this dissertation, I consider three biped models: the Spring Loaded Inverted Pendulum (SLIP), the Compass Gait Biped, and a 6-Link Flat Foot Biped. The SLIP model is composed of a point mass that “walks” via connecting the ball to the ground through massless springs. It is mathematically and conceptually simple, it exhibits kinematic and kinetic behaviors that are extremely similar to key markers of healthy human locomotion [23], and its walking and running behaviors occur naturally without external control. However, the gait of this model is not stable. The Compass Gait Biped is another mathematically simple model that exhibits “passive dynamic walking”, which describes the ability of the biped to walk down a shallow slope under the power of gravity, alone. It has two legs modeled as rigid links with point mass, and a point mass at the hip. While the gait of this model is far less similar to human walking than the SLIP model, the gait is locally asymptotically stable [24]. While most of the literature on the SLIP and Compass Gait models considers their motion through a 2-dimensional plane, they can be extended to the 3-dimensional case [25, 26]. The simplicity of these models makes them useful testbeds and templates for designing controllers that can leverage preexisting limit cycles or gaits, and augment their properties such as speed or step length. However, they are not complex enough to capture the all the salient features of humanoid locomotion [27].

The human body is relatively compliant [28, 29, 30]; in order to use a rigid kinematic chain as an abstraction of human motion certain compromises in model fidelity must be made. For example, some researchers choose to use a rigid curved foot [31] to capture the motion of the center-of-pressure and roll-over shape of the leg [32]. However, this type of



model does not rigorously capture the kinematics and kinetics of the heel, flat foot, toe off gait pattern that is present in human walking [33]. In order to model a human walking with a prosthetic leg, I consider a 6-link biped model with a hip, knees, ankles, heels, and flat feet. This model has been utilized to model a person walking with an exoskeleton in previous work [17]. The treatment of the feet as flat, rigid links is a compromise on fidelity, since foot stiffness and flexion has been shown to be mostly irrelevant [34]. The model lumps the motion of the head, arms, and torso into a large point mass at the hip, which has been demonstrated to be a reasonable approximation in [35].

The principle tools to generate the mathematical description of the motion of these models is Lagrangian mechanics. This chapter reviews a general form for Lagrangian mechanics of rigid kinematic chains, combines this with a dissipative impact model to create a hybrid system, and then gives a definition for orbital stability and a numerical method for checking it. Passivity properties of this system class are reviewed, and finally a detailed description of SLIP, Compass Gait, and 6-Link Flat Foot models is given.

## 2.1 Lagrangian Mechanical Systems with Holonomic Constraints

The state of an  $n$  Degree-Of-Freedom (DOF) mechanical system can be described by a configuration space  $Q$  and its tangent bundle  $TQ = \bigcup_{q \in Q} T_q Q$ , which are generalizations of positions and velocities, respectively. The idea of Lagrangian mechanics is that the differential equations that govern the motion of a mechanical system can be generated by the Euler-Lagrange equation [36]

$$\frac{d}{dt} \frac{\partial \mathcal{L}(q, \dot{q})}{\partial \dot{q}} - \frac{\partial \mathcal{L}(q, \dot{q})}{\partial q} = \tau - A(q)^\top \lambda. \quad (2.1)$$

Here, the generalized position or coordinate vector is  $q \in Q$ , the generalized velocity vector is  $\dot{q} \in TQ$ , and  $\mathcal{L}(q, \dot{q}) : TQ \rightarrow \mathbb{R}$  is a smooth function called the Lagrangian. For mechanical

systems, the Lagrangian takes the form

$$\mathcal{L} = \mathcal{K}(q, \dot{q}) - \mathcal{P}(q) \quad (2.2)$$

$$= \frac{1}{2} \dot{q}^\top M(q) \dot{q} - \mathcal{P}(q), \quad (2.3)$$

which is the difference between the system's kinetic energy  $\mathcal{K}$  and potential energy  $\mathcal{P}$ . The kinetic energy is a quadratic form defined by  $M \in \mathbb{R}^{n \times n}$ , which represents the generalized mass and inertia of the system. The generalized external forces and torques on the system are  $\tau \in \mathbb{R}^n$ , and the constraint forces  $\lambda \in \mathbb{R}^m$  are mapped into the dynamics via the constraint matrix  $A(q) \in \mathbb{R}^{n \times m}$ . The dimensions of the constraint variables indicate that there are  $m$  holonomic constraints on the system. In biped robotics, holonomic constraints are generally used to model interactions with a rigid environment like a wall or the ground that restrict the motion of the biped [37].

The application of the Euler-Lagrange equation (2.1) to the Lagrangian (2.2) yields the 2nd order differential equation that describes the motion of the system,

$$M(q)\ddot{q} + C(q, \dot{q})\dot{q} + N(q) + A(q)^\top \lambda = \tau. \quad (2.4)$$

Here, the matrix  $C(q, \dot{q}) \in \mathbb{R}^{n \times n}$  accounts for Coriolis/centrifugal forces generated by implicit constraints on the rigid components on the system and can be computed from the Christoffel symbols [37] of  $M$ . The matrix  $N(q) = \frac{\partial \mathcal{P}(q)}{\partial q} \in \mathbb{R}^n$  is the effect of potential forces on the system (e.g., gravity). Our ability to control the system comes from the external forces and torques

$$\tau = B(q)u + J^\top(q)F. \quad (2.5)$$

The control torques  $u \in \mathbb{R}^p$  are mapped into the dynamics through the matrix  $B \in \mathbb{R}^{n \times p}$ , while additional unmodeled forces are represented by the wrench  $F \in \mathbb{R}^{6 \times 1}$  are mapped into the dynamics through the Jacobian matrix  $J \in \mathbb{R}^{6 \times n}$ .  $B$  is assumed to have full column rank, i.e.,  $\text{rank}(B) = p$ . If  $p < n - m$ , i.e., the number of actuators is less than the number

of unconstrained DOF's of the system, the system is considered to be *underactuated*. If  $p = n - m$  the system is *fully actuated*, and if  $p > n - m$  the system is *overactuated*.

The constraint forces  $\lambda$  and matrix  $A$  are generated from a function  $\sigma(q) : Q \rightarrow \mathbb{R}^m$ , a holonomic constraint that specifies restrictions on the motion of the system. By taking derivatives of this equation,

$$A = \frac{\partial \sigma}{\partial q}. \quad (2.6)$$

the acceleration variables are revealed with

$$\ddot{\sigma} = A(q)\ddot{q} + \dot{A}(q)\dot{q} = 0. \quad (2.7)$$

The constraint forces can then be solved for by combining (2.7) and (2.4) to arrive at

$$\lambda = (AM^{-1}A^\top)^{-1} \left( AM^{-1}(\tau - C\dot{q} - N) + \dot{A}\dot{q} \right). \quad (2.8)$$

The forces induced by ground contact constraints are exactly the ground reaction forces.  $\lambda$  can then be substituted back into (2.4) to have a complete description of the system dynamics in terms of the state variables  $q, \dot{q}$ . The dimension reduced equivalent constrained dynamics can be obtained by substitution of the constraint equations  $h(q)$  directly into the Lagrangian and computing the dynamics via the Euler-Lagrange equation, in the case that the constraints are holonomic [37]. This eliminates the term  $A(q)^\top \lambda$  from the dynamics and reduces the dimensionality of the system, which can make analysis and simulation simpler. However, the information of the constraint forces is lost. Using the notation from [38], the equivalent constrained dynamics are written as

$$M_\lambda(q_\lambda)\ddot{q}_\lambda + C_\lambda(q_\lambda, \dot{q}_\lambda)\dot{q}_\lambda + N_\lambda(q_\lambda) = B_\lambda u + J_\lambda^\top F. \quad (2.9)$$

The matrices  $M_\lambda, C_\lambda \in \mathbb{R}^{(n-m) \times (n-m)}$ ,  $B_\lambda \in \mathbb{R}^{(n-m) \times p}$ ,  $J \in \mathbb{R}^{6 \times (n-m)}$  and vectors  $\ddot{q}_\lambda, \dot{q}_\lambda, q_\lambda, N_\lambda \in \mathbb{R}^{n-m}$  are subscripted to indicate they are from the equations for the constrained, reduced order system.

The 2nd order differential equation (2.4) can be converted to a 1st order differential equation by defining a new state variable vector  $x^\top = [q^\top, \dot{q}^\top]^\top \in \mathbb{R}^{2n}$ . This allows the system to be written in control affine form [39] as

$$\dot{x} = f(x) + g(x)u, \quad (2.10)$$

where  $f \in \mathbb{R}^{2n}$  and  $g \in \mathbb{R}^{2n \times p}$  are defined as

$$f(x) = \begin{bmatrix} \dot{q} \\ -M^{-1}(C\dot{q} + N + A(q)^\top \lambda - J^\top F) \end{bmatrix}, g(x) = \begin{bmatrix} 0_{n \times p} \\ M^{-1}B \end{bmatrix}. \quad (2.11)$$

A similar method can be applied to obtain a 1st order representation of equation 2.9, as well.

## 2.2 Rigid Impact Dynamics

Impacts are fundamental to locomotion, as opposed to other methods of movement like rolling, slithering, swimming, or flying. Bipedes generally have impacts when the swing leg contacts the ground, and some of their kinetic energy is dissipated by the inelastic nature of the impact. If the biped is modeled as a rigid kinematic chain, the impact dynamics can be modeled using the following assumptions from [40]:

1. The impact is instantaneous.
2. The impact has no rebound and no slippage, so the post-impact contact point/surface is constrained to the ground through the function  $h_I(q)$ .
3. Externally applied forces during impact can be represented by impulses  $F_I$ .
4. The actuators cannot generate impulses, so they can be ignored during impact.
5. The impulsive forces may cause an instantaneous jump in the velocity, but the configuration does not jump.

These modeling assumptions can be combined with the principle of momentum conservation [40] to generate a mathematical formula that gives the post-impact state  $x^+$  as a function of the pre-impact state  $x^-$ . This formula is

$$\begin{aligned} \begin{bmatrix} \dot{q}^+ \\ F_I \end{bmatrix} &= \begin{bmatrix} R & 0 \\ 0 & I_{p \times p} \end{bmatrix} \begin{bmatrix} M(q^-) & -A_I^\top(q^-) \\ A_I(q^-) & 0_{2 \times 2} \end{bmatrix}^{-1} \begin{bmatrix} M(q^-) \\ 0_{2 \times 2} \end{bmatrix} \dot{q}^- \\ q^+ &= R q^-. \end{aligned} \quad (2.12)$$

Here,  $A_I = \frac{\partial \sigma_I}{\partial q} \in \mathbb{R}^p$  and accounts for the unilateral ground constraint during impact, while  $R \in \mathbb{R}^{n \times n}$  is a relabeling matrix that swaps the stance and swing legs at the end of a gait cycle. The exact form of  $R$  depends on the choice of coordinates used to represent the biped configuration, but it must be a circular matrix, i.e.,  $RR = I$ . Some biped models may have multiple contact phases and impacts over a single gait cycle; in the case of intermediate impacts  $R = I_{n \times n}$ . In general, this impact model is inelastic with  $\mathcal{K}^- > \mathcal{K}^+$ , which follows from the mathematical statement of assumption 2,  $A_I \dot{q}^+ = 0$ .

### 2.3 Hybrid Biped Dynamics and Orbital Stability

The description of the motion of a biped involves the combination of the continuous motion equation (2.11) with the discrete impact equation (2.12) to form a hybrid system. In this section, I offer a rigorous general definition of a hybrid system and its solutions. I then give a definition for the stability of an orbit (e.g, a stable biped gait) and discuss Poincaré's method for verifying this stability.

Combining definitions and notations from [40, 41, 42] gives the following general definition:

**Definition 1.** *A hybrid control system  $\mathbb{H}$  has the form*

$$\mathbb{H} : \begin{cases} \dot{x} = f(x) + g(x)u & x \in \mathcal{D} \setminus \mathcal{S} \\ x^+ = \Delta(x^-) & x \in \mathcal{S} \end{cases} \quad (2.13)$$

where the set  $\mathcal{D}$  is called the domain of admissibility, the set  $\mathcal{S}$  is called the switching surface, and the function  $\Delta : \mathcal{S} \rightarrow \mathcal{D}$  is called the impact map. The superscripts “-” and “+” indicate the variables before and after impact.

For rigid bipeds, the reset map can be formulated based on equation (2.12). I consider the domain of admissibility to be the set of the states where the biped is not moving through the ground. The switching surface is the set of states where the biped impacts the ground. The general form of hybrid biped dynamics with a swinging leg is then

$$M(q)\ddot{q} + C(q, \dot{q})\dot{q} + G(q) = Bu + J^\top(q)F \quad \text{if } h(q) > 0 \quad (2.14)$$

$$\begin{bmatrix} \dot{q}^+ \\ F_I \end{bmatrix} = \begin{bmatrix} R & 0 \\ 0 & I_{p \times p} \end{bmatrix} \begin{bmatrix} M & -A^\top \\ A & 0_{2 \times 2} \end{bmatrix}^{-1} \begin{bmatrix} M \\ 0_{2 \times 2} \end{bmatrix} \dot{q}^- \quad \text{if } h(q) = 0 \text{ and } \dot{h} < 0 \quad (2.15)$$

$$q^+ = Rq^-.$$

where  $h$  defines the switching surface and is a function that measures the distance from the ground to the closest point on the swing foot of the biped. In the case that both legs are in contact with the ground and the biped is in double support, the switching surface is set of states where a leg lifts from the ground. Mathematically, this is when  $\lambda_y < 0$  at a contact point, which can be computed from equation (2.8).

In this representation, a stable biped gait is a stable periodic solution (or limit cycle) of the hybrid system. Let  $x(t)$  be the solution of the continuous dynamics of  $\mathbb{H}$ . The solution is *n-periodic* if  $x(t) = x(t + \sum_{i=1}^n T_i)$  where  $T_i$  is constant and is the time between impact  $i$  and  $i + 1$ . From the geometrical point of view, the set of points in the phase space corresponding to  $x(t)$  are an invariant set

$$\mathcal{O} := \{x \in \mathcal{D} \mid x = x(t) \text{ for } t \in [0, T_i]\}, \quad (2.16)$$

called an  $n$ -periodic hybrid orbit. I use the following definition for the stability of  $\mathcal{O}$  from [12]

**Definition 2.**  $\mathcal{O}$  is stable in the sense of Lyapunov if for every  $\epsilon > 0$  there is an open ball  $\mathcal{B}_r(x) := \{y \mid \|y - x\| < r\}$  such that for every  $p \in \mathcal{B}_r$  there is a solution  $\phi(t), \phi(0) = p$  for (2.13) where  $\|\phi(t), \mathcal{O}\| < \epsilon$  for all  $t > 0$ .

In general, it is difficult to analytically demonstrate an orbit is stable because closed form functions for  $x(t)$  do not always exist. However, there is a well-known numerical method, detailed in [12], for checking orbital stability called Poincaré's sections. The basic idea is to identify a fixed point  $x^*$  in the state space about which the step-to-step dynamics are linearized, perturb the system off this point, then compute the eigenvalues of the linearization. Define the Poincaré map  $\mathcal{P}(x) : \mathcal{E} \rightarrow \mathcal{E}$  where the event set  $\mathcal{E} = \{x \mid h(x) = 0\}$  is a section of the state space, and a discrete system  $x(k+1) = P(x(k))$  from event to event. If  $x^*$  is a locally stable point of this system, then  $\mathcal{O}$  is locally stable. This can be verified numerically through a perturbation analysis as described in [24] and then a check that  $\max|\lambda| < 1$  where  $\lambda$  is the set of the eigenvalues of Jacobian  $\nabla_x \mathcal{P}(x^*)$ .

## 2.4 Passivity

Consider the control affine system as described in (2.10) with an output  $y(x) \in \mathbb{R}^n$ . I use the following notion of passivity from [43] for this output:

**Definition 3.** Let  $S(q, \dot{q}) : \mathbb{R}^{2n} \rightarrow \mathbb{R}$  be a continuously differentiable, non-negative scalar function. A system is passive from input  $u$  to output  $y$  with storage function  $S(q, \dot{q})$  if  $y^\top u \geq \dot{S}(q, \dot{q})$ .

The idea of passivity is an extension of the idea of an energy function for a system, where  $S$  plays the role of the energy that can only change due to power input from the control  $u$ .

Passivity is a useful property for a system to have for many reasons. Primarily, it can be used to prove Lyapunov stability under feedback control by the following lemma from [44]:

**Lemma 1.** *If a control-affine system is passive from  $u$  to  $y$  with storage function  $S$ , and  $u = \zeta(y)$  where  $\zeta(y)$  is a continuous function that satisfies  $y^\top \zeta(y) < 0$ , then the zero level-set  $Z = \{y \mid \zeta(y) = 0\}$  is stable in the sense of Lyapunov and is asymptotically attractive.*

A specific choice for  $\zeta(y)$  that satisfies the lemma is

$$u = \zeta(y) = -\kappa\Omega y, \tag{2.17}$$

where  $\kappa > 0$  is a scalar gain while  $\Omega \in \mathbb{R}^{n \times n}$  is a positive definite weighting matrix with each element less than one. This is essentially feedback of a scaled form of the passive output  $y$ . This control retains the passivity property under saturation of  $u$  as

$$y^\top \text{sat}(-\kappa\Omega y) < 0, \tag{2.18}$$

because saturation is a so-called first and third quadrant nonlinearity [45]. Stability is then ensured under saturation of the control input, which occurs in all physically realizable robotic systems.



## CHAPTER 3

### ENERGY SHAPING AND REGULATION CONTROL

The origin of the term “energy shaping” to describe a controller is based on the idea of defining a target virtual dynamical system based on an energy function, and using the control input to cause the plant to act like this target system. Seminal works in this area of research are on “Controlled Lagrangians” [14] by Bloch et al. and “Interconnection and Damping Assignment Passivity-Based Control” (IDA-PBC) by Ortega et al. While the focus of these works is stabilization of an equilibrium point, there has been an effort to extend these methods to generate and stabilize periodic orbits [19]. Energy shaping is particularly useful for emulating walking gaits of passive systems by creating a virtual Lagrangian system, as seen in [15, 16]. In [15], the direction of the virtual gravity vector of the compass gait biped is controlled to emulate a passive walking gait on arbitrary slopes (but the structure of the dynamics remains the same). In [16], new structure/parameters are added to the virtual mass matrix of the compass gait biped, resulting in the generation of new gaits. These ideas have begun to be applied in wearable robotics as in [18], where the virtual gravity of a human-exoskeleton system is controlled to provide motion support or resistance for stroke rehabilitation. A natural extension of this research direction is to apply similar methods to a leg prosthesis.

A closely related idea that is sometimes lumped into “energy shaping” is “energy regulation” (see [19]), where a control explicitly drives the energy of the system to a particular value associated with a walking gait [15, 46, 42, 47]. In autonomous bipeds, this kind of

---

<sup>0</sup>Chapter 3 is in part is a reprint of material published in:

© 2019 ASME. Reprinted, with permission, from M. Yeatman, G. Lv, and R. Gregg, “Decentralized Passivity-Based Control with a Generalized Energy Storage Function for Robust Biped Locomotion,” *ASME Journal of Dynamic Systems, Measurement, and Control*, 141(10): 101007, 2019..

© 2020 ASME. Reprinted, with permission, from M. Yeatman and R. Gregg, “Using Energy Shaping and Tracking to Generate Natural Limit Cycles in Mechanical Systems with Impacts,” *ASME Journal & of Computational and Nonlinear Dynamics*, under review.

method can improve a metric of stability margin or robustness by increasing the so-called basin of attraction (the set of initial conditions of the system that will converge to the limit cycle). As remarked in [15, 42], a key component to this effect is the identification of a limit cycle trajectory where the system energy is conserved so that the energy regulation control is zero on the desired orbit. Energy shaping and energy regulation can be combined [19, 15] to change the virtual closed-loop dynamics, then drive the virtual energy to a desired value to achieve a limit cycle. To-date there has been no research into applying energy regulation methods to any wearable device. Part of the novelty and contribution of this dissertation is to understand how human interaction and assumed passivity can affect systems with energy regulation.

In the following sections I will cover some mathematical theory for energy shaping and regulation control. The open-loop/plant dynamics are a biped with hybrid dynamics (2.14). The control  $u = u_s + u_r$  is partitioned into two components, where  $u_s$  performs energy shaping and  $u_r$  performs energy regulation. These controllers are designed in stages so that  $u_r$  operates on the energy of the shaped system that results from  $u_s$  as seen in the block diagram figure 3.1. I will then propose a specific control structure for a powered prosthetic leg that embeds an energy regulated virtual spring. The idea is that the virtual spring will allow the dynamics of the residual limb and attached prosthesis to behave like the SLIP model, which has forces, motion, and energy properties similar to a healthy leg. The energy regulation control will enable explicit positive work generation of the prosthesis to counteract energy dissipation caused by impact.

### 3.1 Energy Shaping

Here I will review a method of energy shaping with Controlled Lagrangians. For simplicity, I assume that the open-loop biped dynamics are in the equivalent constrained form (2.9) and

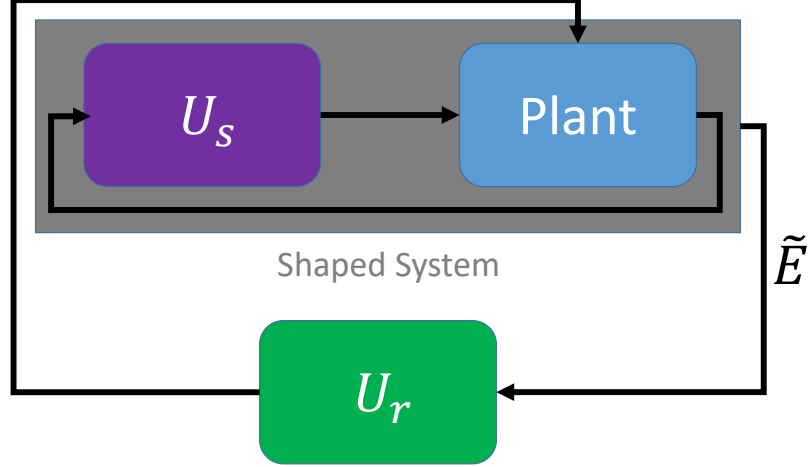


Figure 3.1: Block diagram of the hierarchy for energy shaping and energy regulation control.

drop the subscripts. The system dynamics in terms of the open-loop Lagrangian is

$$\frac{d}{dt} \frac{\partial \mathcal{L}(q, \dot{q})}{\partial \dot{q}} - \frac{\partial \mathcal{L}(q, \dot{q})}{\partial q} = B(q)u + J^\top(q)F. \quad (3.1)$$

Following the methods in [14, 48, 49], I define a desired closed-loop virtual Lagrangian  $\tilde{\mathcal{L}}$  with dynamics of the form

$$\frac{d}{dt} \frac{\partial \tilde{\mathcal{L}}(q, \dot{q})}{\partial \dot{q}} - \frac{\partial \tilde{\mathcal{L}}(q, \dot{q})}{\partial q} = \tilde{B}u_r. \quad (3.2)$$

In [48], it is shown that 3.2 leads to two equations,

$$B^\top \left( \frac{d}{dt} \frac{\partial \tilde{\mathcal{L}}(q, \dot{q})}{\partial \dot{q}} - \frac{\partial \tilde{\mathcal{L}}(q, \dot{q})}{\partial q} \right) = 0 \quad (3.3)$$

$$B^\perp \left( \frac{d}{dt} \frac{\partial \tilde{\mathcal{L}}(q, \dot{q})}{\partial \dot{q}} - \frac{\partial \tilde{\mathcal{L}}(q, \dot{q})}{\partial q} \right) = 0, \quad (3.4)$$

where  $B^\perp$  is a full rank left annihilator of  $B$ , i.e.,  $B^\perp B = 0$ . These two equations are the most general form of the so-called “matching conditions” for energy shaping control. Equation 3.1

is said to match 3.2 if 3.3 and 3.4 hold along the system flow. Matching the systems is easier when the system is fully actuated with  $\text{rank}(B) = n$ . The first equation can be achieved by feedback control, with

$$u_s = (B^\top B)^{-1} B^\top \left( -J^\top(q)F + \left( \frac{d}{dt} \frac{\partial \mathcal{L}}{\partial \dot{q}} - \frac{\partial \mathcal{L}}{\partial q} \right) - \left( \frac{d}{dt} \frac{\partial \tilde{\mathcal{L}}}{\partial \dot{q}} - \frac{\partial \tilde{\mathcal{L}}}{\partial q} \right) \right). \quad (3.5)$$

The second equation is enforced by the assumption of full actuation, because  $B^\perp = 0$ .

If the system is underactuated, then the problem becomes significantly more complicated. Equation 3.4 can lead to a set of nonlinear partial differential equations that must hold along the system flow [48]. In general, the only way to verify these equations hold is to solve them, which is a notoriously challenging prospect and outside the scope of this dissertation. Later in Section 5 I will show that this problem can arise in attaching a virtual spring to the center of pressure of a biped. However, this problem can be made much easier by restricting the class of plant and target systems.

In the case where the plant and target dynamics are restricted to the class of mechanical systems, the virtual Lagrangian of the form

$$\tilde{\mathcal{L}} = \tilde{\mathcal{K}}(q, \dot{q}) - \tilde{\mathcal{P}}(q) = \frac{1}{2} \dot{q}^\top \tilde{M}(q) \dot{q} - \tilde{\mathcal{P}}(q). \quad (3.6)$$

The expression for the target dynamics are derived by applying the Euler Lagrange equation (2.1) to (3.6) which results in

$$\tilde{M}(q)\ddot{q} + \tilde{C}(q, \dot{q})\dot{q} + \tilde{N}(q) = \tilde{M}M^{-1}Bu_r. \quad (3.7)$$

The control that achieves these closed-loop continuous dynamics on system (2.14) is then

$$u_s = (B^\top B)^{-1} B^\top (C\dot{q} + G - M\tilde{M}^{-1}(\tilde{C}\dot{q} + \tilde{G})), \quad (3.8)$$

and the matching condition is simplified to

$$B^\perp (C\dot{q} + G - M\tilde{M}^{-1}(\tilde{C}\dot{q} + \tilde{G})) = 0. \quad (3.9)$$

This matching condition basically ensures that the difference between the plant and target dynamics never has a component in the nullspace of  $B$ . The energy for this closed-loop system is  $\tilde{E} = \tilde{\mathcal{K}}(q, \dot{q}) + \tilde{\mathcal{P}}(q)$ . It is important to note that in all cases the impact dynamics (2.15) remain *unchanged* (because there is no control input in equation (2.12)), meaning the general hybrid dynamics cannot be arbitrarily shaped to match another hybrid system. Additionally, this does not address potential issues with matching the switching surface of the system to some desired behavior.

### 3.2 Energy Regulation

The method of energy regulation presented here is based on the work in [15] and is “passivity-based”, meaning the control is a form of negative feedback of a passive output as given in Definition 3. This stands in contrast to other energy regulation control techniques that do *not* preserve passivity, such as [42] and [46]. I begin by defining the storage function

$$S = \frac{1}{2}(\tilde{E} - E_{\text{ref}})^2, \quad (3.10)$$

where  $\tilde{E}$  is the virtual energy of the closed-loop system from equation 3.7 and  $E_{\text{ref}}$  is the reference energy. The time derivative of this storage function is

$$\dot{S} = (\dot{\tilde{E}} - \dot{E}_{\text{ref}})(\tilde{E} - E_{\text{ref}}). \quad (3.11)$$

From equation 3.7, the instantaneous change in energy is

$$\dot{\tilde{E}} = \dot{q}^\top \tilde{M} M^{-1} B u_r \quad (3.12)$$

$$= \dot{q}^\top \tilde{B} u_r \quad (3.13)$$

$$\dot{S} = (\dot{q}^\top \tilde{B} u_r - \dot{E}_{\text{ref}})(\tilde{E} - E_{\text{ref}}). \quad (3.14)$$

First, I will consider the case where the reference energy is constant, i.e.,  $\dot{E}_{\text{ref}} = 0$ . From substitution,

$$\dot{S} = \dot{q}^\top \tilde{B} u_r (\tilde{E} - E_{\text{ref}}), \quad (3.15)$$

and by Definition 3 the energy-based passive output can be identified as

$$y(q, \dot{q})^\top = (\tilde{E} - E_{\text{ref}}) \dot{q}^\top B_u. \quad (3.16)$$

Using the paradigm of negative passive feedback [43],  $\dot{S}$  can be rendered negative semi-definite by feedback of the scaled output with

$$u_r = -\kappa \Omega y = -\kappa (\tilde{E} - E_{\text{ref}}) \Omega \tilde{B}^\top \dot{q}. \quad (3.17)$$

Here,  $\kappa > 0$  is a scalar gain while the weighting matrix  $\Omega \in \mathbb{R}^{n \times n}$  is positive definite with each element less than one. The storage function and its time derivative are related by

$$\dot{S} = -\kappa (\tilde{E} - E_{\text{ref}})^2 \dot{q}^\top \tilde{B} \Omega \tilde{B}^\top \dot{q} \quad (3.18)$$

$$= -2\kappa \|\dot{q}\|_\Omega^2 S, \quad (3.19)$$

where the term  $\dot{q}^\top \tilde{B} \Omega \tilde{B}^\top \dot{q}$  is a norm. The asymptotic convergence of the virtual energy to the target reference energy is guaranteed if the system state cannot enter some positively invariant set where  $\|\dot{q}\|_\Omega = 0$ .

While it is possible to regulate a general non-constant reference energy  $E_{\text{ref}}(q, \dot{q}, t)$  function that varies with state and time, I argue that the result is identical to the technique of partitioning the control into an energy shaping step and then an energy regulation step. Furthermore, the result of directly regulating the varying reference energy is unclear without this partitioning. I can define a new energy function  $\tilde{E} = E - E_{\text{ref}}(q, \dot{q}, t)$  then use the Legendre transformation to derive the associated Lagrangian  $\tilde{\mathcal{L}}$ , assuming that the transformation is well-defined. The target dynamics can be obtained through the EL equation and the Controlled Lagrangians technique used to arrive at an energy shaping control (because of this more general form of  $E_{\text{ref}}$ , more general matching conditions from [48] must be satisfied). If the reference energy has some constant term  $C$  such that  $E_{\text{ref}} = f(q, \dot{q}, t) + C$ , it will vanish after the EL equations are applied. However, the desired convergence can be recovered by

applying an outer-loop energy regulating control with  $\tilde{E} = E - f(q, \dot{q}, t)$  and  $E_{\text{ref}} = C$ . This two step procedure allows us to clearly interpret the effect of the control as determining the shape of an energy level set through the shaping step and then stabilizing the set through energy regulation, similar to [19]. Directly regulating a time-state varying reference energy results in a less clear effect. This point is particularly salient in the next section on using a time-integral based energy function that accounts for the work done by dissipative forces in the system.

### 3.2.1 Regulation of a Work-Based Energy Function

As shown in [42, 47], I can define a generalized system energy as

$$E(q, \dot{q}, v, t) = K(q, \dot{q}) + P(q) - W(q, \dot{q}, v, t). \quad (3.20)$$

where the work done by some torque/force input  $v$  is

$$W = \int_0^t \dot{q}^\top B_v v \, d\tau. \quad (3.21)$$

The work  $W$  accounts for the energy stored, added, and dissipated over time  $t$  by  $v$ . Note that the exact form of this input is left arbitrary; the important feature is that it generates a limit cycle for the biped. The time derivative of this new work-based energy function is

$$\dot{E} = \frac{d(K + P)}{dt} - \frac{dW}{dt}. \quad (3.22)$$

From the definition of  $W$ , the application of the fundamental theorem of calculus, and the conservation of energy in a mechanical system,

$$\dot{E} = (\dot{q}^\top B_u u + \dot{q}^\top B_v v) - \dot{q}^\top B_v v = \dot{q}^\top B_u u. \quad (3.23)$$

Achieving this power relation is the main “trick” behind including  $W$  in the system energy function 3.20. In term of the biped dynamics 2.14, we can consider  $B_v v = J^\top F$ .

From here, the analysis follows the same pattern as in the previous section. Reusing the storage function from equation 3.10 and its time derivative 3.11, I again assume  $E_{ref}$  is constant so that

$$\dot{S} = (E - E_{ref})\dot{q}^\top B_u u, \quad (3.24)$$

with passive output

$$y(q, \dot{q}, v, t)^\top = (E - E_{ref})\dot{q}^\top B_u. \quad (3.25)$$

A critical difference between 3.16 and 3.25 is that the new output is now dependent on time and the input  $v$ . This output can be substituted into the energy regulation control 4.45.

### 3.3 Application to Hybrid Locomotive Systems

Autonomous walking systems have limit cycles with trajectories, stability properties, and other gait characteristics that can depend on the value of the system parameters [24, 23]. This means that by changing these parameters, it is possible to change the limit cycle properties to make a biped change speeds or walk up a slope [15]. The basin of attraction of these limit cycles are typically small, hence I will use energy regulation to increase the basin in order to make gait transitions more robust as shown in [15]. This method of gait transition is basically the idea of Lyapunov funneling, see [50, 51]. However, the hybrid nature of the dynamics can present conceptual challenges to the application of both energy shaping and regulation control methods.

If the impact map  $\Delta$  depends on the system parameters and the system is limited only to continuous/non-impulsive control, then arbitrary virtual hybrid systems cannot be exactly emulated. This idea is related to work on energy shaping and Controlled Symmetries [52], of which a key component was demonstrating that the impact dynamics of a rigid biped are invariant with respect to the ground slope parameter. However, it is completely possible to



change the virtual parameters of only the closed-loop continuous dynamics, while using the original open-loop impact dynamics. I expect that the qualitative relationship between gait characteristics (e.g., walking speed) and parameters will be similar between the true system and partially emulated virtual system.

The impact map also influences the construction of an energy regulating control. If a passive walker has a conserved energy on its periodic orbit in the continuous dynamics, then the energy must be conserved across the discrete dynamics as well. This implies an equilibrium between the kinetic energy lost from dissipative impact and the potential energy gained from shifting the world frame [53]. This equilibrium can be unstable, such that a small perturbation will cause the impact dynamics to drive the energy away from the limit cycle [24]. However, it could be possible to use energy regulation to stabilize these passively unstable limit cycles. The idea is that over the flow of the continuous dynamics, the energy regulating controller compensates for the destabilizing effect of the impact dynamics. Consider the step to step storage function

$$S_{i+1}^- = \int_0^{t_i} (\dot{q}^\top B u_r)(E - E_{\text{ref}}) d\tau + S_i^+ \quad (3.26)$$

$$= \int_0^{t_i} (\dot{q}^\top B u_r)(E - E_{\text{ref}}) d\tau + \Delta_S(q^-, \dot{q}^-) + S_i^-, \quad (3.27)$$

where  $t_i$  is the time between impacts and  $\Delta_S$  is the change in the storage function at impact.

If

$$0 \geq \int_0^{t_i} (\dot{q}^\top B u_r)(E - E_{\text{ref}}) d\tau + \Delta_S(q^-, \dot{q}^-), \quad (3.28)$$

then  $S_{i+1}^- \leq S_i^-$ , meaning the storage function is always decreasing between impacts and the energy is converging to the target energy. This is basically the notion of a hybrid storage function and so-called “jump and flow passivity” [54], but applied to orbital stabilization. For an unstable passive limit cycle,  $\Delta_S > 0$ , while a stable one corresponds to  $\Delta_S < 0$ . From equation (3.18), the amount of storage dissipated over the continuous dynamics can be modulated with the gain  $\kappa$ . Again, even if the inequality (3.28) is satisfied and the

reference energy is asymptotically stable, this is only a necessary but not sufficient condition for achieving a limit cycle in general.

### 3.4 A Hopping Robot Example

This section considers a simple model of a hopping robot with 1 degree-of-freedom (DOF). The simplicity of the model allows analytical proofs of stability and performance due to the linear open-loop continuous dynamics and low dimensionality. Some of the information on the passive dynamics is similar to other works on hoppers [55] and the rimless wheel [56]. The model serves as a simple non-abstract example to demonstrate and develop methods for application on higher order and more interesting models later in the dissertation.

#### 3.4.1 Hopper Dynamics

Consider an actuated mass-spring system hopping on a static flat surface and constrained to move along the vertical axis (a simplified version of the SLIP model). The continuous dynamics has two phases/equations

$$\mathbf{Stance (ST)} \quad u = m\ddot{y} + k(y - y_0) + mg \quad (3.29)$$

$$\mathbf{Flight (FL)} \quad 0 = m\ddot{y} + mg \quad (3.30)$$

where the mass of the point is  $m$ , the distance from the point to the ground is  $y$ , the relaxed length of the spring is  $y_0$ , the gravitational acceleration constant is  $g$ , and the actuation force is  $u$ . The discrete dynamics that govern the switch between these phases are

$$\text{if } \mathbf{phase} == \mathbf{FL} \quad \text{and} \quad y \leq y_c \quad (3.31)$$

$$\dot{y}^+ = e \dot{y}^-$$

$$\mathbf{phase} := \mathbf{ST}$$

$$\text{if } \mathbf{phase} == \mathbf{ST} \quad \text{and} \quad y \geq y_0 \quad (3.32)$$

$$\mathbf{phase} := \mathbf{FL}$$

where the superscripts - and + indicate pre-impact and post-impact states, respectively. The spring length at impact is  $y_c \leq y_0$ , and  $e$  is the coefficient of restitution. If  $e = 1$ , then the impact is elastic. If  $0 < e < 1$ , the impact is plastic.

Periodic orbits in Lagrangian systems necessarily have a conserved energy, which implies the system energy must be conserved at impact. For the passive hopper, this means the energy added in by the spring length offset must equal the energy dissipated by the impact, i.e.,  $\frac{1}{2}k(y_0 - y_c)^2 = \frac{1}{2}m(1 - e)^2(\dot{y}^-)^2$ . If the impact is plastic, then the orbit can be shown to be locally exponentially stable in the sense of Lyapunov by considering the energy state from impact to impact. Before impact,

$$E_i^- = \frac{1}{2}m(\dot{y}^-)^2 + mgy_c, \quad (3.33)$$

and after

$$E_i^+ = \frac{1}{2}m(e\dot{y}^-)^2 + \frac{1}{2}k(y_0 - y_c)^2 + mgy_c. \quad (3.34)$$

Since energy is conserved over the continuous dynamics,  $E_i^+ = E_{i+1}^-$ , which implies that

$$E_{i+1}^- = e^2 E_i^- + \frac{1}{2}k(y_0 - y_c)^2 + (1 - e^2)mgy_c. \quad (3.35)$$

Because  $0 < e < 1$ , this discrete system is exponentially stable and

$$E \rightarrow \frac{k(y_0 - y_c)^2}{2(1 - e^2)} + mgy_c = E_{\text{lim}}. \quad (3.36)$$

This forms an analytical Poincaré map [12], thus there is always a locally exponentially stable hybrid limit cycle for the hopper.

For all parameter cases of the passive hopper, the system will get stuck in the stance phase if the energy is too low to achieve liftoff. In addition, the mass can bottom out against the ground if the energy is too large, which we consider to be a system failure. This implies that basin of attraction is bounded by these two energy level sets as

$$mgy_0 < E < \frac{1}{2}ky_0^2. \quad (3.37)$$

If  $e = 1$  and  $y_c = y_0$ , the energy is always conserved across all dynamic regimes and there is a family of marginally stable periodic orbits within these energy bounds.

### 3.4.2 Hopper Control

The hopping height  $y_{\text{apex}}$  is limited by the upper bound on the energy with the expression

$$y_{\text{apex}} < \frac{ky_0^2}{2mg}. \quad (3.38)$$

The good news is that energy shaping can be used to change the virtual spring stiffness  $\tilde{k}$  to increase the basin ceiling and achieve arbitrary hopping heights, while energy regulation can be used to create energy for liftoff and minimize the basin floor. The resulting control and closed loop stance dynamics are

$$u = u_s + u_r \quad (3.39)$$

$$= (k - \tilde{k})(y - y_0) - \kappa(\tilde{E} - E_{\text{ref}})\dot{y} \quad (3.40)$$

$$0 = m\ddot{y} + \kappa(\tilde{E} - E_{\text{ref}})\dot{y} + \tilde{k}(y - y_0) + mg, \quad (3.41)$$

where  $\tilde{E} = \frac{1}{2}m\dot{y}^2 + \frac{1}{2}\tilde{k}(y - y_0)^2 + mgy$ . If there is a linear damping term ( $d \cdot \dot{y}$ ) in the stance dynamics, it acts as a shift on the reference energy as  $E_{\text{new}} = E_{\text{ref}} - \frac{d}{\kappa}$  so the damped hopper system can be addressed by this example as well. Interestingly, the new stance dynamics correspond exactly to the harmonic Rayleigh-Van-der-Pol oscillator from [57].

In the case of  $e = 1$  and  $y_c = y_0$ , we can choose any reference energy that satisfies equation (3.37) to achieve a virtual passive limit cycle. In the case of  $0 < e < 1$  and  $0 < y_c < y_0$ , we must choose  $E_{\text{ref}}$  to be exactly equal to  $E_{\text{lim}}$  from equation (3.36) if we want to ensure that the hopping limit cycle mimics a passive system. Consider the step-to-step storage function at impact,

$$S_i^+ = \frac{1}{2}(E^+ - E_{\text{ref}})^2 \quad (3.42)$$

$$= \frac{1}{2}(e^2 E_i^- + \frac{1}{2}k(y_0 - y_c)^2 - E_{\text{ref}})^2. \quad (3.43)$$

If  $0 < e < 1$  and  $E_{\text{ref}} = E_{\text{lim}}$ , then  $S_i^+ = e^4 S_i^-$  and the storage function decreases after impact, i.e.,  $S_i^+ \leq S_i^-$ . The energy regulation control causes the storage to decrease over the

continuous dynamics, implying  $S_{i+1}^- \leq S_i^+$ . It follows then that  $S_{i+1}^- \leq S_i^-$ ; the post impact storage function monotonically decreases from event to event. Thus, the hybrid limit cycle of the system under the energy regulation control is asymptotically stable.

### 3.4.3 An Impact-to-Impact Energy Update Law

One can generally expect a hopping robot to encounter many different surfaces that result in varying coefficients of restitution that cannot be estimated beforehand, implying different natural energy levels associated with the natural limit cycle. So it would be useful in practice to have a method of updating  $E_{\text{ref}}$ . Inspired by structure of the impact dynamics, we propose the update policy

$$E_{\text{ref}_{i+1}} = E_{\text{ref}_i} + \Lambda(E_i^+ - E_i^-) \quad (3.44)$$

$$= E_{\text{ref}_i} + (e^2 - 1)\Lambda E_i^- + \Lambda \left( \frac{1}{2}k(y_0 - y_c)^2 + (1 - e^2)mgy_c \right). \quad (3.45)$$

where  $\Lambda$  is a scaling gain. Essentially, if the impact dynamics cause a net gain in  $E$  then  $E_{\text{ref}}$  is increased, and vice-versa. From the convergence of  $S$  in the continuous dynamics,

$$|E_{i+1}^- - E_{\text{ref}_i}| \leq |E_i^+ - E_{\text{ref}_i}|, \quad (3.46)$$

The triangle inequality [58] can be applied so that

$$E_{i+1}^- \leq e^2 E_i^- + \frac{1}{2}k(y_0 - y_c)^2 + (1 - e^2)mgy_c \quad (3.47)$$

$$E_{i+1}^- \geq -e^2 E_i^- - \frac{1}{2}k(y_0 - y_c)^2 - (1 - e^2)mgy_c. \quad (3.48)$$

This allows the discrete system

$$\begin{bmatrix} E_{\text{ref}_{i+1}} \\ E_{i+1}^- \end{bmatrix} = f(E_{\text{ref}_i}, E_i^-) \quad (3.49)$$

to be bound as

$$\begin{bmatrix} E_{\text{ref}_{i+1}} \\ E_{i+1}^- \end{bmatrix} \leq \begin{bmatrix} 1 & \Lambda(e^2 - 1) \\ 0 & e^2 \end{bmatrix} \begin{bmatrix} E_{\text{ref}_i} \\ E_i^- \end{bmatrix} + \begin{bmatrix} \Lambda \mathbf{c} \\ \mathbf{c} \end{bmatrix} \quad (3.50)$$

$$\begin{bmatrix} E_{\text{ref}_{i+1}} \\ E_{i+1}^- \end{bmatrix} \geq \begin{bmatrix} 1 & \Lambda(e^2 - 1) \\ 0 & -e^2 \end{bmatrix} \begin{bmatrix} E_{\text{ref}_i} \\ E_i^- \end{bmatrix} + \begin{bmatrix} \Lambda \mathbf{c} \\ -\mathbf{c} \end{bmatrix} \quad (3.51)$$

$$\mathbf{c} = \frac{1}{2}k(y_0 - y_c)^2 + (1 - e^2)mgy_c \quad (3.52)$$

By inspection, both of bounding systems are linear and exponentially stable when  $0 < e < 1$  and  $0 < \Lambda < 1$ . The contraction mapping theorem [59] can be applied to show that  $E_{\text{ref}_i}$  and  $E_i^-$  both converge to  $E_{\text{lim}}$ .

This update law can generalize to higher dimensional systems, which we show through numerical simulation on the compass gait biped in a later section. We remark that in practice, using a different constant value of  $E_{\text{ref}}$  can still result in a limit cycle as in [55], but the asymptotic trajectory will not emulate a virtual passive system and is dependent on the value of the gain  $\kappa$ . Finally, the stability of the system with the update law relies on the stability properties of the passive limit cycle,  $0 < e < 1$ . This leads us to believe that in general, the energy associated with an unstable limit cycle cannot be arrived at via (3.44).

## CHAPTER 4

### APPLICATION ON BIPED ROBOTS

In this Chapter I present, from simple to complex, a series of locomotive mechanical systems and use energy shaping and regulation control to stabilize and generate walking and running gaits. In simple walking models, like the Spring Loaded Inverted Pendulum and the Compass Gait Biped, characteristics of a gait such as walking speed and step length are directly linked to model parameters like spring stiffness and mass. Thus, it makes sense to use energy shaping to virtually change the model parameters to induce desired properties like increasing the walking speed. However, this type of control does nothing to increase the basin of attraction of the virtual system. Thus, it makes sense to use energy regulation to increase the basin and facilitate transitions during parameter switching. By using these techniques, the simple models can then be embedded into more complex biped systems and serve as templates to generate motion, similar to the ideas in [60]. This gives a baseline of how to use templates for human locomotion to control complex models of powered prostheses and orthoses.

#### 4.1 The Spring Loaded Inverted Pendulum

The SLIP is a widely known walking model that exhibits behaviors and properties similar to human walking [23]. It is comprised of a point mass that “walks” via connecting the ball to the ground through massless springs. Because it is *not* a rigid kinematic chain, there is no rigid impact. The SLIP model considered in this dissertation moves in a two-dimensional

---

<sup>0</sup>Chapter 4 is in part is a reprint of material published in:

© 2019 ASME. Reprinted, with permission, from M. Yeatman, G. Lv, and R. Gregg, “Decentralized Passivity-Based Control with a Generalized Energy Storage Function for Robust Biped Locomotion,” *ASME Journal of Dynamic Systems, Measurement, and Control*, 141(10): 101007, 2019.

© 2020 ASME. Reprinted, with permission, from M. Yeatman and R. Gregg, “Using Energy Shaping and Tracking to Generate Natural Limit Cycles in Mechanical Systems with Impacts,” *ASME Journal & of Computational and Nonlinear Dynamics*, under review.

plane, can exhibit both walking and running behaviors, and has additional actuation along the spring axis. The walking behavior alternates between a single support phase and a double support phase, while the running behavior alternates between a single support phase and a flight phase. The system has no dissipation, which implies that the energy is always conserved and that the model is not physically realizable. A diagram of the system is given in Fig. 4.1.

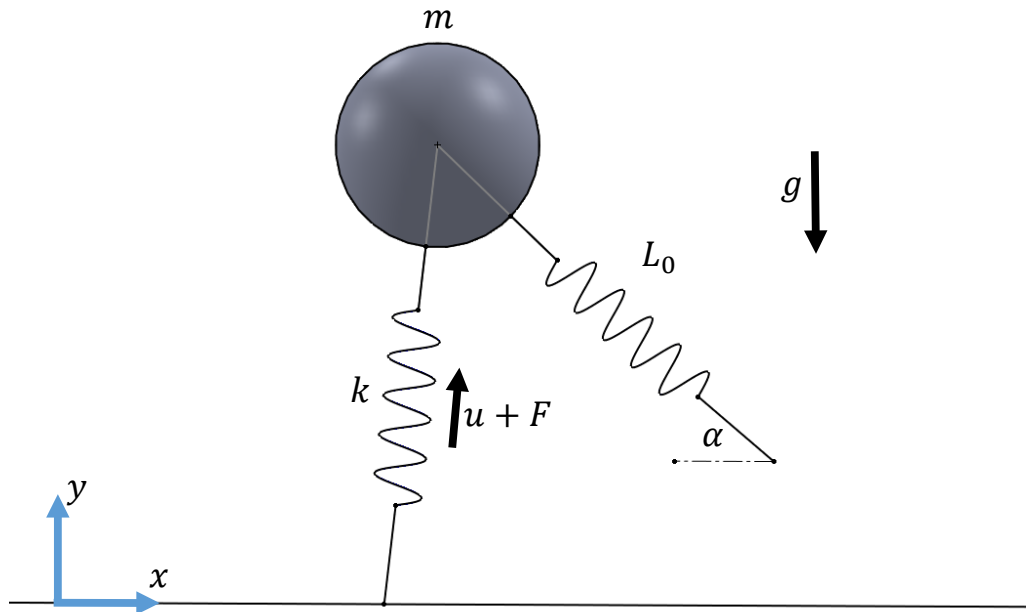


Figure 4.1: Diagram of the spring loaded inverted pendulum.

In general, the energy of the system is

$$E = \mathcal{K}(\dot{q}) + \mathcal{P}(q) \quad (4.1)$$

$$= \frac{1}{2}(m)(\dot{x}^2 + \dot{y}^2) + \frac{1}{2}k(L_1(x, y) - L_0)^2 + \frac{1}{2}k(L_2(x, y) - L_0)^2 + mgy \quad (4.2)$$

The configuration vector of the model is  $q = [x, y]^T$ , the point mass is  $m$ , and the length and stiffness of the springs are  $L$  and  $k$ , respectively. The gravitational acceleration constant is  $g$ , and is along the vertical coordinate  $y$ . At  $L = L_0$ , the system releases a spring from the



ground and engages the spring again at the contact angle  $\alpha$  when  $y = L \sin(\alpha)$ . This gives the ground contact point pf. The springs are labeled 1 and 2, left to right, when they are in contact with the ground. The rules for releasing and engaging the springs imply that the system energy does not jump at these switches, thus the spring energy and force expressions can be dropped when they are not engaged with the ground. These switching rules and the application of the Euler-Lagrange equation (2.1) lead to the following equations of motion:

$$\mathbf{Double\ Support\ (DS)} \quad J_1^\top u_1 + J_2^\top u_2 = M\ddot{q} + J_1^\top F_1 + J_2^\top F_2 + G \quad (4.3)$$

$$\mathbf{Single\ Support\ (SS)} \quad J_1^\top u_1 = M\ddot{q} + J_1 F_1 + G \quad (4.4)$$

$$\mathbf{Flight\ (FL)} \quad 0 = M\ddot{q} + G \quad (4.5)$$

$$\text{if } \mathbf{phase == DS} \quad \text{and} \quad L_2 \geq L_o \quad (4.6)$$

$$\mathbf{phase := SS}$$

$$\text{if } \mathbf{phase == SS} \quad \text{and} \quad y \leq L_o \sin(\alpha) \quad (4.7)$$

$$\mathbf{phase := DS}$$

$$\text{if } \mathbf{phase == FL} \quad \text{and} \quad y \leq L_o \sin(\alpha) \quad (4.8)$$

$$\mathbf{phase := SS}$$

$$\text{if } \mathbf{phase == SS} \quad \text{and} \quad L_1 \geq L_o \quad (4.9)$$

$$\mathbf{phase := FL}$$

$$M = \begin{bmatrix} m & 0 \\ 0 & m \end{bmatrix}, G = \begin{bmatrix} 0 \\ mg \end{bmatrix}, J_i = \begin{bmatrix} \frac{x - \text{pf}_{x_i}}{L_i} \\ \frac{y - \text{pf}_{y_i}}{L_i} \end{bmatrix},$$

$$L_i = \sqrt{(x - \text{pf}_{x_i})^2 + (y - \text{pf}_{y_i})^2}, F_i = k(L_i - L_o)$$

The motion of the mass is extremely similar to the motion of a human's center of mass in the sagittal plane, and the qualitative “double hump” in the ground reaction force is characteristic of both human walking and the SLIP model[23] as seen in Figures 4.2 and 4.3.

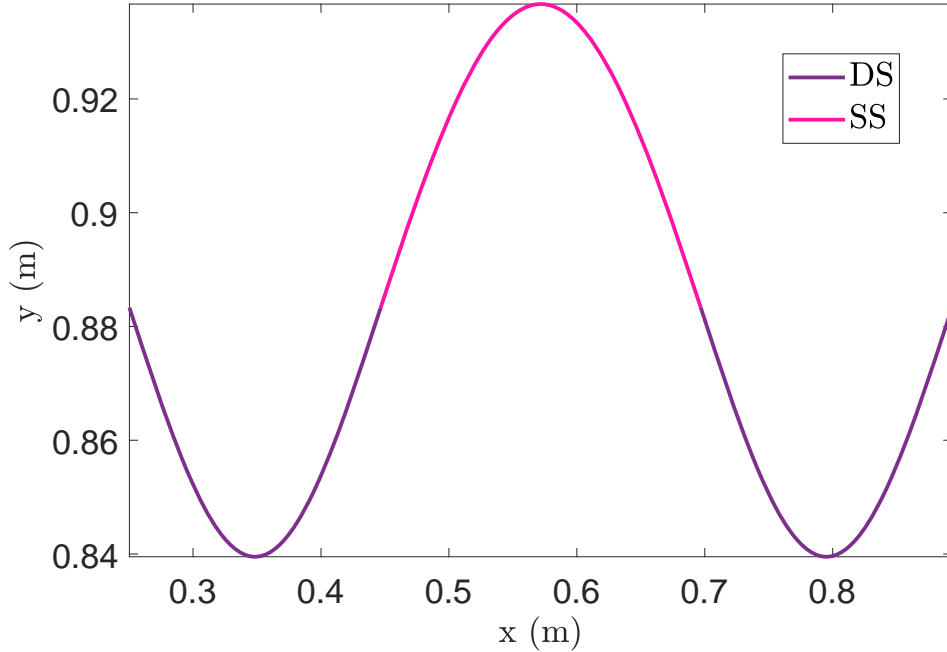


Figure 4.2: Sample walking trajectory of the SLIP model, average walking speeds of  $1.1\text{ms}^{-1}$ .  $m = 70\text{kg}$ ,  $k = 12250\text{Nm}^{-1}$ ,  $L_o = 0.94\text{m}$ .

#### 4.1.1 Control

In [23], it is shown that for a constant spring stiffness  $k$  and touchdown angle  $\alpha$ , there is a compact set of energies that correspond to walking or running periodic orbits in the SLIP model. They also show that these energy sets exist and change for a range of stiffnesses and touchdown angles. This is our motivation to use energy shaping to change the spring stiffness. Because the energy of the open-loop system is conserved, any periodic orbit is only marginally stable. Thus, it is reasonable to use energy regulation to stabilize the orbit. However, because the SLIP model has a 4 dimensional state space instead of the 2 dimensional space of the hopper, a single energy value does not uniquely define a trajectory of the open-loop system. Additionally, work in both [23] and [61] indicates that controlling the contact angle is critical to the stability of this model. Inspired by [61], we use the policy

$$\alpha_{i+1} = \frac{1}{2}(\alpha_i + \pi - \theta_i) \quad (4.10)$$

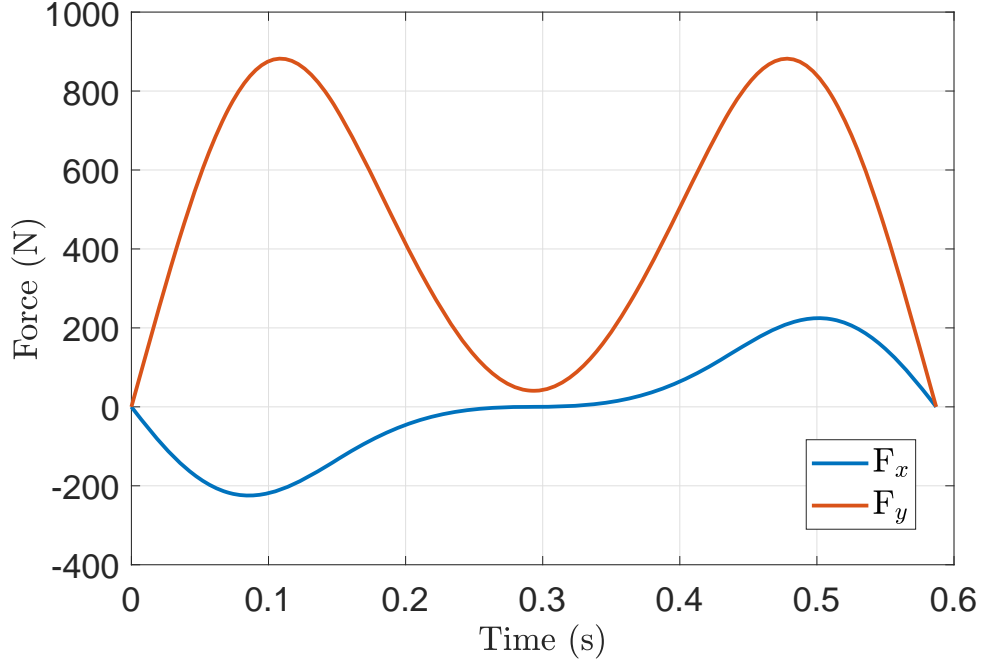


Figure 4.3: The ground reaction force of one “foot” along the sample trajectory, starting at touchdown.

to update the contact angle, where  $\theta_i$  is the take off angle. This policy reaches an equilibrium when the touchdown and liftoff positions are symmetric about the  $y$  axis.

The control is partitioned into  $u = u_s + u_r$ . The stiffness change is accomplished with  $u_s = (k - \tilde{k})(L - L_o)$ . Using the storage function of equation (3.10), the time derivative is

$$\dot{S} = (\tilde{E} - E_{\text{ref}})\dot{q}^\top J^\top u_r \quad (4.11)$$

which means we should choose

$$u_r = -\kappa J\dot{q}(\tilde{E} - E_{\text{ref}}) \quad (4.12)$$

$$= -\kappa \dot{L}(\tilde{E} - E_{\text{ref}}) \quad (4.13)$$

to ensure that  $\dot{S}$  is negative semi-definite. The closed loop dynamics of this system are then

$$0 = M\ddot{q} + J^\top \tilde{F} + G + J^\top (\kappa \dot{L}(\tilde{E} - E_{\text{ref}})) \quad (4.14)$$

In section 3.4.2 we mentioned that the energy regulation control caused the closed-loop hopper system to take the form of a harmonic Rayleigh-Van-der-Pol oscillator. By inserting these closed loop dynamics into the SLIP model, we can examine the effect of the “unmodeled” rotational dynamics around the spring contact point. The motivation is that this will be suggestive of qualitative behavior of embedding this energy regulated SLIP model into higher order biped models as in [46] without aggressive compensation of dynamics transverse to the spring action. The recycling of the 1-DOF hopper controller for the SLIP model is accomplished by using only the energy of the SLIP model along the spring axis as

$$u_r = -\kappa\dot{L}(\tilde{E}_L - E_{\text{ref}}) \quad (4.15)$$

$$\tilde{E}_L = \frac{1}{2}m\dot{L}^2 + \frac{1}{2}\tilde{k}(L - L_o)^2. \quad (4.16)$$

The closed loop dynamics are then

$$0 = M\ddot{q} + J^\top \tilde{F} + G + J^\top (\kappa\dot{L}(\tilde{E}_L - E_{\text{ref}})). \quad (4.17)$$

The potential benefit of controller (4.15) over (4.12) is that it requires less state information, but with the drawback that the limit cycle trajectory will certainly not emulate a passive system.

### 4.1.2 Simulations

This section offers simulation results that demonstrate the ability to use energy shaping regulation methods to achieve different running speeds on the SLIP model. The control in equation (4.12) is termed the regulation control while equation (4.15) is termed the oscillator control. We started with an initial known running gait from [61], with  $m = 70$  kg,  $L_o = 1$  m,  $\alpha = 55^\circ$ ,  $\tilde{k} = k = 8200\frac{N}{m}$ , and  $E = 1860J$  (marked as a red dot in Fig. 4.4-4.8). For all cases,  $\kappa = 1$ . For the oscillator, we heuristically found a reference energy value  $E = 583J$  that resulted in an average speed similar to the known gait ( $\approx 6\frac{m}{s}$ ). We created a grid of target

energies and stiffnesses around this configuration, used the flight apex of the known gait as the initial condition for every grid point, and allowed the system to converge to a new limit cycle. This means that every stable grid point is a stable transition from the initial limit cycle to a new limit cycle due to a single change in reference energy and/or virtual stiffness. The existence and stability of the limit cycle were confirmed via the numerical linearization of the Poincaré return map via the method from [12].

The results for the stable average running speed of the model under the energy shaping and regulation control and the embedded harmonic Rayleigh-Van-der-Pol oscillator are given in Fig. 4.4 and 4.6. The edge of each surface indicates the edge of the sampling grid, or a case where the model fell through the floor or went backwards. For the regulation control in Fig. 4.4, the speed level set projections indicate that stiffness does not determine the average speed which agrees with the results of [23] that show a range of walking speeds for a given spring stiffness. However, the oscillator control causes a qualitative change in this relationship so that the average speed does depend on stiffness and reference energy as seen in Fig. 4.6. The two methods give a similar range of achievable walking speeds. We emphasize again that these new gaits are all the result of stable transitions from the passive known gait. A sample trajectory for the energy regulation controller is given in Fig. 4.5, where the known gait is run for 3 steps then the parameters are switched and the trajectory and contact angle converge to a new gait.

Plots of the equilibrium contact angle as a function of stiffness and energy are given in Fig. 4.7 and 4.8 for direct comparison to the results in [23]. Both methods have a similar range of contact angles; the difference between them is largely that the embedded oscillator surface in Fig. 4.8 seems to be flatter than the surface in Fig. 4.7. This indicates that there might be some constant normal vector in this space associated with stability for the system under the embedded oscillator.

The most important take away from these simulation results is that a single change in parameters using energy shaping and regulation can achieve a stable transition between

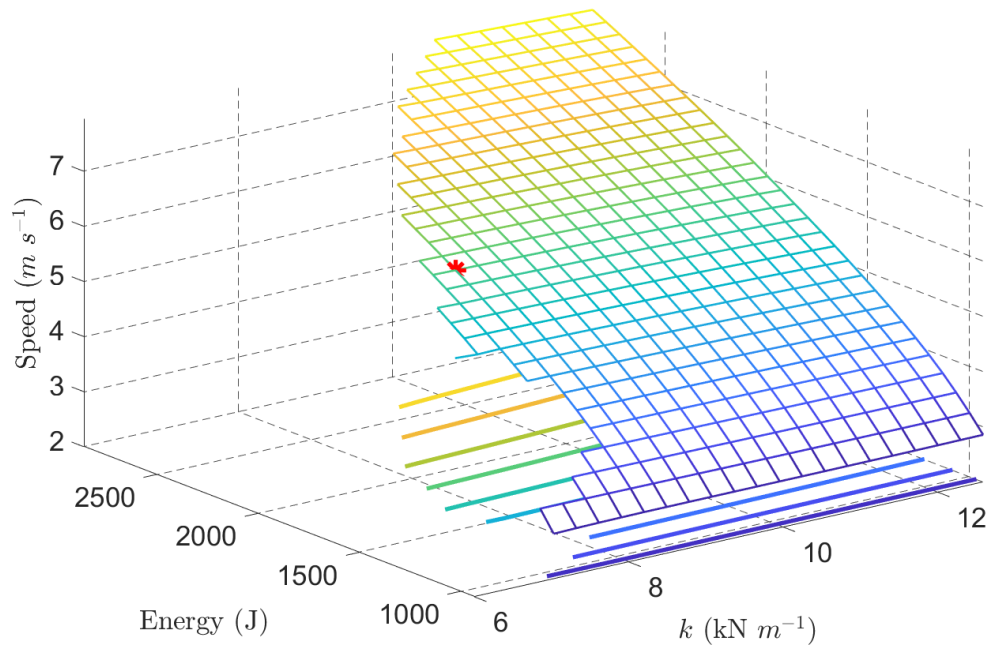


Figure 4.4: Speed-Energy-Stiffness surface for the SLIP model under the regulation control. The minimum speed achieved was  $2.82 \frac{m}{s}$ , the maximum  $7.95 \frac{m}{s}$ .

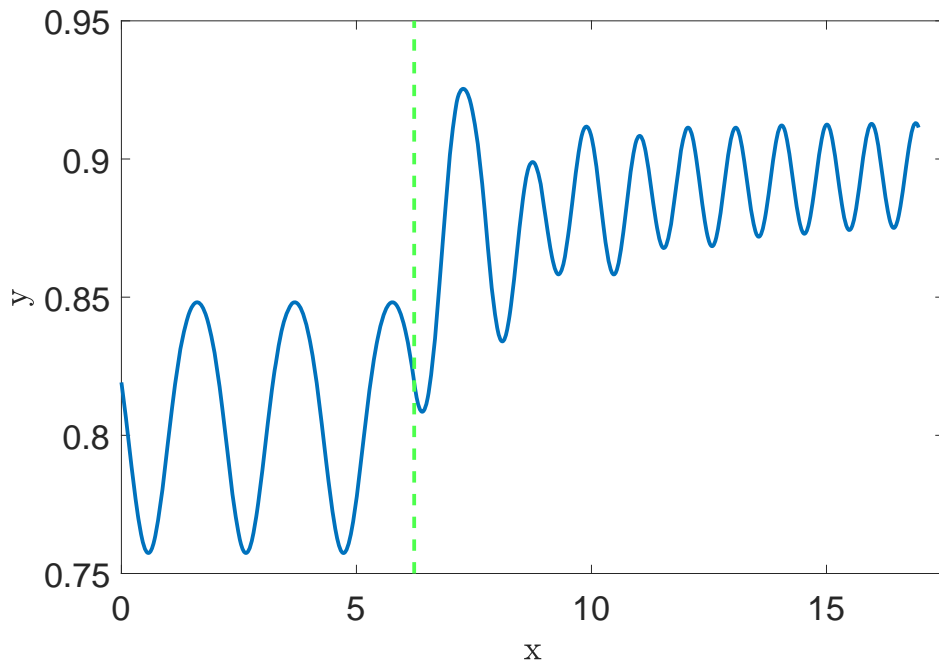


Figure 4.5: Sample trajectory of transition from  $6 \frac{m}{s}$  to  $3 \frac{m}{s}$  under the regulation control. The stiffness and reference energy were switched at the horizontal dashed line.

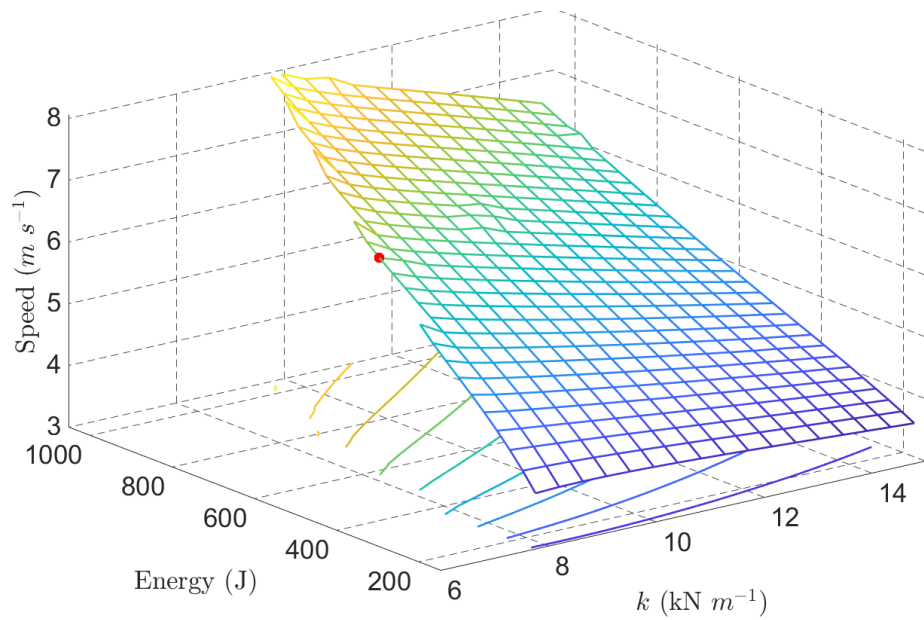


Figure 4.6: Speed-Energy-Stiffness surface for the SLIP model under the oscillator control. The minimum speed achieved was  $3.65 \frac{m}{s}$ , the maximum  $8.05 \frac{m}{s}$ .

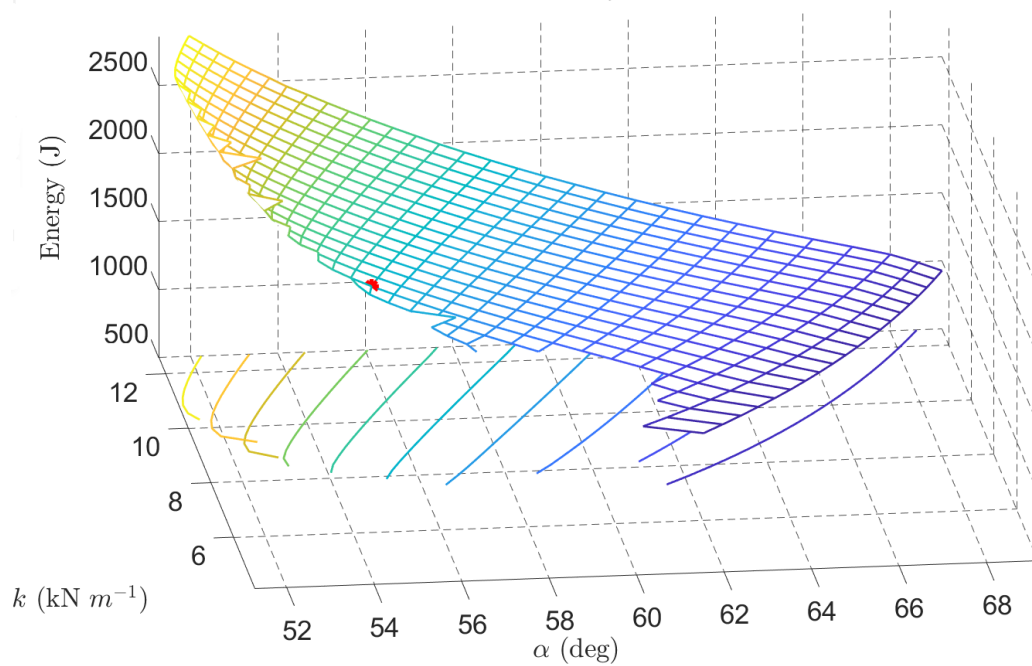


Figure 4.7: Contact Angle-Energy-Stiffness surface for the SLIP model under regulation control.

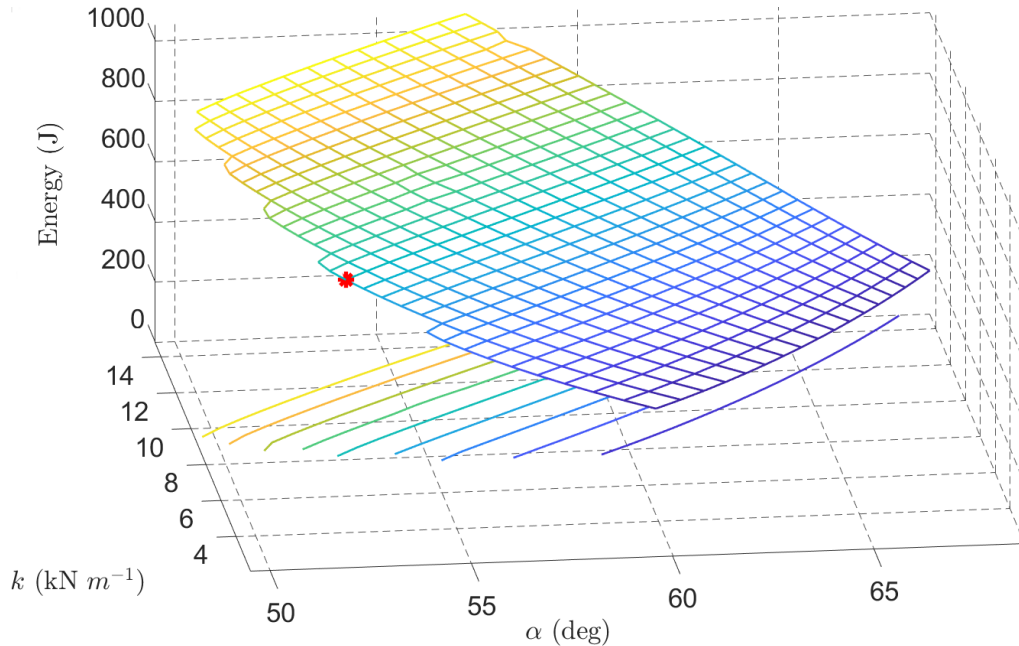


Figure 4.8: Contact Angle-Energy-Stiffness surface for the SLIP model under the oscillator control.

fast and slow running. Also, the principles of energy shaping and regulation control can be applied to a subcomponent of the system to achieve qualitatively similar behavior. We expect that this could be extremely useful in the application of these methods to wearable devices to assist locomotion, like a powered prosthesis [11] or orthosis [18], where measuring the total energy of the combined human-robot system is infeasible.

## 4.2 The Compass Gait Biped

The compass gait biped is titled as such because it has two rigged legs and looks like a compass drawing tool [62]. It is composed of two legs modeled as rigid links with point mass, and a point mass attached at the hip connection. The compass gait biped has historically served as a test bed to explore new walking controllers because it is viewed as “the simplest walking model” [63] that can account for plastic impact dynamics, underactuation, and swing leg dynamics. Historically, much of the literature on the model has considered the case where



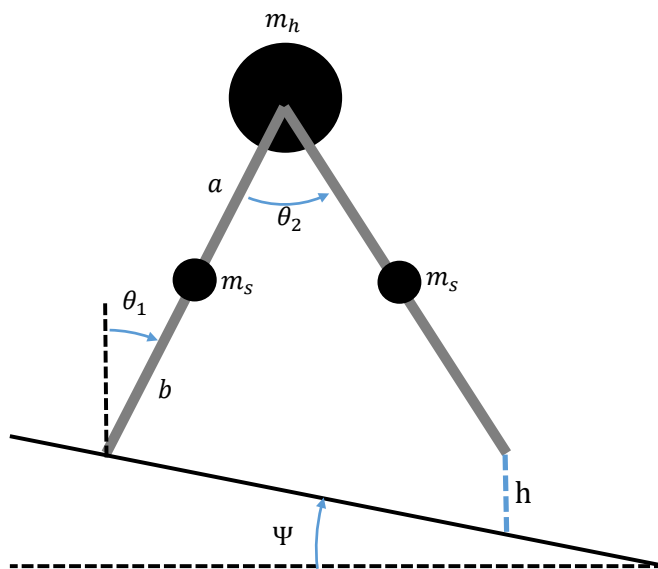


Figure 4.9: Diagram of the compass gait biped.

the biped is on a shallow slope and thus exhibits the “passive dynamic walking” phenomena [53]. More recent work has considered random terrain [64] and stair environments [65] as well. Some authors have posited similarity between human locomotion and the compass gait model in terms of passive swing leg mechanics [66], but this a very rough generalization that does not hold in general [67]. Similar to the SLIP model, there is no dissipation in the continuous dynamics and the passive walking motion cannot be physically realized without adding a swing leg that retracts. A diagram of the model is given in Figure 4.9.

The energy of the system is

$$E = \mathcal{K}(q, \dot{q}) + \mathcal{P}(q) \quad (4.18)$$

$$= \frac{1}{2} \dot{q}^\top M(q) \dot{q} + g \sum_{i=1}^3 m_i y_i \quad (4.19)$$

where the configuration vector  $q = [x; y; \theta_1; \theta_2]$ , the mass matrix is  $M$ , and the summation  $\sum_{i=1}^3 m_i y_i$  accounts for the three point masses and locates their vertical position  $y_i$  relative to the potential energy datum at  $y = 0$ . The position of the stance foot is located in the

world frame by  $(x, y)$ , and is constrained to the ground by equations  $x = 0, y = 0$ . Thus, the world frame is shifted to the contact point after every impact.

The constrained continuous dynamics where  $q_\lambda = [\theta_1; \theta_2]$  are described by (2.14), where

$$M = \begin{bmatrix} m_s (a - \cos(\theta_2) (a + b))^2 + m_s b^2 + (m_h + m_s \sin(\theta_2))^2 (a + b)^2 & m_s a (a - \cos(\theta_2) (a + b)) \\ m_s a (a - \cos(\theta_2) (a + b)) & m_s a^2 \end{bmatrix} \quad (4.20)$$

$$C = \begin{bmatrix} m_s a \dot{\theta}_2 \sin(\theta_2) (a + b) & m_s a \sin(\theta_2) (a + b) (\dot{\theta}_1 + \dot{\theta}_2) \\ -m_s a \dot{\theta}_1 \sin(\theta_2) (a + b) & 0 \end{bmatrix} \quad (4.21)$$

$$G = \begin{bmatrix} -g (\sin(\theta_1) (m_s (a + 2b) + m_h (a + b)) - m_s a \sin(\theta_1 + \theta_2)) \\ m_s a g \sin(\theta_1 + \theta_2) \end{bmatrix} \quad (4.22)$$

$$h = (a + b) (\cos(\theta_1 + \theta_2) - \cos(\theta_1)) \quad (4.23)$$

The discrete dynamics are described by equation (2.15) where

$$A = \begin{bmatrix} (a + b) (\cos(\theta_1 + \theta_2) - \cos(\theta_1)) & \cos(\theta_1 + \theta_2) (a + b) \\ (a + b) (\sin(\theta_1 + \theta_2) - \sin(\theta_1)) & \sin(\theta_1 + \theta_2) (a + b) \end{bmatrix} \quad (4.24)$$

$$R = \begin{bmatrix} 1 & 1 \\ 0 & -1 \end{bmatrix} \quad (4.25)$$

There is an additional rule for the switching surface,  $\theta_2 > 0$  which ensures that the swing leg is in front of stance leg at impact. This allows the swing leg to clip through the ground. Unlike the SLIP model, the compass gait biped has only one phase of continuous motion, single support. This is because a double support phase would completely constrain the motion of the biped (there are 4 DOF's, constraining both feet in the Cartesian  $x$  and  $y$  coordinates is 4 constraints).

Passive dynamic walking describes a stable limit cycle that emerges due to the combination of both the continuous and discrete dynamics. On this cycle, the kinetic energy lost from the impact dynamics is exactly equal to the potential energy gained by the shift of the potential energy datum to the impact foot. An example plot of the phase portrait of a passive walking limit cycle is given in Figure 4.10.

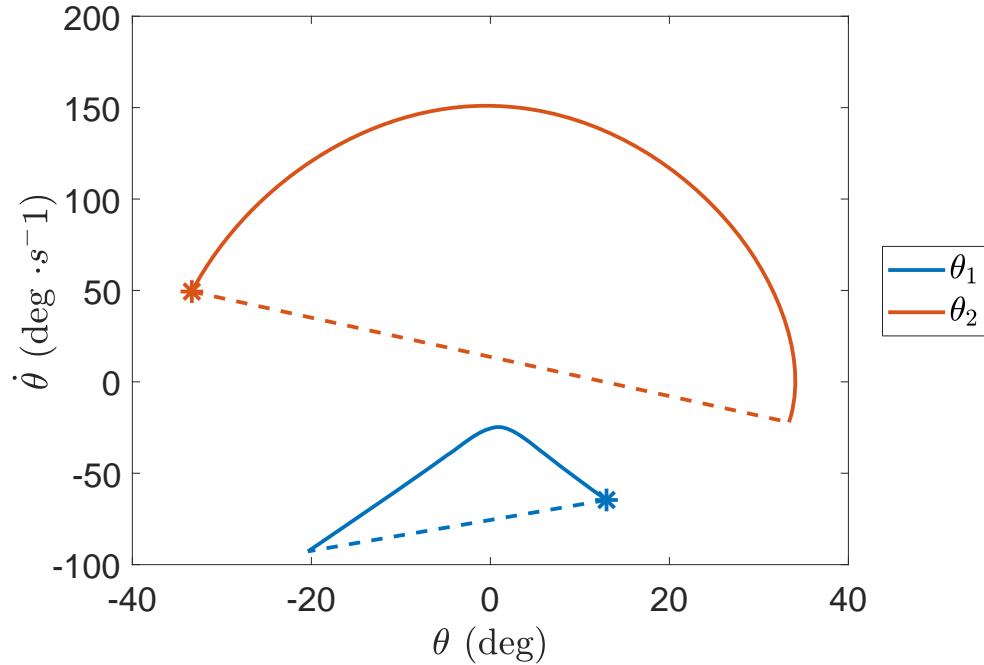


Figure 4.10: Projected phase portrait of a passive limit cycle. The trajectory starts at the starred points.  $m_h = 10\text{kg}$ ,  $m_s = 5\text{kg}$ ,  $a = 0.5\text{m}$ ,  $b = 0.5\text{m}$ .

#### 4.2.1 Control

Using the framework from Chapter 3, the energy shaping control is

$$u_s = -M\tilde{M}^{-1}(\tilde{C}\dot{q} + \tilde{G}) + C\dot{q} + G, \quad (4.26)$$

while the energy regulation control is

$$u_t = -\kappa(\tilde{E} - E_{\text{ref}})M\tilde{M}^{-1}\Omega\dot{q}. \quad (4.27)$$

The closed-loop dynamics are then

$$\widetilde{M}\ddot{q} + (\widetilde{C} + \kappa(\widetilde{E} - E_{\text{ref}})\Omega)\dot{q} + \widetilde{G} = 0. \quad (4.28)$$

The parameters available for shaping in the energy function of the system are:  $\widetilde{m}_h, \widetilde{m}_s, \widetilde{a}, \widetilde{b}$  and  $\widetilde{g}$ . The question then becomes: how should we choose these values? In [68], the effect of gravity shaping on the compass gait biped is thoroughly explored, indicating that average walking speed is proportional to  $\sqrt{\widetilde{g}}$ . In [24], it is shown that the dynamics can be normalized to depend on the mass ratio  $\mu = \frac{m_h}{m_s}$  and the length ratio  $\beta = \frac{b}{a}$ , which both influence the average speed. Because the impact dynamics depend only on  $M$ , we can exactly emulate a target  $\widetilde{g}$  but not for  $\widetilde{\beta}$  and  $\widetilde{\mu}$ . This means we can exactly reproduce the results from [68] in the closed-loop hybrid dynamics, but changing  $\widetilde{\mu}$  and  $\widetilde{\beta}$  will give different results from [24]. A well-known effect of mass parameter variation in the compass gait biped is bifurcation induced when the period-1 gait becomes unstable. However, a new result that we show in simulation is that energy regulation can be used to stabilize these gaits and increase the range of achievable passive period-1 limit cycles.

In the hopper with plastic impacts, we were able to analytically compute the  $E_{\text{ref}}$  for a given passive limit cycle using equation (3.36). In general, it is not possible to know the energy of a passive biped limit cycle without simulating it numerically. This poses a challenge to dynamically changing the virtual parameters and reference energy to achieve new passive limit cycles without making a library of pre-computed gaits. In [66], a discrete step-by-step update law for  $E_{\text{ref}}$  in an energy regulation control is proposed, as

$$E_{\text{ref}_{i+1}} = E_{\text{ref}_i} + \lambda(v_{\text{ref}} - v_i). \quad (4.29)$$

This law achieves a desired average walking speed  $v_{\text{ref}}$ , where  $\lambda$  is a scaling gain and  $v_i$  is the average walking speed for the  $i_{th}$  step. However this law simply shifts the problem to picking the  $v_{\text{ref}}$  associated with a natural limit cycle before hand, instead of  $E_{\text{ref}}$ . Instead,

we can reuse the update law in equation (3.44) from the 1-DOF hopper and apply it to the compass gait biped. A comparison between these strategies on a simulated biped is given in the following section. We use  $u^{\text{nat}}$  to denote the control under equation (3.44) and  $u^{\text{vel}}$  for equation (4.29).

### 4.2.2 Simulations

We now present simulation results for the compass gait biped under the energy shaping and regulation controls. The baseline parameters we use are  $m_h = 10\text{kg}$ ,  $m_s = 5\text{kg}$ ,  $a = 0.5\text{m}$ ,  $b = 0.5\text{m}$ ,  $\Psi = 3.7^\circ$  with a known initial condition for a stable limit cycle from [24]. We compare changes in the true ratios  $\beta$  against changes in the virtual ratios  $\tilde{\beta}$  during the continuous dynamics. We omit results for  $\mu$  and  $\tilde{\mu}$  for brevity. The energy regulation controls  $u_t^{\text{vel}}$  and  $u_t^{\text{nat}}$  are applied to the system with the virtual ratios, using the control parameters  $\lambda = 0.5$ ,  $\kappa = 100$ , and  $\Omega = \text{diag}([1, 0])$ . Each reference velocity  $v_{\text{ref}}$  for a given ratio is taken from the corresponding physical ratio limit cycle. The ratios that we sample are on a uniform grid from 0.5 to 1, and we do not display data points in the grid range that either bifurcated or were unstable within our search tolerance. We confirm the stability of the limit cycles using the linearized Poincaré return map.

The results are shown in Figs. 4.11, 4.12, and 4.13. We can see that shaping the continuous dynamics alone through  $\tilde{\beta}$  does not reproduce the same limit cycle as physically changing the parameters. In Fig. 4.11, the virtual length ratio  $\tilde{\beta}$  has the same general trend between ratio and speed as  $\beta$ , but it causes a larger increase in walking speed. The introduction of  $u_t^{\text{nat}}$  enables  $E_{\text{ref}}$  to converge to  $\tilde{E}_{\text{nat}}$ , as evidenced where the circle and cross data points overlap in the figures. It also increases the range of achievable speeds, as seen by the circle data points that do not overlap the cross points. The velocity update law  $u_t^{\text{vel}}$  causes the shaped system to converge to the targeted walking speed of the associated physical system, as seen by the overlap of the squares and stars. Fig. 4.12 shows the energies that

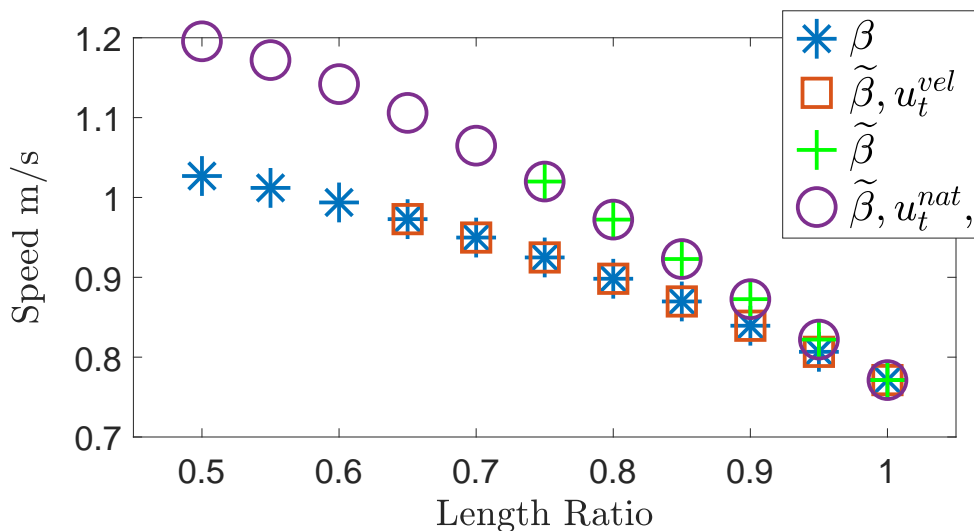


Figure 4.11: Length ratio versus average speed for physical and virtual dynamics.  $\beta$  is the physical length ratio,  $\tilde{\beta}$  is the virtual length ratio,  $u_t^{vel}$  converges to a desired walking speed,  $u_t^{nat}$  converges to the energy equilibrium induced by the discrete dynamics. Data points that bifurcated or were unstable are not displayed.

the update laws converge to, indicating the real parameters shift energy down more than the virtual ones. In Fig. 4.13, we can see that  $u_t^{vel}$  causes limit cycles that are less efficient compared to those from  $u_t^{nat}$ , in the sense that they require more torque output from the control to achieve the same walking speed. These inefficient cycles are due to the fact that they are unnatural and must compensate for the energy mismatch between  $\tilde{E}_{ref}$  and  $\tilde{E}_{nat}$ .

Finally, we offer a simulation example of using energy regulation to stabilize an unstable limit cycle. In this case, the terrain is changed from a slope to stairs of a similar geometry. Thus, the impact map  $\Delta(q, \dot{q})$  remains the same but the switching surface  $\mathbf{S}$  and distance function  $h$  are changed. The stair impact map still admits the energy equilibrium from the slope dynamics, however as seen in Fig. 4.14 this is not associated with a stable period-1 limit cycle for the passive system. In Fig. 4.15, we present a stair walking simulation where we switch on the energy regulation control after 4 steps and run it for 10 more steps. This causes the biped to converge to the period 1 slope limit cycle while walking on the stairs terrain, indicating that we have stabilized this previously unstable gait.

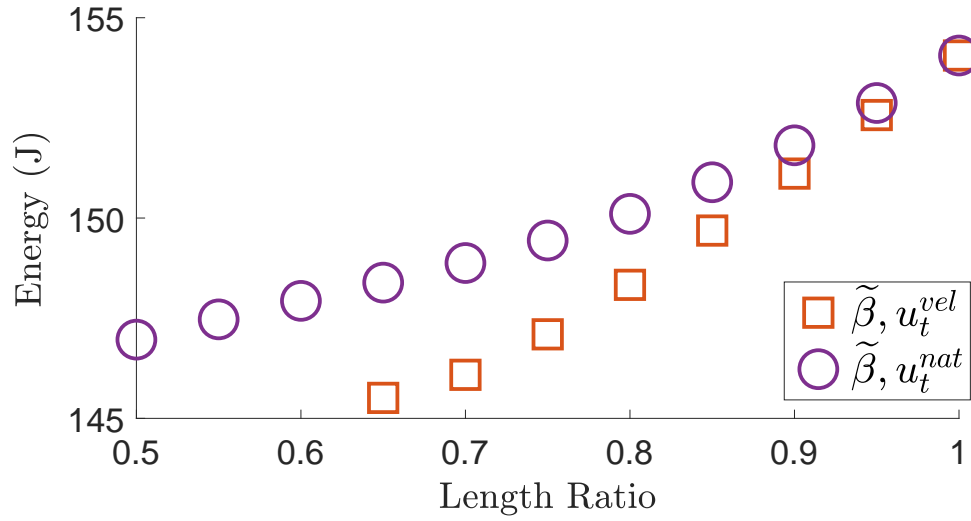


Figure 4.12: Energy versus length ratio for the adaptive energy regulation controllers. Data points that bifurcated or were unstable are not displayed.

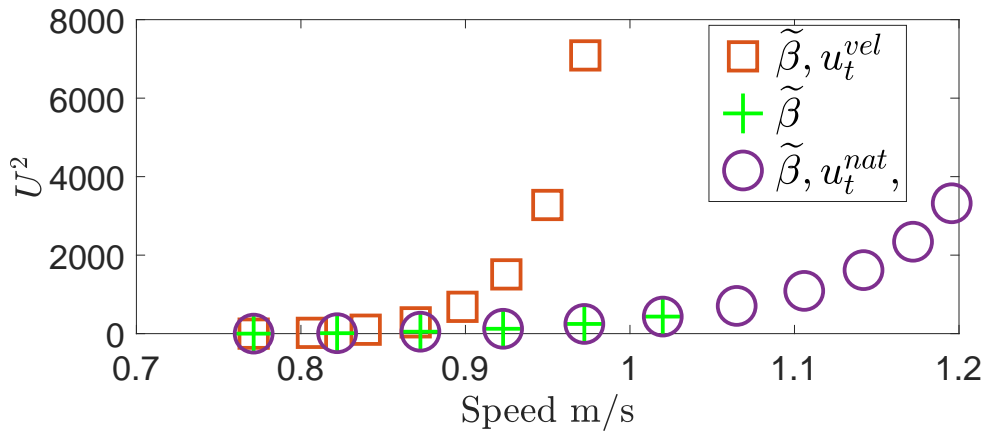


Figure 4.13: Time integral of torque squared versus average speed for physical and virtual dynamics length ratio changes. Data points that bifurcated or were unstable are not displayed.

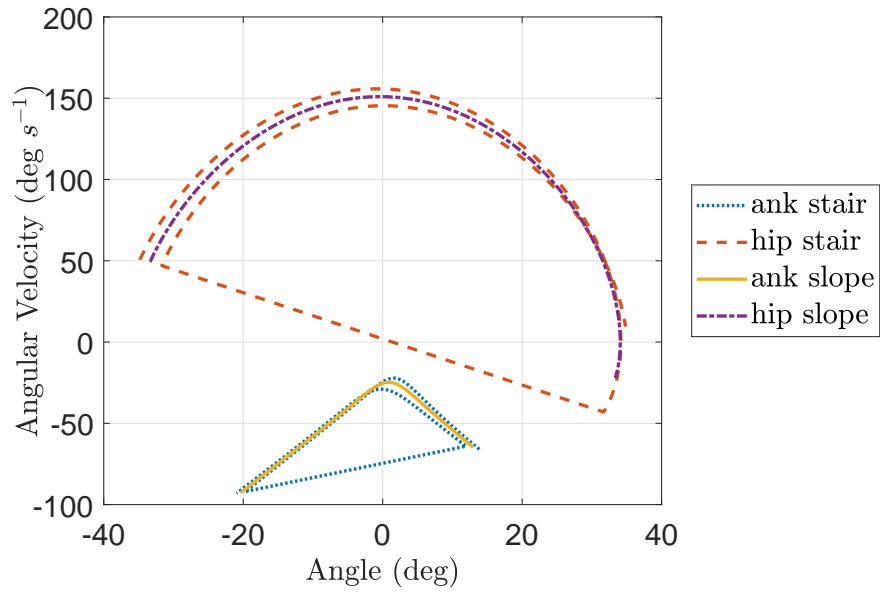


Figure 4.14: The slope period-1 passive limit cycle versus the stairs period-2 passive limit cycle.

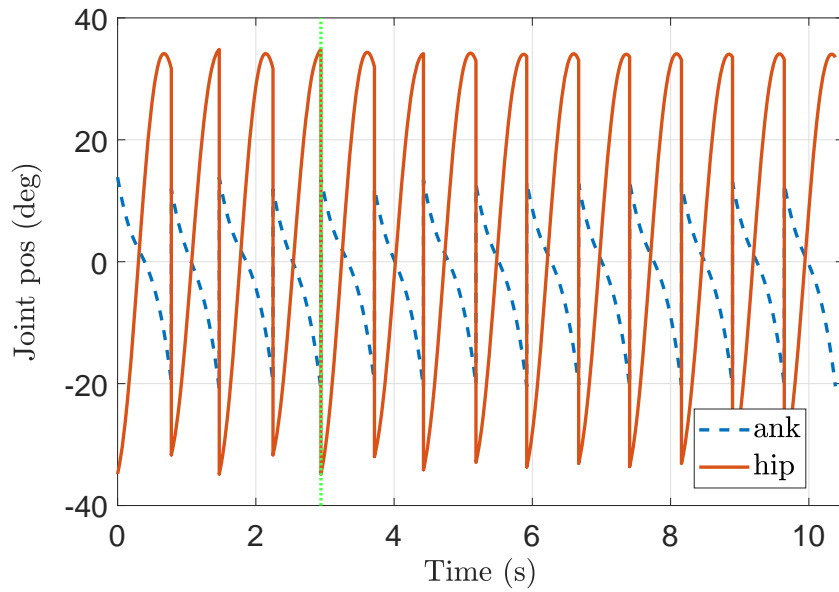


Figure 4.15: Transition from passive period-2 limit cycle to an energy regulated period-1 limit cycle. The energy regulation control is turned on after 4 steps, at the green vertical line.



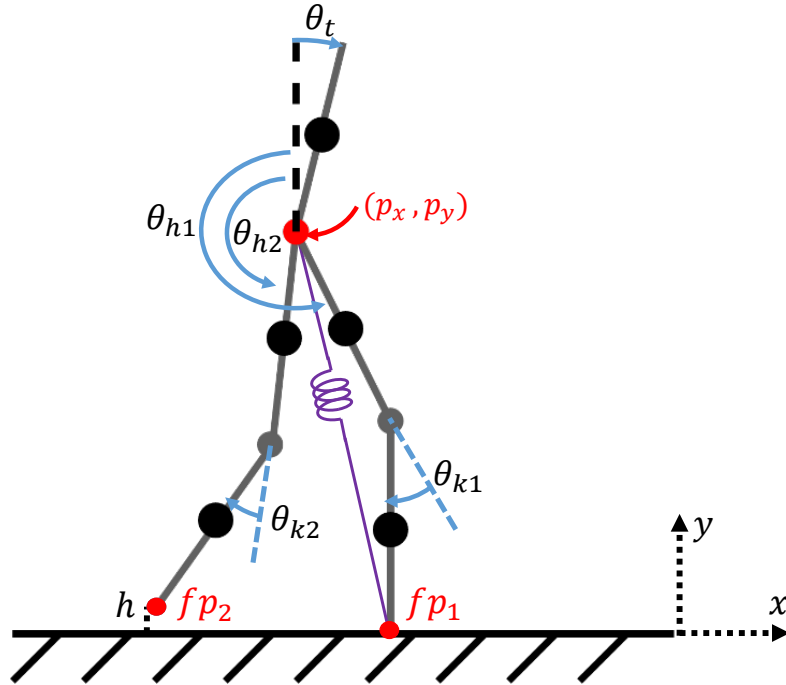


Figure 4.16: Diagram of the Rabbit biped, a 5 Link robot with a torso and knees. The virtual spring between the hip and the ground is shown in purple.

### 4.3 The RABBIT Model

The RABBIT walking model is a 5 link biped with knees, a hip, and a torso. It is based of hardware developed in the early 2000s in France that served a one of the first truly dynamic walking bipeds that did not rely on quasi-static/ Zero-Moment-Point control techniques [69], and is the primary biped model used in the definitive book on control of dynamic biped locomotion [12]. Details of the modeling and equations of motion can be found in [12], the general methods used are the same as specified in Chapter 2. The RABBIT model is an improvement on the compass gait model in the sense that 1) the swing leg does not need to pass through the ground 2) it is capable of a meaningful double support phase. A visualization of the model is given in Figure 4.16.

The configuration vector of the biped is  $q = [p_x, p_y, \theta_{h1}, \theta_{k1}, \theta_{h2}, \theta_{k2}, \theta_t]^T \in \mathbb{R}^{7 \times 1}$ , where  $p_x$  and  $p_y$  are the Cartesian position of the hip joint in the inertial reference frame. The legs are

labeled 1 (stance) and 2 (swing) until the legs are swapped at the end of double support. The mass  $m_j$ , length  $l_j$  and inertia  $I_j$  of the links are indexed by the subscript  $j \in \{\text{tor, th, sh}\}$  which denotes the torso, thigh, and shank respectively. The model switches between single support and double support phases as the trailing leg lifts from the ground and the swing leg impacts the ground, respectively. The point feet are constrained to a static point on ground at the point of impact, leading to the constraint equation  $\sigma_{SS} = [\text{fp}_{x1}, \text{fp}_{y1}]^\top$  during single support and  $\sigma_{DS} = [\text{fp}_{x1}, \text{fp}_{y1}, \text{fp}_{x2}, \text{fp}_{y2}]^\top$  during double support. These functions induce the constraint matrices  $A_{SS}$  and  $A_{DS}$  respectively. The equations of motion have the form of the hybrid biped dynamics from Section 2.3 where

$$\text{Double Support (DS)} \quad M\ddot{q} + C\dot{q} + G + A_{DS}^\top \lambda = Bu \quad (4.30)$$

$$\text{Single Support (SS)} \quad M\ddot{q} + C\dot{q} + G + A_{SS}^\top \lambda = Bu \quad (4.31)$$

if **phase == DS** and  $\lambda_{y2} \leq 0$

$$\begin{bmatrix} \dot{q}^+ \\ F_I \end{bmatrix} = \begin{bmatrix} R & 0 \\ 0 & I_{p \times p} \end{bmatrix} \begin{bmatrix} M(q^-) & -A_{SS}^\top(q^-) \\ A_{SS}(q^-) & 0_{2 \times 2} \end{bmatrix}^{-1} \begin{bmatrix} M(q^-) \\ 0_{2 \times 2} \end{bmatrix} \dot{q}^-$$

$$q^+ = R q^-.$$

**phase := SS**

if **phase == SS** and  $\text{fp}_{y2} \leq 0$

$$\begin{bmatrix} \dot{q}^+ \\ F_I \end{bmatrix} = \begin{bmatrix} R & 0 \\ 0 & I_{p \times p} \end{bmatrix} \begin{bmatrix} M(q^-) & -A_{DS}^\top(q^-) \\ A_{DS}(q^-) & 0_{2 \times 2} \end{bmatrix}^{-1} \begin{bmatrix} M(q^-) \\ 0_{2 \times 2} \end{bmatrix} \dot{q}^-$$

$$q^+ = R q^-.$$

**phase := DS**

### 4.3.1 Control

The goal of this section is to embed the dynamics of the lower dimensional energy regulated SLIP model into the higher dimensional RABBIT model via energy shaping and regulation control. Similar previous work exists in [46], however this dissertation improves upon it by demonstrating a stable period 1 limit cycle using the method of Poincaré. In addition, I match the dynamics of the hip joint in Cartesian space to the SLIP model, rather than the COM. This brings the problem much closer to the human-prosthesis application since its COM cannot be reliably estimated without motion capture. Finally, in this section the swing leg trajectory is generated by embedding the dynamics of a pendulum instead of by virtual constraints as in [46]. The torso angle is regulated to a set-point using a PD Feedback Linearization controller [45].

As in the previous section, I partition the control into  $u = u_s + u_r$  that perform energy shaping and regulation. Since I want to match the SLIP dynamics to the hip joint of the RABBIT model in the Cartesian plane, I need to express the hip joint coordinates. Let  $z = [\text{hp}_x, \text{hp}_y]^\top$  be a vector of the hip x-y position. The equations of motion in these coordinates are then

$$\dot{z} = J_h \dot{q} \quad (4.32)$$

$$\ddot{z} = J_h \ddot{q} + \dot{J}_h \dot{q}, \quad (4.33)$$

where  $J_h$  is the hip Jacobian. The desired dynamics for  $\ddot{z}$  are the energy regulated SLIP equations of (4.14). The SLIP single support should be matched to the RABBIT single support, and the same for double support. This means the desired closed loop behavior should be

$$\ddot{z}_S = M_S^{-1} \left( -J_S^\top F_S - G_S - J_S^\top (\kappa \dot{L}(\tilde{E}_S - E_{\text{ref}})) \right) \quad (4.34)$$

$$\tilde{E}_S = \frac{1}{2} \dot{z}^\top M_S \dot{z} + m_h(g)(\text{hp}_y) + \frac{1}{2} k(L_S - L_o)^2 \quad (4.35)$$

where  $F_S$  and  $J_S$  are the target virtual spring force and its mapping Jacobian, while  $M_S$  and  $G_S$  are constant target mass and gravity matrices from the SLIP model. In the coordinates for RABBIT during single support,  $F_S = -k(L_S - L_o)$ ,  $L_S = \|\vec{hp} - \vec{pf}\|$ , and  $J_S = J_f - J_h$  where  $J_f$  is the foot Jacobian. These expressions are copied and stacked so that the SLIP-to-RABBIT embedding is consistent during double support. While in physical implementation it is advisable to obtain the equivalent constrained dynamics from equation (2.9) for the system and/or use force sensors to estimate  $\lambda$ , in simulation the values for  $\lambda$  are determined by satisfying

$$A_{\text{phase}}\ddot{q} + \dot{A}_{\text{phase}}\dot{q} = 0. \quad (4.36)$$

as shown in equation (2.8). Mathematical manipulation the following equations,

$$\begin{aligned} A_{\text{phase}}\ddot{q} + \dot{A}_{\text{phase}}\dot{q} &= 0 \\ J_h\ddot{q} + \dot{J}_h\dot{q} &= \ddot{z}_S \\ M\ddot{q} + C\dot{q} + G &= \begin{bmatrix} B & -A_{\text{phase}}^\top \end{bmatrix} \begin{bmatrix} u_s \\ \lambda \end{bmatrix}, \end{aligned}$$

to eliminate  $\ddot{q}$  can yield the initial version of the energy shaping and regulation problem as solving

$$Q \begin{bmatrix} u_s \\ \lambda \end{bmatrix} = \begin{bmatrix} A_{\text{phase}} \\ J_h \end{bmatrix} M^{-1}(-C\dot{q} - G) + \begin{bmatrix} -\dot{A}_{\text{phase}}\dot{q} \\ \ddot{z}_S - \dot{J}_h\dot{q} \end{bmatrix} \quad (4.37)$$

$$Q = \begin{bmatrix} A_{\text{phase}} \\ J_h \end{bmatrix} M^{-1} \begin{bmatrix} B & -A_{\text{phase}}^\top \end{bmatrix} \quad (4.38)$$

for  $u_s$  and  $\lambda$ .

However matching the full hybrid dynamics of the SLIP to RABBIT requires more than just solving equation (4.37) for  $u_s$ , the switching surfaces and impact dynamics need to match as well. For single support, this means that 1) the position and velocity of the hip joint should

be invariant over the impact dynamics, 2) the virtual spring is relaxed at touchdown, and 3) the angle between the ground and  $\vec{hp} - \vec{pf}$  is equal to  $\alpha$ . For double support, this means that the trailing leg should lift from the ground when  $L_2 = L_o$ . Equation (4.37) can be modified to control the normal contact force between the trailing leg and the ground by partitioning the constraint matrix into  $A_o$  and  $A_d$  (0 for open and  $d$  for desired), where  $A_o$  is derived from  $\sigma_o = [fp_{x1}, fp_{y1}, fp_{x2}]^\top$  and  $A_d$  from  $\sigma_d = fp_{y2}$ . I then specify the normal contact force as  $\lambda_{y2} = \lambda_d = F_{sy2}$ , the trailing leg  $y$  force from the slip model, and obtain a control that performs force control and energy shaping as

$$Q \begin{bmatrix} u_s \\ \lambda_o \end{bmatrix} = \begin{bmatrix} A_{\text{phase}} \\ J_h \end{bmatrix} M^{-1}(-C\dot{q} - G + A_d^\top \lambda_d) + \begin{bmatrix} -\dot{A}_{\text{phase}}\dot{q} \\ \ddot{z}_S - \dot{J}_h\dot{q} \end{bmatrix} \quad (4.39)$$

$$Q = \begin{bmatrix} A_{\text{phase}} \\ J_h \end{bmatrix} M^{-1} \begin{bmatrix} B & -A_o^\top \end{bmatrix}. \quad (4.40)$$

This ensures that  $\lambda_{y2} \rightarrow 0$  as  $L_2 \rightarrow L_o$  so that the timing of trailing leg of RABBIT lifting matches the SLIP model.

There are no swing leg dynamics in the SLIP model; the assumption is that contact angle can be arbitrarily controlled. This poses an issue for embedding the SLIP dynamics because it means I have to generate the motion of the swing leg to coordinate the motion of the swing foot with the hip so that the contact angle is emulated and the energy of the virtual model is conserved. In order to stay in the energy shaping framework, I match the dynamics of the swing foot to that of a pendulum. The parameters of the target pendulum system are chosen via an optimization procedure that ensures the swing foot impacts the ground with contact angle  $\alpha$  and zero velocity when  $hp_y = L_o \sin(\alpha)$ . Thus, the energy shaping control during single support is also a modification of equation (4.37), with coordinates and desired

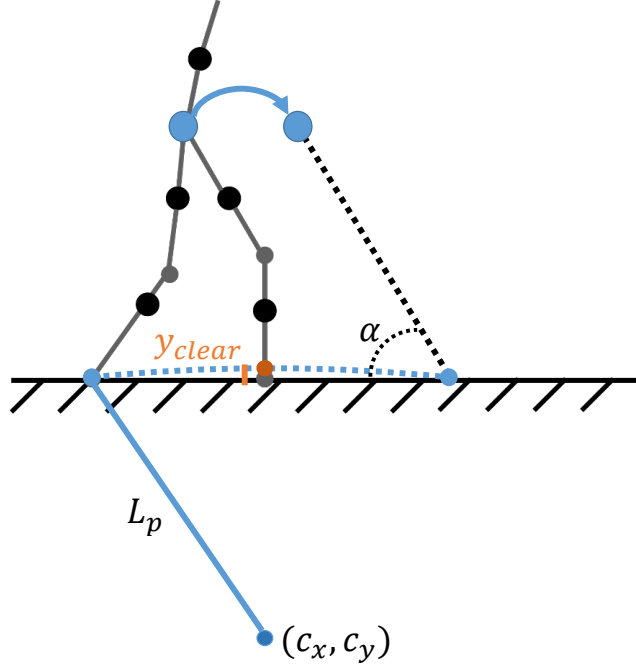


Figure 4.17: Diagram of the embedded virtual pendulum and swing foot trajectory.

dynamics

$$z = [hp_x, hp_y, fp_{x2}, fp_{y2}]^T \quad (4.41)$$

$$\ddot{z} = \begin{bmatrix} \ddot{z}_S \\ M_P^{-1}(-C_P \dot{z}_{fp} - G_P) \end{bmatrix} \quad (4.42)$$

where  $M_P$ ,  $C_P$ , and  $G_P$  are the matrices of the pendulum system with free parameters  $c_x, c_y, L_p$ , and  $g_p$  as the pendulum center location, length, and gravitational acceleration constant. The values for  $c_x, c_y$ , and  $L_p$  are chosen by constraining the geometry of the problem as in Figure 4.17 so that the point of maximum height  $y_{clear}$  is collinear with the stance foot along the horizontal axis. The center point  $(c_x, c_y)$  and contact angle  $\alpha$  are updated at every the beginning of every transition to single support. The contact angle is determined by policy in equation (4.10). The expected hip position at foot strike is assumed to be symmetrical about the stance foot, which is then used calculate the desired

foot position. The center point  $(c_x, c_y)$  is derived from the circle of radius  $L_p$  that passes through the starting, ending, and  $y_{clear}$  foot positions. The virtual gravity  $g_p$  chosen via off-line optimization and kept constant during operation.

### 4.3.2 Simulation

The control was verified in a simulation using MATLAB. I attempted to generate the example trajectory from Figure 4.2 in the section on the SLIP model. Using the initial conditions from there, the limit cycle for the closed-loop RABBIT biped under the energy shaping and regulation was found via numerical search. The parameters of the model that were used are given in Table 4.1. The trajectory from the SLIP was not stable, but the simulation converged to a new limit near the target cycle as seen in Figure 4.18. This new trajectory has a much smaller oscillation amplitude (and energy) in the  $y$  direction, thus some of this energy is transferred into the  $x$  direction and the average walking speed increases slightly. There is also a sort of phase shift in the trajectory; in the pure SLIP model the mass achieves its nadir in double support and its apex is single support, however in the new trajectory on the RABBIT this is flipped. The energy of the new limit cycle is also *not* conserved at impact, which is shown in Figure 4.19. The energy regulation controller dissipates some energy that is injected to the hip via momentum transfer at impact. In the context of the overall approach of energy shaping plus regulation control, this example highlights the point that the discrete dynamics can not be shaped. Thus, the attempt to match hybrid systems with different impact maps and switching surfaces is not exact. However, energy regulation can add some robustness against this issue, in the sense that a stable limit cycle in the neighborhood of the target can still emerge.

Table 4.1: Rabbit Model Simulation Parameters

Parameter	Variable	Value
Torso mass	$m_{\text{tor}}$	40 [kg]
Thigh mass	$m_{\text{th}}$	10 [kg]
Shank mass	$m_{\text{sh}}$	5 [kg]
Torso moment of inertia	$I_{\text{tor}}$	0 [kg·m <sup>2</sup> ]
Thigh moment of inertia	$I_{\text{th}}$	0 [kg·m <sup>2</sup> ]
Shank moment of inertia	$I_{\text{sh}}$	0 [kg·m <sup>2</sup> ]
Thigh length	$l_{\text{tor}}$	0.5 [m]
Shank length	$l_{\text{th}}$	0.5 [m]
Heel length	$l_{\text{sh}}$	0.5 [m]
Spring stiffness	$k$	12250 [N·m <sup>-1</sup> ]
Spring relaxed length	$L_0$	0.94 [m]
SLIP mass	$m_s$	70 [kg]
Torso set point	$\bar{\theta}_{\text{tor}}$	-5 [deg]
Energy regulation gain	$\kappa$	10
Swing clearance	$y_{\text{clear}}$	0.1 [m]
Pendulum gravity	$g_p$	192 [m·s <sup>-2</sup> ]

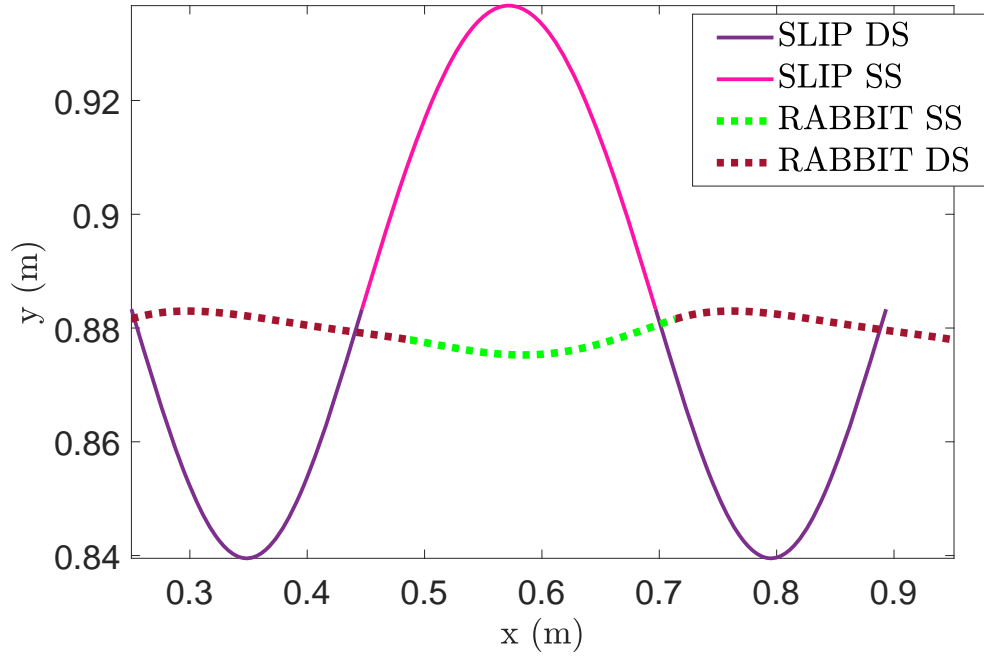


Figure 4.18: Simulation of the RABBIT biped with embedding of the energy regulated SLIP model versus the true SLIP model.



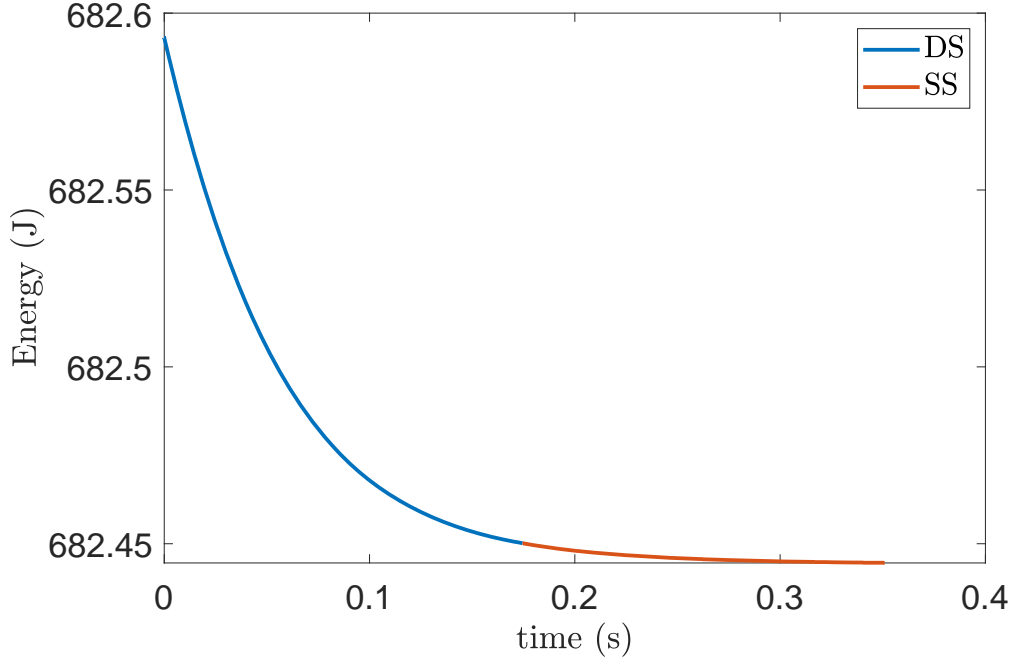


Figure 4.19: Energy over the Rabbit-SLIP embedded limit cycle.

#### 4.4 The Flat Foot Biped

The equations of motion for the 6 link flat foot biped model have the form given in 2.14 and 2.15. A diagram of the model with the coordinates is given in Figure 4.20. The generalized coordinates are defined as  $q = [p_x, p_y, \phi, \theta_s, \theta_t, \theta_h, \theta_{sk}, \theta_{sa}]^\top \in \mathbb{R}^{8 \times 1}$ , where  $p_x$  and  $p_y$  represent the Cartesian position of the stance heel in the inertial reference frame, and  $\phi$  is the angle of the heel-to-ankle vector with respect to the vertical axis. The subscript  $i \in \{a, k, h, sk, sa\}$  denotes the ankle, knee, hip, stance knee, and stance ankle, respectively, and is used to describe the angles  $\theta_i$  between each link. The mass  $m_j$ , length  $l_j$  and inertia  $I_j$  of the links are indexed by the subscript  $j \in \{f, s, t, h, st, ss, sf\}$  which denotes the stance foot, stance shank, stance thigh, hip, swing thigh, swing shank, and swing foot, respectively.

Besides the increased dimension of the state space, the primary difference between this model and the compass gait biped is flat versus point feet. Flat feet induce contract constraints than change as the biped progresses through a gait cycle. For the stance leg in a

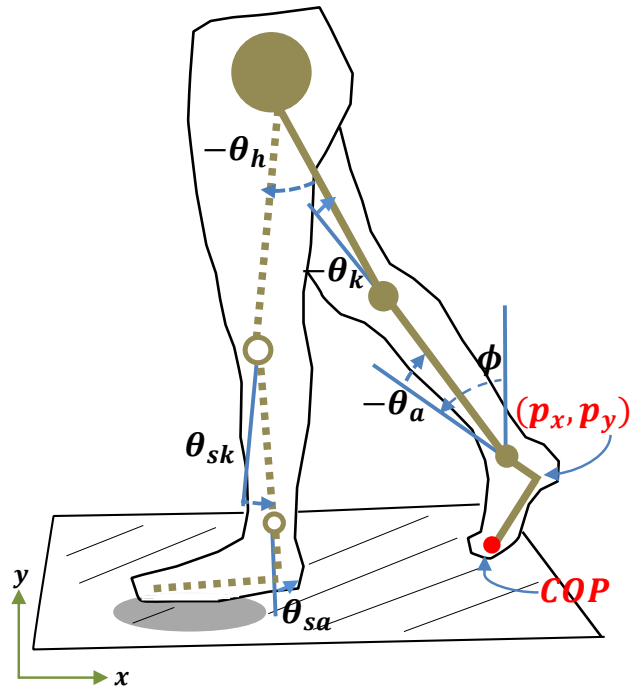


Figure 4.20: Diagram of an 8-DOF flat foot humanoid biped with overlaid coordinate system.

human-like gait, the heel strikes the ground, then the biped rolls over the heel until the foot slaps the ground, until finally the center of pressure reaches the toe and the heel pickups while rolling over the toe. During this process, the swing leg is moving until it hits the ground in front of the stance leg. The biped can enter a brief period of double support until the trailing toe lifts from the ground. Thus, there are 4 phases of continuous dynamical phases and constraint matrices: heel, flat, toe, and double support (DS). Backwards transitions are not allowed and are considered system failures.

Using the methods in Chapter 2, the hybrid dynamic regimes over one step are computed in the following sequence:

heel regime :

1.  $M\ddot{q} + T(q, \dot{q}) + A_{\text{heel}}^\top \lambda = \tau$  if  $a_{\text{flat}} \neq 0$ ,
2.  $\dot{q}^+ = (I - X(A_{\text{flat}}X)^{-1}A_{\text{flat}})\dot{q}^-$  if  $a_{\text{flat}} = 0$ ,

flat regime :

3.  $M\ddot{q} + T(q, \dot{q}) + A_{\text{flat}}^\top \lambda = \tau$  if  $|c_p(q, \dot{q})| < l_f$ ,
4.  $\dot{q}^+ = \dot{q}^-, (q(1)^+, q(2)^+)^\top = \mathcal{G}$  if  $|c_p(q, \dot{q})| = l_f$ ,

toe regime :

5.  $M\ddot{q} + T(q, \dot{q}) + A_{\text{toe}}^\top \lambda = \tau$  if  $h(q) \geq 0$ ,
6.  $(q^+, \dot{q}^+) = R(q^-, \dot{q}^-)$  if  $h(q) = 0$

The vector  $T$  groups the Coriolis/centrifugal terms and potential forces for brevity. The superscripts “ $-$ ” and “ $+$ ” indicate the pre-impact and the post-impact values, respectively. The terms  $X = M^{-1}A_{\text{flat}}^\top$  and  $\mathcal{G} = (l_f \cos(\gamma), l_f \sin(\gamma))^\top$  model the change in inertial reference frame,  $c_p$  is the location of the center of pressure,  $\gamma$  is the ground slope angle, and  $l_f$  is the foot length. The ground clearance of the swing heel is denoted by  $h(q)$ , and  $R$  denotes the swing heel ground-strike impact map derived based on [40].

Part of the model from [38] is a set-point Proportional-Derivative (PD) controller that generates a stable limit cycle while walking down a shallow slope. It has the form

$$v = -K_p(q_m - \bar{\theta}) - K_d \dot{q}_m. \quad (4.43)$$

Here,  $q_m$  is the actuated coordinates vector,  $\bar{\theta}$  is the equilibrium vector, and the diagonal control gain matrices are denoted as  $K_p, K_d \in \mathbb{R}^{5 \times 5}$ . The mapping matrix  $B_v$  is constructed such that the PD controller actuates the ankles, knees, and hip of the biped. This PD

controller  $v$  is termed the “inner loop” and the to-be-derived PBC  $u$  the “outer loop”, since the PBC relies on the existence a limit cycle.

In Section 3.2.1 I went over the details of regulating a time-varying energy function that accounts for non-conservative work done on a system. That method is relevant in this context of a PD controller generating a walking gait on the 6 Link Flat Foot biped. The work done by  $v$  is

$$W_v = \int_0^t \dot{q}^\top B_v v d\tau \quad (4.44)$$

and the generalized system energy is  $E = K + P - W$ . The energy regulation controller that results from the procedure in Section 3.2.1 is then

$$u_r = -\kappa(\tilde{E} - E_{\text{ref}})\Omega\tilde{B}_u^\top\dot{q}. \quad (4.45)$$

#### 4.4.1 Centralized Simulations

This section offers simulations to exemplify how the centralized PBC affects the qualitative behavior of the biped system and demonstrate the analysis methods we used to quantify performance. A nominal limit cycle was found in [38] for a walking gait down on a slope of  $\alpha = 0.095$  radians. This limit cycle is used to determine the reference energies for the PBC. The exact parameters used in the biped model and in the PD control are specified in Tab. 4.2, which are adopted from [38] and are human inspired. The PBC is applied as an outer loop of the PD control (inner loop). Since  $p_x, p_y$  are always constrained to the ground, the biped is fully-actuated during the flat foot phase and underactuated with degree one during heel and toe contact due to  $\phi$ . The entries in the diagonal vector for  $\Omega$  that correspond to  $p_x, p_y$  are, and  $\phi$  are always zero since they are unactuated. The PBC is always saturated at 50 Nm, as a reasonable limit of the physical capability of the actuators on an exoskeleton [18].

The PD controlled biped has three contact configurations which cause the nominal limit cycle to transition between three different constant system energies,  $E_{\text{heel}} \rightarrow E_{\text{flat}} \rightarrow E_{\text{toe}}$ .

Table 4.2: Flat Foot Model Simulation Parameters

Parameter	Variable	Value
Hip mass	$m_h$	31.73 [kg]
Thigh mass	$m_t$	9.457 [kg]
Shank mass	$m_s$	4.053 [kg]
Foot mass	$m_f$	1 [kg]
Thigh moment of inertia	$I_t$	0.1995 [kg·m <sup>2</sup> ]
Shank moment of inertia	$I_s$	0.0369 [kg·m <sup>2</sup> ]
Full biped thigh length	$l_t$	0.428 [m]
Full biped shank length	$l_s$	0.428 [m]
Full biped heel length	$l_a$	0.07 [m]
Full biped foot length	$l_f$	0.2 [m]
Hip equilibrium angle	$\theta_h$	-0.5 [rad]
Hip proportional gain	$K_{ph}$	182.250 [N·m/rad]
Hip derivative gain	$K_{dh}$	35.100 [N·m·s/rad]
Swing knee equilibrium angle	$\bar{\theta}_{sk}$	0.2 [rad]
Swing knee proportional gain	$K_{psk}$	182.250 [N·m/rad]
Swing knee derivative gain	$K_{dsk}$	18.900 [N·m·s/rad]
Swing ankle equilibrium angle	$\bar{\theta}_{sa}$	-0.25 [rad]
Swing ankle proportional gain	$K_{psa}$	182.250 [N·m/rad]
Swing ankle derivative gain	$K_{dsa}$	0.810 [N·m·s/rad]
Stance ankle equilibrium angle	$\theta_a$	0.01 [rad]
Stance ankle proportional gain	$K_{pa}$	546.750 [N·m/rad]
Stance ankle derivative gain	$K_{da}$	21.278 [N·m·s/rad]
Stance knee equilibrium angle	$\theta_k$	-0.05 [rad]
Stance knee proportional gain	$K_{pk}$	546.750 [N·m/rad]
Stance knee derivative gain	$K_{dk}$	21.278 [N·m·s/rad]

This can be seen in the periodic, constant jumps in Fig. 4.21, which shows the trajectory for the generalized energy  $E = K + P - W$  versus time, for three steps. The jumps are an artifact caused by the physical decrease in kinetic energy due to an impact, the shift of the virtual potential energy datum between different locations on the biped, and the reset of the work integral between steps. The three distinct energies  $E_{\text{heel}}$ ,  $E_{\text{flat}}$ , and  $E_{\text{toe}}$  are used as the reference values for the centralized PBC during the corresponding contact constraint.

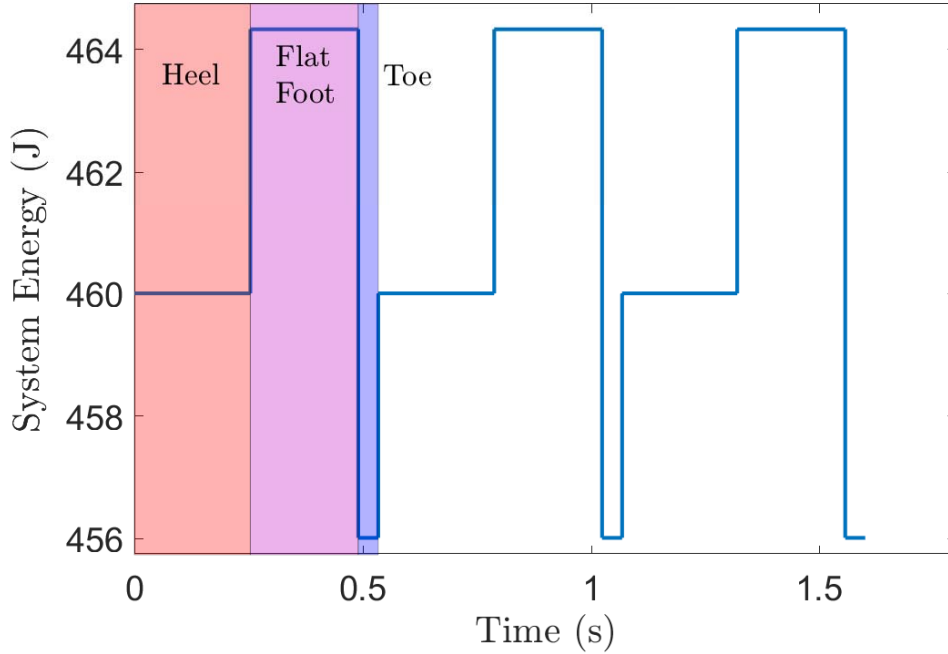


Figure 4.21: Generalized energy ( $E$ ) of the PD controlled (inner-loop) biped system while traversing the limit cycle. There are three constant energy levels with discrete jumps between them.

### Storage Convergence

When the system is solely under the influence of the PD controller, the storage function  $S$  and system energy  $E$  remain constant during the continuous dynamics, and are only changed by the discrete dynamics (i.e., impacts). Implementing the PBC on top of the PD controller qualitatively changes the system behavior by forcing the storage function to converge during the continuous dynamics as well. This is demonstrated in Fig. 4.22, which gives the storage over time of the biped system perturbed by  $\Delta x_o = [0_{8 \times 1}; 0.4 \dot{q}_o]$ . Here, the control parameters  $\Omega = [0, 0, 0, 1, 1, 0.001, 1, 1] I_{8 \times 8}$  and  $k = 1$  were chosen for simplicity and to respect the physical symmetry of the biped. Similar to Fig. 4.21, the discrete jumps in the storage are caused by the impact dynamics. The storage decreases between periods of the same contact configuration (e.g., the second instance of the heel phase has less storage than the first) with or without PBC, which is important for the notion of hybrid passivity

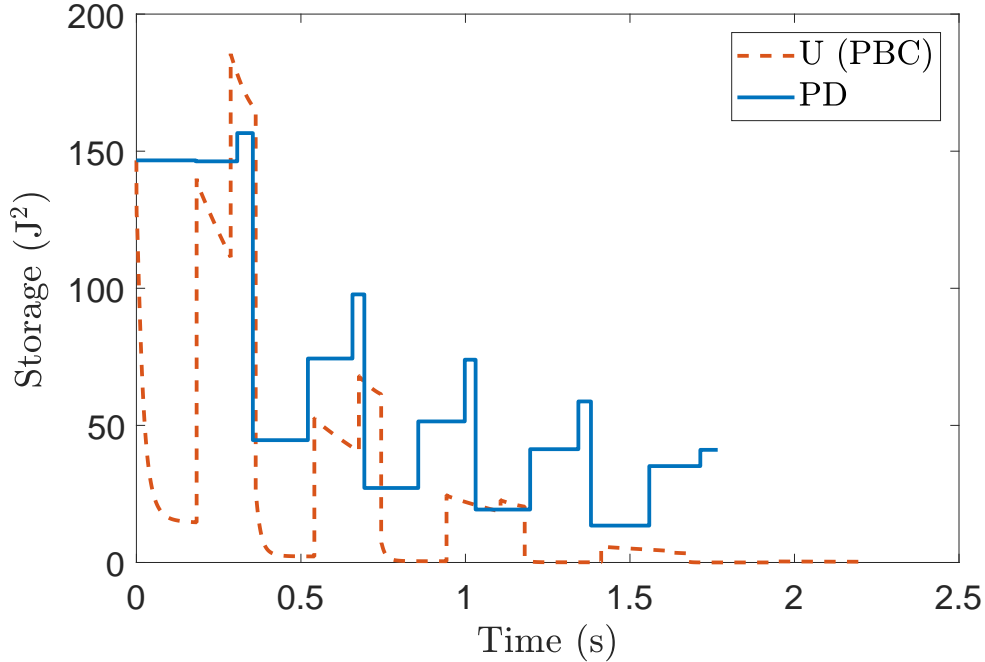


Figure 4.22: Centralized storage function for the perturbed system with PBC and without PBC, over 5 steps. The transition between steps is marked by a large decrease in storage, caused by heel impact.

from [70]. The convergence of the storage function during the continuous dynamics appears to be exponential for the PBC case, with different rates for each contact condition. The effect of this behavior is that the centralized PBC forces the storage close to zero in 5 steps, which is much faster than the PD control alone. If we consider the storage as a metric for how close the biped is to the nominal limit cycle, then we can conclude that the PBC causes the biped to reach steady-state walking faster. However, the storage only gives an indication of convergence speed. It does not definitively demonstrate stability of the hybrid limit cycle nor does it demonstrate a notion of robustness; these ideas are discussed in Sec 4.4.1.

### Control Torques

The torques of PBC for the first three steps of the simulation from Fig. 4.22 are given in Fig. 4.23. The specific joint where the control torque  $u_i$  acts is indicated by the subscript

$i \in \{a, k, h, sk, sa\}$ . The figure indicates that the saturation effect does significantly influence the torque profile, especially for the stance ankle actuator. It is interesting to note that the torques for the stance leg are generally larger than those for the swing leg; this is because the velocities of the joints in the swing leg are smaller in general. The torque trajectory in the first phase has an exponential like trajectory for all the joints, which corresponds to the exponential convergence of the energy to the reference since the torque is proportional to this term. When the energy error becomes small enough, the dynamics of the joint velocities begin to have a larger influence on the control torques. Again, the jumps in the control torque are caused by the instantaneous changes in velocity and energy at impact.

### Stability and Robustness

I stated that the stability of the limit cycle of the hybrid system can be determined by calculating the eigenvalues of the linearized Poincaré map. If the eigenvalues  $\Lambda$  of the linearization lie within the unit circle, then the limit cycle is locally exponentially stable [12]. Fig. 4.24 displays the largest magnitude of all the eigenvalues as  $k$  is varied from 0 to 10 with  $\Omega = [0, 0, 0, 1, 1, 0.001, 1, 1]I_{8 \times 8}$ . This single value is displayed for clarity and conciseness, because the linearization has 16 eigenvalues. The figure indicates that the system is stable for this range of gains since the value is always less than one.

The linearization of the Poincaré map can give some notion of robustness, namely the margin from largest eigenvalue to the unit circle (basically a gain margin). However, there is not a consensus in the field of biped locomotion on what exactly “robustness” means. Many researchers use the eigenvalues as described and say that an increased margin indicates a more robust walking gait [71, 72]. This has drawbacks, namely that eigenvalues characterize local stability and rate of convergence; they contain little information about global properties of the nonlinear system like basin of attraction or robustness. Furthermore, sensitivity to numerical error can result in unstable eigenvalues for a stable orbit (an effect we saw while



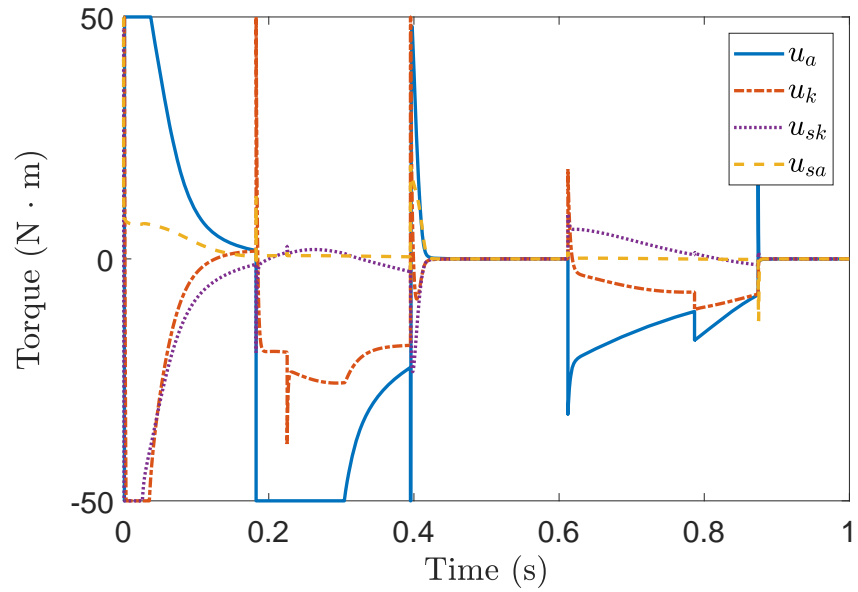


Figure 4.23: Torque over time for the centralized controller  $U$  for the first three steps.

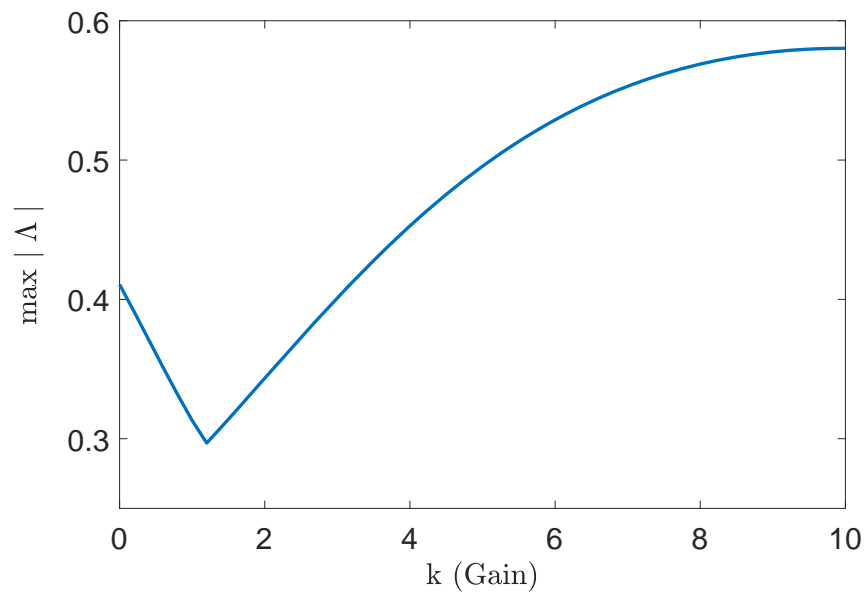


Figure 4.24: Maximum absolute value of the eigenvalues of the linearization of the Poincaré map as the gain  $k$  is varied from 0 to 10.

working with these simulations). A more thorough discussion of the robustness of walking bipeds exists in other works [73, 74]. Because of these issues, we turn to a modification of this metric.

A metric called the “gait sensitivity norm”, with the notation  $\|\partial g/\partial e\|_2$ , was proposed in [74] to provide a measure of the robustness of bipedal gait. It has been subsequently utilized in several other works [75, 76, 77]. We use it to compare the effectiveness of the different controls in our simulations by considering an increase in  $1/\|\partial g/\partial e\|_2$  as an increase in robustness. The calculation of this norm requires gait indicators, gait perturbations, and a linearization of the Poincaré return map. The indicators are essentially failure modes of the system and the perturbations are characteristic of actions on the system that cause failure. We regard “failure” as the biped ceasing to walk. The gait indicators are step length, step time, and the minimum ground clearance of the swing leg heel over the duration of midstance. The disturbances are a change of slope by  $+/- 1$  radian and a perturbation vector  $\Delta x_o = [0_{8 \times 1}; 0.4 \dot{q}_o]$  that introduces a scaled initial velocity at heel strike. We calculate the Poincaré return map [12] at heel strike after 3 steps in our analysis. Based on our choice of indicators and perturbations, we can interpret limit cycles with “better” gait sensitivity norms as being robust to changes in ground slope and velocity disturbances, in the sense that they are farther away from the minimum “allowable” indicator values.

The nominal limit cycle of biped system under PD control alone has a reciprocal norm of  $1/\|\partial g/\partial e\|_2 = 0.1584$ . The biped with the centralized PBC with the parameters used to generate Fig. 4.22 has a reciprocal norm of  $1/\|\partial g/\partial e\|_2 = 0.0248$ , which indicates a less robust system. This might seem to indicate that the PBC cannot achieve the goal of improving the robustness of the biped. However, by simply changing the PBC parameters to  $\Omega = [0, 0, 0, 1, 1, 0.001, 1, \mathbf{0}]J_{8 \times 8}$  (removing the PBC actuator at the swing ankle and keeping everything else the same), we find an increase in robustness with  $1/\|\partial g/\partial e\|_2 = 0.6341$ . This demonstrates that it is important to judiciously choose values in  $\Omega$ . To understand

why such a dramatic change occurs, consider an edge case when  $\Omega = [0, 0, 0, 0, 0, 0, 0, \mathbf{1}]I_{8 \times 8}$ . Essentially, this causes the swing foot to act as a reaction wheel pendulum in a similar manner to [78]. Since the impact map is extremely sensitive to the state of the swing foot at impact, this control parameter choice contracts the basin of attraction of the desired limit cycle dramatically. This causes the biped to fall over when the generalized energy is slightly perturbed.

#### 4.4.2 Decentralized Model

The controller in the previous section relies on the ability to measure all inertial and geometrical properties of the biped. It also relies on measuring all the joint positions and velocities, inner-loop torques, and external forces applied to the system in order to continuously calculate the generalized system energy. In the context of the application to a powered prosthesis or exoskeleton, one generally has an accurate model of the powered device and rough estimates of the user’s mass distribution and geometry. The biggest challenge relates to the inability to measure all of the user’s joint velocities and torques. The straightforward approach might seem to be to partition the system into user and device [79], and then use the energy of the device to construct a PBC. However, we can improve upon this with a partitioning scheme that utilizes all the available model parameter and state information to construct a PBC that is robust to parametric error.

The actuation for the UTD Leg 2 design has knee and ankle joints driven by electric motors. The sensing mechanisms available are: laser-based digital rotary encoders on the joints, an inertial measurement unit (IMU) with accelerometers and gyroscopes mounted above the knee on the shank, and a 6-axis load cell/force sensor. Because none of these sensors are capable of giving explicit measurements of the motion of the human body, there is a motivation to create a decentralized model of the human-prosthesis system that utilizes the maximal amount of available state information. A diagram is given in 4.25.

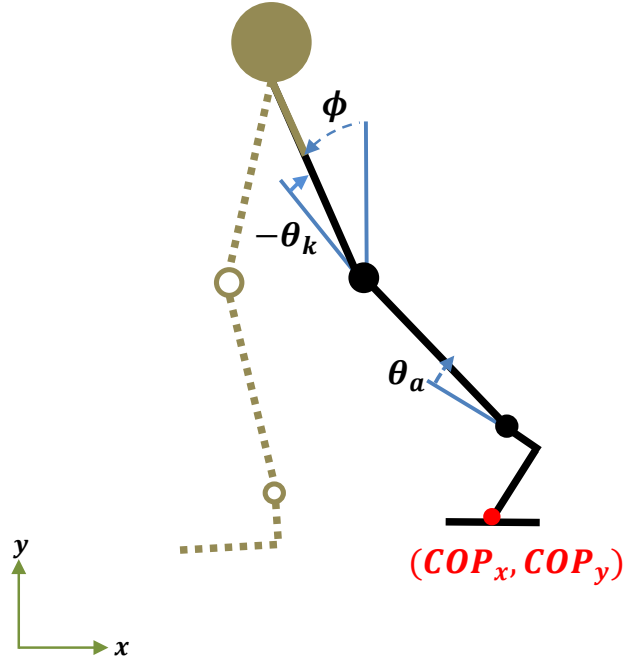


Figure 4.25: Diagram of a decentralized model of the human-prosthesis system.

Let the set of model parameters be  $\Theta$  and contain all of the mass, inertia, and link length parameters of the biped given in 4.20. Let the set of measured parameters be  $\Theta_O \subset \Theta$  and collect all of the model parameters that are measurable. Similarly, a vector of measurable states  $x_O = [q_O; \dot{q}_O] \in \mathbb{R}^{2b \times 1}$  can be extracted from the state vector  $x = [q; \dot{q}]$ , where the vectors of measured position and velocity variables are  $q_O \in \mathbb{R}^{b \times 1}$  and  $\dot{q}_O \in \mathbb{R}^{b \times 1}$ , respectively. The number of joints with position and velocity measurements is given by  $b$ . Equipped with  $\Theta_O$  and  $x_O$ , I can find a subexpression in the Lagrangian of the mechanical system  $\mathcal{L}(x, \Theta) = K - P$  that represents the measurable subsystem  $\mathcal{L}_O(x_O, \Theta_O)$  such that

$$\mathcal{L} = \mathcal{L}_O + \mathcal{L}_{\bar{O}}, \quad (4.46)$$

where  $\mathcal{L}_{\bar{O}}$  is an unmeasured or unmodeled part of the system that cannot explicitly enter into the controller. To do this, I proceed by finding a subexpression  $K_O(q_O, \dot{q}_O, \Theta_O)$  for the kinetic energy and  $P_O(q_O, \Theta_O)$  for the potential energy such that  $\mathcal{L}_O(q_O, \dot{q}_O, \Theta_O) = K_O - P_O$ .

Beginning with the kinetic energy, the mass matrix  $M$  can be calculated using the method from [37] as

$$M = \sum_{j=1}^{n-1} J_j^\top(q) \mathcal{M}_j J_j(q). \quad (4.47)$$

This method constructs the mass matrix link by link, where  $J_j \in \mathbb{R}^{6 \times n}$  and  $\mathcal{M}_j \in \mathbb{R}^{6 \times 6}$  are the body Jacobian and generalized inertia matrix of the  $j$ th link, respectively. The sum is from 1 to  $n - 1$  because the biped models I consider are in a 2-dimensional plane. The mass matrix can be partitioned into

$$M = M_O(q_O, \Theta_O) + \Psi \quad (4.48)$$

$$M_O = \sum_{j=1}^{n-1} J_{jO}^\top \mathcal{M}_{jO} J_{jO}, \quad (4.49)$$

where  $M_O(q_O, \Theta_O)$  is a modified mass matrix that collects additive terms in  $M$  that are functions of the symbols in  $\Theta_O$  and  $x_O$ , exclusively. As it will be shown,  $M_O$  is constructed by obtaining a modified body Jacobian  $J_{jO}(q_O, \Theta_O)$  and a modified inertia matrix  $\mathcal{M}_{jO}(\Theta_O)$  for each link through a partitioning scheme. The remainders of the terms from this scheme are all collected in the variable  $\Psi$ , and no claims about its properties are made.

The matrix  $\mathcal{M}_j$  is always positive definite by construction because it has the form

$$\mathcal{M}_j = \text{diag}(m_j, m_j, m_j, I_{jxx}, I_{jyy}, I_{jzz}) \quad (4.50)$$

which contains on the diagonal the mass and the inertias about the principal axes of the link. It can be decomposed into

$$\mathcal{M}_j = \mathcal{M}_{jO} + \mathcal{M}_{j\bar{O}}, \quad (4.51)$$

where  $\mathcal{M}_{j_O}$  is a diagonal matrix that extracts all the symbols in  $\mathcal{M}_j$  that are also in  $\Theta_O$ . It is important to note that any  $\mathcal{M}_{j_O}$  is positive semi-definite as long as  $\mathcal{M}_j$  contains at least one symbol in  $\Theta_O$ . The remainder  $\mathcal{M}_{j_{\bar{O}}}$  is collected into  $\Psi$ .

Consider the body Jacobian, specifically that each element  $\epsilon_{i,k}$  in  $J_j$  has the form

$$\epsilon_{i,k} = \sum_{z=1}^{n-1} f_z(q_z, \Theta_z) \quad (4.52)$$

based on [37]. The exact form of  $f_z$  depends on the type of joints, revolute or prismatic, that make up the kinematic chain. However, in general, each  $f_z$  is a function of a vector of position state variables  $q_z$  and a set of system parameters  $\Theta_z$ . Each element can be partitioned into

$$\epsilon_{i,k} = \epsilon_{O_{i,k}} + \epsilon_{\bar{O}_{i,k}}, \quad (4.53)$$

where  $\epsilon_{O_{i,k}}$  is the summation of the terms where  $\Theta_z \in \Theta_O$  and all the symbols in  $q_z$  are in  $x_O$ . The term  $\epsilon_{\bar{O}_{i,k}}$  is collected into the remainder  $\Psi$ . The body Jacobian matrix can then be partitioned element-by-element so that  $J_{j_O}$  is constructed from the  $\epsilon_{O_{i,k}}$  elements.

Thus I have demonstrated the methods for constructing the  $J_{j_O}$  and  $\mathcal{M}_{j_O}$  terms in (24). As previously noted, each  $\mathcal{M}_{j_O}$  is positive semi-definite, which implies  $M_O$  is also positive semi-definite. By substitution of (4.48), the kinetic energy can be written as

$$K = \frac{1}{2} \begin{bmatrix} \dot{q}_O^\top & \dot{q}_{\bar{O}}^\top \end{bmatrix} (M_O + \Psi) \begin{bmatrix} \dot{q}_O \\ \dot{q}_{\bar{O}} \end{bmatrix}. \quad (4.54)$$

The subexpression  $K_O$  retains a quadratic form of

$$K_O = \frac{1}{2} \begin{bmatrix} \dot{q}_O^\top & 0 \end{bmatrix} M_O \begin{bmatrix} \dot{q}_O \\ 0 \end{bmatrix} \quad (4.55)$$

so that  $K_O \geq 0$ . This means that  $K_O$  can be treated as the kinetic energy of a subsystem.

Similarly, I can partition the potential energy into two components. To see this, consider the definition for the potential energy

$$P(q) = \sum_{n=1} m_j h_j(q, \Theta) g. \quad (4.56)$$

It is also possible to partition this energy into

$$P = P_O(q_O, \Theta_O) + P_{\bar{O}}, \quad (4.57)$$

by extracting the terms in the summation that belong to  $q_O$  and  $\Theta_O$ . Since  $P$  depends only on position state information, any subexpression  $P_O$  will also depend on only position state information and as such can be considered a new potential energy. Thus, the subexpression  $\mathcal{L}_O$  is Lagrangian and defines a Lagrangian subsystem. The subsystem dynamics are

$$\begin{aligned} M_O(q_O, \Theta_O)\ddot{q}_O + C_O(q_O, \dot{q}_O, \Theta_O)\dot{q}_O + N_O(q_O, \Theta_O) = \\ \Gamma(q, \dot{q}, \Theta, v, u_O) + B_O u_O, \end{aligned} \quad (4.58)$$

where  $M_O \in \mathbb{R}^{b \times b}$  is the mass matrix for the subsystem,  $C_O \in \mathbb{R}^{b \times b}$  is the corresponding Coriolis/centrifugal matrix, and  $N_O \in \mathbb{R}^{b \times 1}$  is a gravitational force vector. Torques generated by both the interaction with the un-modeled system  $\mathcal{L}_{\bar{O}}$  and the inner-loop control  $v$  are represented by  $\Gamma$ , while the torques applied by local actuators and their mapping into the subsystem are represented by the term  $B_O u_O$ .

#### 4.4.3 Decentralized Energy Regulation

This kind of regulation of a generalized system energy is useful in the control of the decentralized biped system presented in Section 4.4.2. Over the flow of the biped moving along a limit cycle, energy is exchanged between the measurable system derived from  $\mathcal{L}_O$  and the un-measurable system  $\mathcal{L}_{\bar{O}}$ . In general, the dynamics of this exchange are crucial to the walking behavior and largely governed by forces generated from outside the measurable subsystem. An attempt to regulate the true mechanical energy of the subsystem  $K_O + P_O$  to a constant value would inhibit/destroy this flow, and could be counterproductive to supporting walking behavior. Because the generalized system energy can account for external work done on the system, if measured properly, the energy flow between  $\mathcal{L}_O$  and  $\mathcal{L}_{\bar{O}}$  can remain unperturbed along the trajectory of a stable limit cycle.

The mathematical demonstration of this is as follows: begin with

$$E_O(q_O, \dot{q}_O, \Theta_O, \Gamma, t) = K_O + P_O - W_O(q_O, \dot{q}_O^\top, \Gamma, t) \quad (4.59)$$

where

$$W_O = \int_0^t \dot{q}_O^\top \Gamma \, d\tau, \quad (4.60)$$

and define a storage function for the decentralized subsystem as

$$S_O(q_O, \dot{q}_O, \Theta_O, \Gamma, t) = \frac{1}{2}(E_O - E_{O\text{ref}})^2. \quad (4.61)$$

Take the time-derivative of  $S_O$  to find

$$\dot{S}_O = (E_O - E_{O\text{ref}})(\dot{E}_O - \dot{E}_{O\text{ref}}), \quad (4.62)$$

and  $E_O$  to find

$$\dot{E}_O = \frac{d(K_O + P_O)}{dt} - \frac{dW_O}{dt} \quad (4.63)$$

$$\begin{aligned} &= (\dot{q}_O^\top B_O u_O + \dot{q}_O^\top \Gamma) - \dot{q}_O^\top \Gamma \\ &= \dot{q}_O^\top B_O u_O, \end{aligned} \quad (4.64)$$

which follows from (4.58) and (4.60). By substituting  $\dot{E}_O$  into  $\dot{S}_O$ , the storage time derivative is

$$\dot{S}_O = (E_O - E_{O\text{ref}})(\dot{q}_O^\top B_O u_O - \dot{E}_{O\text{ref}}). \quad (4.65)$$

Upon inspection of  $\dot{E}_O$ , it is apparent that the generalized energy does indeed take a constant value on the limit cycle, since  $\dot{E}_O = 0$  when  $u_O = 0$ . This means  $\dot{E}_{O\text{ref}} = 0$  on the limit cycle for the uncontrolled subsystem. The decentralized controller is then

$$u_O(q_O, \dot{q}_O, \Theta_O, \Gamma, t) = -k_O \Omega_O (E_O - E_{O\text{ref}}) B_O^\top \dot{q}_O \quad (4.66)$$

with similar passivity, saturation, and exponential convergence properties to the centralized case.



#### 4.4.4 Decentralized Simulations

This section explores the behavior of the biped with two different decentralized controls while comparing them amongst each other, to the centralized PBC, and to the biped with only PD control. The motivation behind these comparisons is to gain an understanding for the potential application to an exoskeleton. The centralized PBC represents the theoretical case if we could get perfect measurements of the human parameters and motion, while the decentralized cases represent the compromise made by the choice of the system model. The PD control alone represents the human walking without any assistance. Again, all the PBC controllers were saturated at 50 Nm.

We have the two decentralized controls  $U_\zeta, U_\xi$  and the centralized control  $U$ . The main difference between the two decentralized controls is the model information that they use. Specifically,  $U_\zeta$  utilizes the same full model parameter set  $\Theta$  as the centralized control  $U$ , but it restricts the state information to a vector  $x_O$  local to the stance leg such that

$$x_O = [p_x, p_y, \phi, \theta_s, \theta_t, \dot{p}_x, \dot{p}_y, \dot{\phi}, \dot{\theta}_s, \dot{\theta}_t]^\top. \quad (4.67)$$

The second decentralized PBC  $U_\xi$  uses the restricted state information  $x_O$  and also uses a restricted model parameter set

$$\Theta_O = \{m_f, m_s, I_f, I_s, l_f, l_s\} \quad (4.68)$$

that is also local to the stance leg. This is essentially modeling the stance leg as a completely separate subsystem. This gives rise to subsystems with generalized energies  $E_\zeta(x_O, \Theta)$  and  $E_\xi(x_O, \Theta_O)$  that are used to construct the controls  $U_\zeta$  and  $U_\xi$ , respectively. The energy  $E_\xi$  has a physical interpretation: it is the energy of the stance shank and foot. The energy  $E_\zeta$  does not have such an intuitive meaning.

In order to implement the decentralized controllers  $U_\zeta$  and  $U_\xi$ , we need target reference energies for each of them at each contact configuration. These can be found in simulation

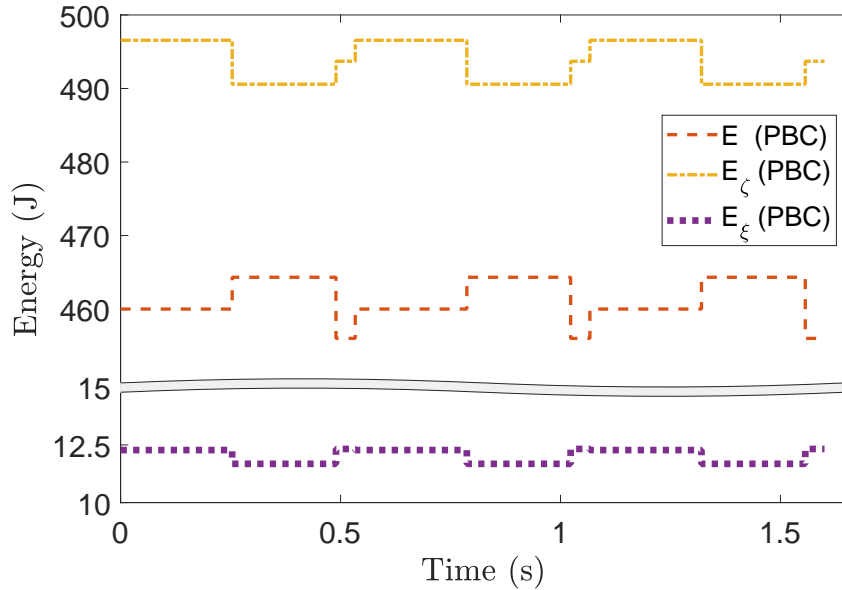


Figure 4.26: Generalized energy of all three systems while traversing the limit cycle. There is a break in the y-axis of the graph to accommodate the difference in average magnitude of the energy trajectories.

by simply computing the value of their generalized energies over the nominal limit cycle of the biped under PD control alone. We see in Fig. 4.26 that the decentralized energies take constant values on the limit cycle, as expected. Since the construction of  $E_\zeta$  ignores the majority of the mass and inertia terms of the biped system, it is expected that its value along the limit cycle is significantly smaller compared to the other two energies. In contrast, when  $E_\zeta$  is compared to the real system energy  $E$ , it has an increased virtual potential energy which makes it larger than  $E$ .

### Storage Convergence

We constructed an experiment of four simulations with a perturbation to the biped's initial condition on the limit cycle. The independent variable is the control method used in each simulation. The control parameters for all three PBC controllers were kept the same, with  $\Omega = [0, 0, 0, 1, 1, 0, 0, 0]I_{8 \times 8}$  and  $k = 1$ , which limits actuation to the stance side knee and

ankle. The same perturbation to the state of the biped on the limit cycle at heel strike  $\Delta x_o = [0_{8 \times 1}; 0.4 \dot{q}_o]$  was used in each simulation. Since the point of introducing control into the system is to make the *entire* biped system converge back to the limit cycle, we examined the *centralized* storage function that utilizes the full state and model parameter information. By contrast, the storage function of one of the decentralized systems only gives information about the convergence of a portion of the biped.

From Fig. 4.27, we can see that the behavior for the PBC  $U_\xi$  is very close to the system with PD control only, while the decentralized PBC  $U_\zeta$  is very close to the “best case” scenario of the centralized system. Again, the convergence rate back to the limit cycle is significantly faster for  $U$  and  $U_\zeta$  than for  $U_\xi$  and PD control alone. This confirms that there a gain in performance from the decentralized partitioning scheme to generate  $U_\zeta$  rather than simply modeling the stance leg as a localized subsystem to generate  $U_\xi$ . The decentralized control  $U_\zeta$  does not converge quite as quickly as  $U$ , but this is to be expected since it does not utilize the full state feedback.

The reason why the decentralized control  $U_\xi$  essentially acts like the biped with PD control alone is because the magnitude of the energy error is small compared to the other controls. This means less storage is injected to the system at each impact and since this storage does not accurately account for the “real distance” to the limit cycle, the control is less effective. The decentralized PBC  $U_\xi$  resembles the performance of to the centralized control  $U$  precisely because the generalized energy for that decentralized subsystem is close to the centralized energy.

## Robustness

The robustness properties of each system are characterized by the gait sensitivity norm. We performed a simulation experiment to examine this across an array of different scaling gains  $k$  for each control while maintaining the same weighting matrix  $\Omega = [0, 0, 0, 1, 1, 0, 0, 0]I_{8 \times 8}$ .

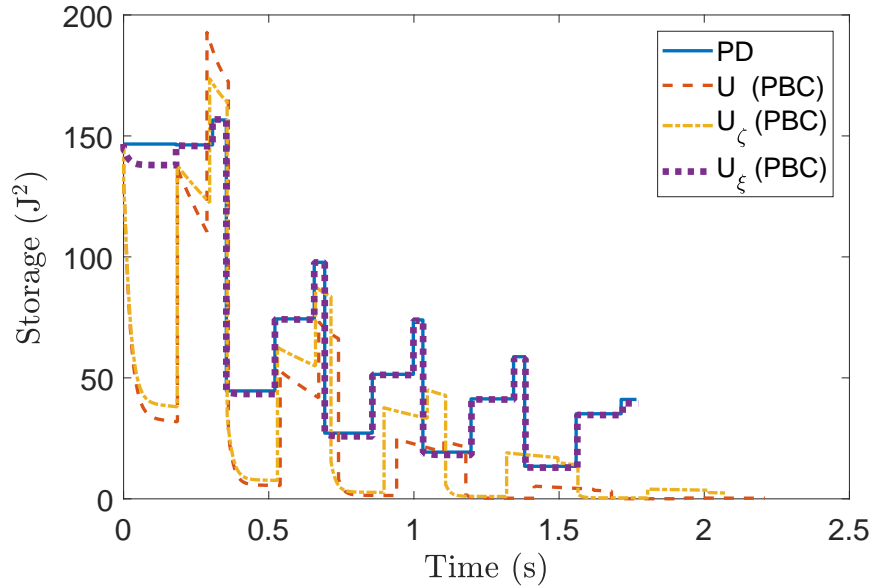


Figure 4.27: System storage function across PBC implementations.

This allows a rigorous comparison of the robustness of the different controls. The results of this experiment are displayed in Tab. 4.3. This table demonstrates the same relationship observed in the storage analysis; that  $U$  and  $U_\zeta$  are similar in behavior while  $U_\xi$  acts more like PD control alone. Also, there is a strict ordering of the control methods across all the selected gains, in terms of robustness, that correlates with the amount of information available to the control. In other words, utilizing a larger information set to construct the PBC makes the biped more robust. While the table seems to indicate that increasing the scaling gain always makes the gait more robust, this is not always the case. For example, increasing the gain of the centralized control to  $k = 100$  makes the reciprocal of the gait sensitivity norm  $1/||\partial g/\partial e||_2 = 2.0055$ , and increasing further still to  $k = 1000$  makes  $1/||\partial g/\partial e||_2 = 0.001$ , which is a large decrease in robustness. These results reveal that there exists a limit on the scaling gain such that exceeding the limit actually makes the system performance worse.

Table 4.3: Reciprocal of the gait sensitivity norm calculated across controllers and scaling gains

Reciprocal of Gait Sensitivity Norm ( $1/  \partial g/\partial e  _2$ )			
	$k = 0.01$	$k = 1$	$k = 10$
$U$	0.1614	0.6614	3.0454
$U_\zeta$	0.1594	0.3345	2.2086
$U_\xi$	0.1584	0.1597	0.1755
$PD$	0.1584		

#### 4.4.5 Model Parameter Error

In this section we explore the effect of parameter error in the energy function of the decentralized control  $U_\zeta$ . Based on the results in the previous section, this control represents the best version that could be implemented on a wearable device. However, it is practically guaranteed that measures or estimates of the inertia of the user will have some error. Furthermore, we believe that the characteristics of the parameter error in this scenario should generalize to the other control cases. An example simulation is given in Fig. 4.28 that uses  $U_\zeta$  with control parameters  $\Omega = [0, 0, 0, 1, 1, 0, 0, 0]I_{8 \times 8}$ ,  $k = 1$ , and a set of arbitrarily chosen model parameter errors of  $\pm 30\%$  difference from the parameters in  $\Theta$ . It is perturbed off the limit cycle at heel strike by  $\Delta x_o = [0_{8 \times 1}; 0.4\dot{q}_o]$ . It is important to note that the reference energies are calculated with the inaccurate model parameters and then used in the control with the same error. This method ensures the storage function is zero along the limit cycle and also is reflective of a real-world implementation.

Even with model parameter error, the decentralized control still causes the biped to converge to the limit cycle in less steps than without PBC, as seen in Fig. 4.28. During heel contact of the second and third step, it seems that the storage function is larger than the non-PBC case but this behavior is transient and quickly disappears. In addition, the value of the

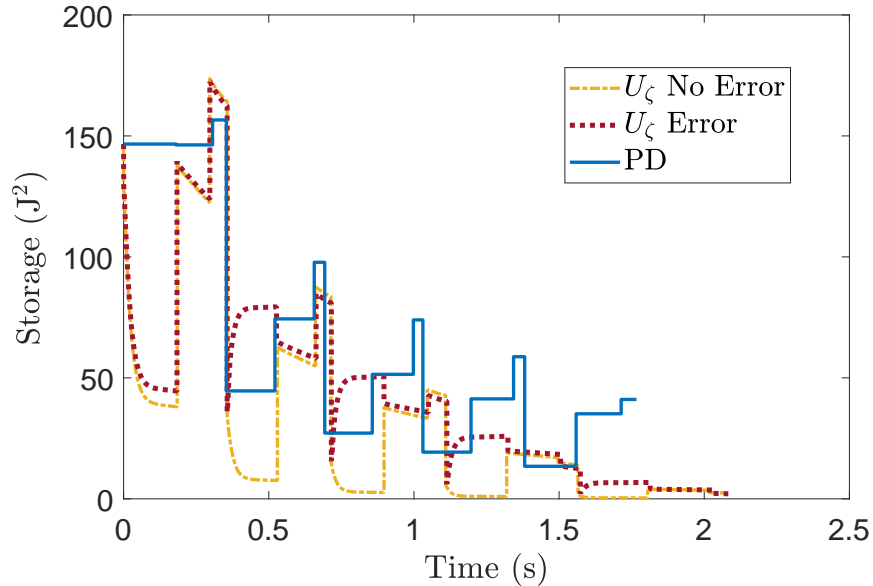


Figure 4.28: System storage function for a decentralized PBC with perfect model parameters versus a decentralized PBC with random  $\pm 30\%$  error in the model parameters.

reciprocal gait sensitivity norm for the control with parameter error is  $1/\|\partial g/\partial e\|_2 = 0.6614$ , which is greater than the non-PBC system.

To investigate the general behavior of the PBC under model parameter error, we ran an experiment with consistent control parameters where we calculated the gait sensitivity norm for the system with 30 random sets of model parameter errors. The error multiple for each parameter  $\mu \in \Theta$  was a uniform random variable in  $\pm 0.3$ , and we calculated the parameter error norm as the 2-norm of all these error values. A scatter plot of the results is given in Fig. 4.29. All of the values on the plot are significantly larger than the gait sensitivity norm for the PD control alone. These results support the idea that as long as the scheme for calculating the storage injection at each impact correlates with the energy of the system, the control should make the system more robust. The major point of the experiment is to show the efficacy of the PBC under random parametric error and not some “cherry-picked” values.

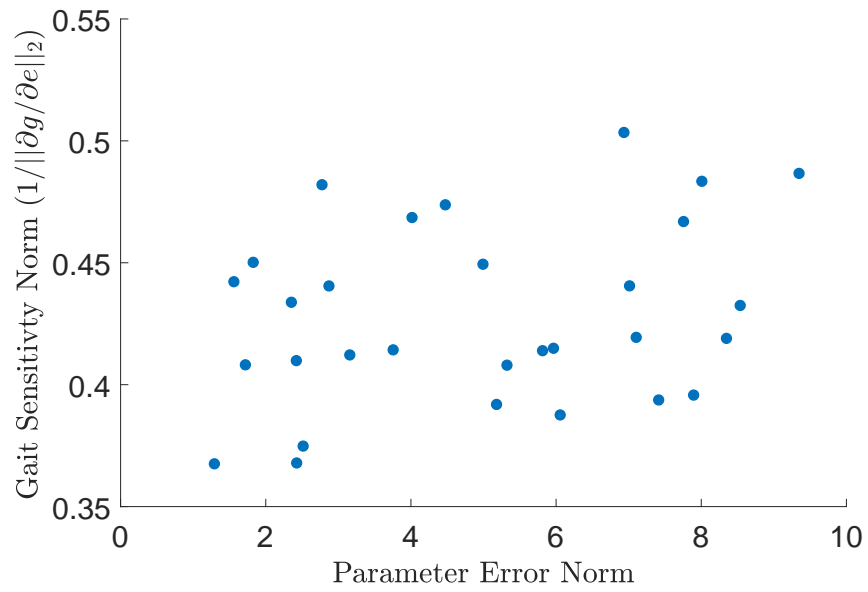


Figure 4.29: Robustness of decentralized control vs model parameter error norm with  $k = 1$ .

## CHAPTER 5

### APPLICATION ON A POWERED PROSTHETIC LEG

This chapter focuses specifically on the control of a powered knee-ankle prosthetic leg to aid people with trans-femoral amputations. The additional capability of a powered device over a passive device is two-pronged; it can enable more reliable and precise position control, and it can impart positive work to the user. The success of recent research on translating methods of autonomous biped control into prosthesis leg control has largely been related to the position control aspect. In [11], knee and ankle trajectories for an entire stride are parameterized by the position of the user’s hip angle, which automatically synchronizes the motion of the device to the user and allows highly volitional motion. In [80], a virtual constraint to maintain the so called “roll-over shape” is used to support the user during stance. The primary issue with these examples and other trajectory based control methods is that they are not explicitly designed to propel the user or perform positive work. Impedance based control methods such as the one from [81], which has a tunable pushoff impulse and emulates estimates of human joint impedances, are more effective at directly restoring energy. This chapter seeks to expand upon this paradigm by using energy shaping control to cause the prosthesis to emulate a virtual spring similar to the SLIP model, and then use energy regulation to explicitly perform positive work on the human-prosthesis system.

#### 5.1 Model and Hardware

While a human using a wearable device is not the same as an autonomous biped, many of the principles of modeling, motion, and control are the same in both applications. The additional challenge of controlling a wearable system is predicting/sensing what the user is doing. In the case of a prosthesis, it is desirable to keep the sensing localized so that donning/doffing is easy and the mechanical components remain relatively unobtrusive. However, this makes



the problem of controlling the prosthesis to influence the combine human-prosthesis system a decentralized control problem. The human body has 320 skeletal muscle pairs [82] that allow volitional motion, so any tractable model that gives meaningful insight into walking behavior will necessarily be an abstraction of the rich dynamics of the human body. The model of the system that I use is the decentralized variation of the Flat Foot model from [38] detailed in Section 4.4.2. On the specific hardware that I used, the UTD Leg 2, a controller is limited to sensing positions of the global thigh angle, the knee angle, and ankle angle of the prosthesis. It can also sense the net wrench applied at the physical interface of the foot with the shank. A picture of the hardware is shown in Figure 5.1.

## 5.2 Control

In Section 4.3.1, I embedded the energy regulated SLIP model into the RABBIT biped and achieved an exact match of the hip point energy to the SLIP energy. This required both full state information and full actuation. The prosthesis system has neither of these properties. In order to address this issue I will add in the dynamics of a virtual spring without compensating for the natural nonlinear dynamics, which has been demonstrated to be a viable approach for generating walking motion on a biped robot in [46]. The key distinction is that I will use the user hip joint as a proxy for the COM, which allows the virtual spring dynamics to be a function of only the knee and ankle positions. The oscillator dynamics of equation (4.15), which uses the energy of the SLIP model that can be calculated using just the spring position and velocity, will be added in as well to perform positive work generation while again only using local sensing. This virtual spring control will only be active during stance; in swing, the phase variable based joint trajectory controller from [11] will be used. This choice is motivated from the biomechanics of human walking in which push-off at the end of stance provides the majority of the propulsive force, and that the main

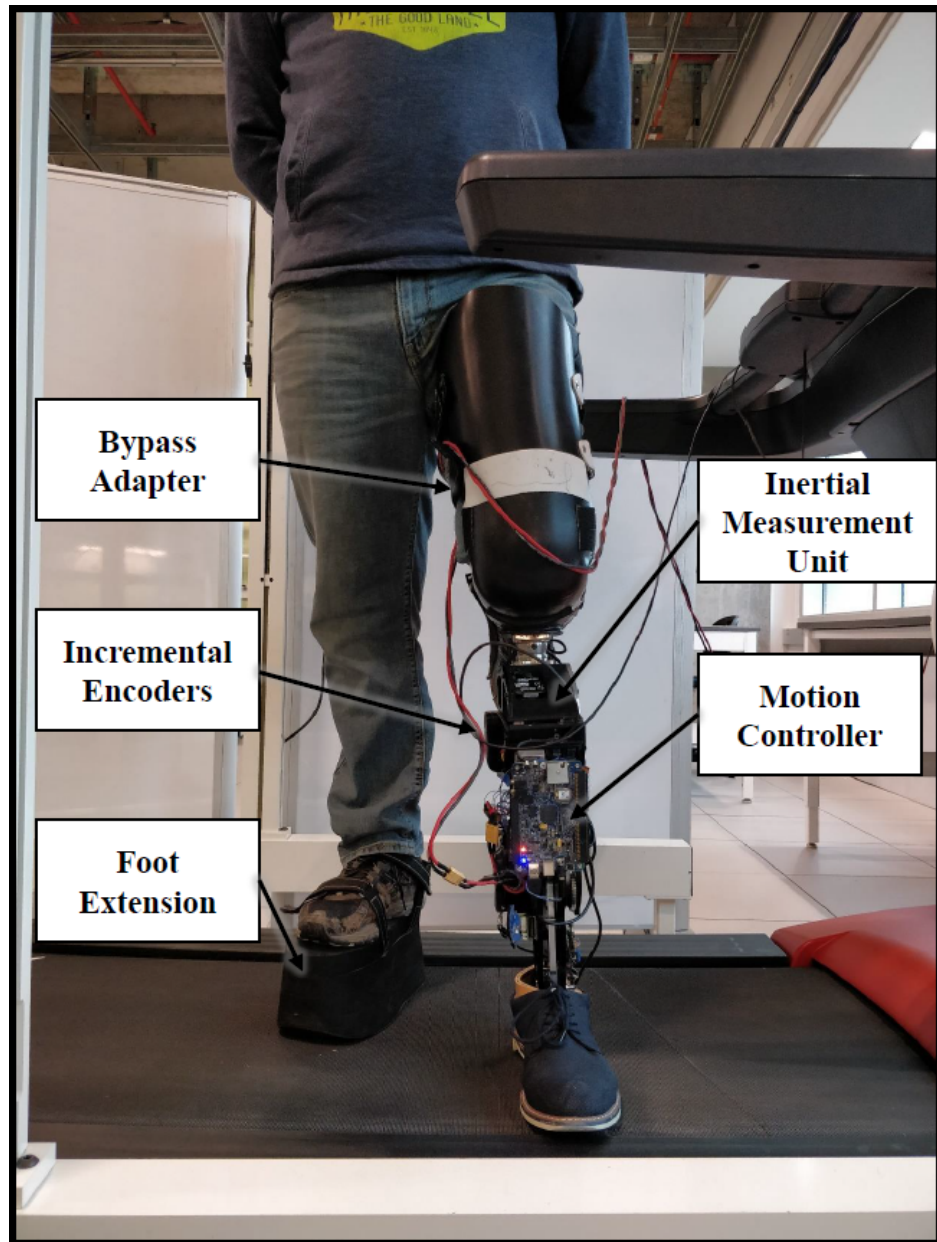


Figure 5.1: A picture of the experimental setup with UTD Leg 2.

outcome of swing is the placement of the foot in front of the user’s hip which is more suited to position/trajectory control.

A critical difference between the RABBIT model and the prosthesis model is the geometry of the feet and a changing contact condition. The prosthesis model has a flat foot which experiences the heel-flat-toe contact pattern from Section 4.4. In the heel and toe configurations, the ground contact is at a single point and the virtual spring connection points are obvious. The connection point needs to travel from the heel to the toe in a smooth manner over the flat foot phase; to this purpose I will use the local center of pressure as the virtual spring connection point. I will show how attempting to use a pure energy shaping approach requires solving a partial differential equation, thus it is helpful to use a force sensor to calculate the COP as a system input. A diagram is given in Figure 5.2.

### The Virtual Spring

In the biped model, the COP can be calculated from the constraint forces  $\lambda(q, \dot{q}, u, F)$  (as defined in 2.8). Directly using this expression to formulate an energy shaping control has two challenges. First, because  $\lambda$  depends on  $u$ , a partial differential equation must be solved in order to even compute the expression for the virtual spring control. Consider the expression for the energy stored in a virtual spring between the hip center and COP,

$$P_s(q, \lambda) = \frac{1}{2}k(L(q, \lambda) - L_o)^2. \quad (5.1)$$

The spring length  $L$  is the distance between the hip center and COP. The expression for this is

$$L = \|\overrightarrow{\text{Hip}}(q) - \overrightarrow{\text{COP}}(q, \lambda)\| \quad (5.2)$$

At heel and toe phases, the COP is simply at the heel and toe and only thus depends on  $q$ . During the flat foot phase, the constrained coordinate vector is  $h = [x, y, \phi]^\top$  and the

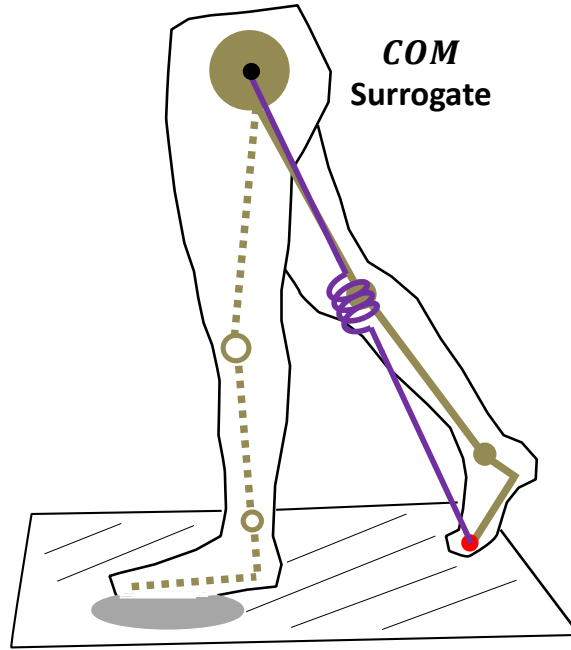


Figure 5.2: Virtual spring between the center of pressure and a surrogate for the center of mass.

corresponding generalized constraint force is  $\lambda = [\lambda_x, \lambda_y, \lambda_m]^\top$ . The center of pressure can be calculated from

$$\text{COP}_{fx} = \frac{\lambda_m - l_a \cdot \lambda_t}{\lambda_n} \quad (5.3)$$

where  $\lambda_n, \lambda_t$  are the normal and tangential force components relative to the ground and  $\text{COP}_{fx}$  is the distance along the foot from the heel to the COP. A constant rotation matrix based on the ground slope and its inverse can be used to convert between  $\lambda_n, \lambda_t$  and  $\lambda_x, \lambda_y$ . A diagram is given in Figure 5.3. From 2.8, the COP becomes a function of  $q, \dot{q}$ , and  $u$ , and thus  $P_s(q, \dot{q}, u)$  does not fit the form for the potential energy of a mechanical system. So the

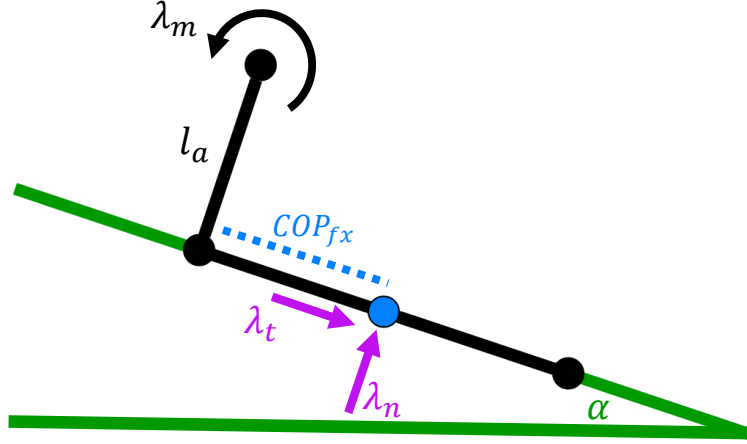


Figure 5.3: Diagram of relation of COP to constraint forces for the flat foot contact condition.

more general energy shaping control 3.5 must be used, leading to

$$u_s = (B^\top B)^{-1} B^\top \left( \left( \frac{d}{dt} \frac{\partial \mathcal{L}(q, \dot{q})}{\partial \dot{q}} - \frac{\partial \mathcal{L}(q, \dot{q})}{\partial q} \right) - \left( \frac{d}{dt} \frac{\partial \tilde{\mathcal{L}}(q, \dot{q}, \lambda)}{\partial \dot{q}} - \frac{\partial \tilde{\mathcal{L}}(q, \dot{q}, \lambda)}{\partial q} \right) \right) \quad (5.4)$$

$$= (B^\top B)^{-1} B^\top \left( -\frac{d}{dt} \frac{\partial P_s(q, \dot{q}, \lambda)}{\partial \dot{q}} + \frac{\partial P_s(q, \dot{q}, \lambda)}{\partial q} \right) \quad (5.5)$$

Expanding the expressions for the potential energy partial derivatives yields

$$\frac{\partial P_s(q, \dot{q}, \lambda(q, \dot{q}, u_s))}{\partial \dot{q}} = \frac{\partial P_s}{\partial L} \frac{\partial L(q, \lambda(q, \dot{q}, u_s))}{\partial \dot{q}} = \frac{\partial P_s}{\partial L} \frac{\partial L}{\partial \lambda} \frac{\partial \lambda}{\partial u_s} \frac{\partial u_s}{\partial \dot{q}} \quad (5.6)$$

$$\frac{\partial P_s(q, \dot{q}, \lambda(q, \dot{q}, u_s))}{\partial q} = \frac{\partial P_s}{\partial L} \left( \frac{\partial L}{\partial q} + \frac{\partial L}{\partial \lambda} \frac{\partial \lambda}{\partial u_s} \frac{\partial u_s}{\partial q} \right), \quad (5.7)$$

and when substituted back into equation (5.5) they reveal the existence of a partial differential equation in  $u_s$  (emphasized by the highlighted portions of the equations). Practically, this means even with full state and parameter information, the control to achieve both the matching conditions for this problem is intractable.

There is an approximation of the desired effect that can be made. Because the prosthesis is equipped with a load cell, I will treat  $\lambda$  as an input to the system using this sensor and consider  $\frac{\partial \lambda}{\partial q} = \frac{\partial \lambda}{\partial \dot{q}} = 0$  in order to reduce the problem complexity and view  $P_s(q, \lambda)$  as a

mechanical potential energy. In addition, because the hip center is calculated using local state and parameter information, the second matching condition is trivially satisfied. So the approximate energy shaping law takes the form

$$u_s = (B^\top B)^{-1} B^\top \left( -\frac{\partial P_s}{\partial q} \right) \quad (5.8)$$

$$= (B^\top B)^{-1} B^\top \left( -\frac{\partial P_s}{\partial L} \frac{\partial L}{\partial q} \right) \quad (5.9)$$

$$= -k_s (L(q, \lambda) - L_o) (B^\top B)^{-1} B^\top \frac{\partial L(q, \lambda)}{\partial q}. \quad (5.10)$$

The conceptual downside of this method is that the energy in the virtual spring can be changed by the motion of the COP which muddles the physical interpretation of an energy regulation control even further.

## Energy Regulation

Ideally, an energy regulation controller would act directly on a measurement of the energy of the human-prosthesis system. As has been discussed, lack of sensing makes this difficult/intractable. Instead, I will use a modification of the energy based method from equation (4.15)

$$u_r = -\kappa \dot{L} (\tilde{E}_L - E_{\text{ref}}) \quad (5.11)$$

$$\tilde{E}_L = \frac{1}{2} m \dot{L}^2 + \frac{1}{2} \tilde{k} (L - L_o)^2, \quad (5.12)$$

that creates a harmonic Van-der-Pol Rayleigh oscillator along the virtual spring axis. As seen in Section 4.2.2, this can create walking behavior similar to the dynamics that result from controlling the total energy in simulation. The physical prosthesis system and virtual spring control have nonlinear dynamics and a moving virtual spring connection point that add additional complexity to this approximation. In human walking, different joints contribute different proportions to the total power output [83, 84]. The most significant contribution

of net positive work comes from the ankle during pushoff [85, 1] and net negative work from the knee during heel strike. This behavior can be emulated through a biomimetic torque saturation scheme on the energy regulation portion. This ensures that the only “extra” work performed, outside of the virtual spring, is positive from the ankle and negative from the knee. This is especially useful since the energy function is not the total system energy, so it is guaranteed to fluctuate. This saturation preserves passivity (see equation 2.18).

Energy regulation is additionally challenged by the need for velocity estimation, since the sensing is limited to joint encoders at the knee and ankle. A straightforward method to estimate velocity from the position signal is to use a numerical difference

$$v(t_k) = \frac{p(t_k) - p(t_{k-1})}{t_k - t_{k-1}}, \quad (5.13)$$

which divides the difference in position between two position readings by the sampling period. This is well-known to encounter issues related to quantization in the physical sensing mechanism of an encoder and the sampling rate versus dynamics time scales [86]. The velocity estimation can be improved by using “exponential smoothing” [87], which stores previous samples of the estimated velocity and outputs a weighted linear combination of estimates. The method used on the prosthesis system is

$$\mathbf{v}(t_k) = \beta_v \cdot v(t_k) + (1 - \beta_v) \cdot \mathbf{v}(t_{k-1}), \quad (5.14)$$

where  $\mathbf{v}(t_k)$  is the smoothed velocity and  $v(t_k)$  is the numerical difference. The parameter  $\beta_v$  is a “forgetting factor” that controls how much influence the summed older samples  $\mathbf{v}(t_{k-1})$  have.  $\beta_v = 1$  corresponds to having no smoothing effect. The exponential smoothing can be viewed as storing all of the previous samples with weight that exponentially decays over time, and has the effect of reducing “ripples” that can occur when an encoder moves across a tick [78] and other forms of noise. By inspecting the equation for energy regulation, one can see that the velocity of the virtual spring enters the control as a cubic polynomial. This

can amplify noise effects on a much larger order of magnitude than traditional PD control techniques. Therefore, I implement additional layers of smoothing on the output of the energy regulation control and saturate its rate of change as

$$\mathbf{u}_r(t_k) = \beta_v \left( \mathbf{u}_r(t_{k-1}) + \text{sat}\left(\frac{u_r - \mathbf{u}_r(t_{k-1})}{t_k - t_{k-1}}\right) \right) + (1 - \beta_v) (\mathbf{u}_r(t_{k-1})), \quad (5.15)$$

The biomimetic power saturation is then implemented on the smoothed output  $\mathbf{u}_r(t_k)$  as

$$\begin{aligned} & \text{if } \mathbf{u}_{r,knee} \dot{q}_{knee} > 0 \\ & \quad \mathbf{u}_{r,knee} := 0 \\ & \text{if } \mathbf{u}_{r,ankle} \dot{q}_{ankle} < 0 \\ & \quad \mathbf{u}_{r,ankle} := 0. \end{aligned}$$

## Energy Regulation with a Velocity Observer

An alternative approach to these smoothing techniques is Kalman filters or observers, which exploit knowledge of the model/system dynamics to obtain velocity estimations. While there is some evidence that the performance difference between model based filters and exponential smoothing is negligible [87], the model based designs better lend themselves to rigorous analytical proofs of stability and performance. In this section, I will recapitulate a passivity-based velocity observer from [86] for a rigid robot with position sensing only, then demonstrate local asymptotic stability when combined with a passivity based energy regulation controller. This is simply presented as a theoretical alternative, and is not actually implemented in the experiment section.

The structure of the observer is based on the general model for rigid robots from equation (2.14), and is

$$\dot{\hat{q}} = z + \mathfrak{L}_d \hat{q} \quad (5.16)$$

$$\dot{z} = M^{-1}(q) (Bu + J^\top F - C(q, \dot{q}_0) \dot{q}_0 - G(q)) + \mathfrak{L}_p (q - \hat{q}), \quad (5.17)$$



where  $[\hat{q}; z]$  is the observer state. The variable  $\dot{q}_0 = \dot{\hat{q}} - \Lambda(q - \hat{q})$  (with  $\Lambda$  positive definite) is a weighting between the velocity estimation and the observer position error, which serves to exploit passivity properties of the robot dynamics and ensure convergence of the estimated velocity to the true velocity.  $\mathfrak{L}_d = \mathfrak{r}I_{n \times n} + \Lambda$  and  $\mathfrak{L}_p = \mathfrak{r}\Lambda$  are positive definite observer gain matrices, and  $\mathfrak{r} > 0$  is the scaling gain. Under some assumptions: 1) there are bounds on the magnitude of norms  $\mathbf{V}_p, \mathbf{M}_m, \mathbf{C}_m$  of the velocity vector, mass matrix, and Coriolis/centrifugal matrix, respectively, 2) that  $\mathfrak{r} > \mathbf{M}_m^{-1} \mathbf{C}_m \mathbf{V}_p$ , then the observer position and velocity are guaranteed to locally exponentially converge to the true states. The region of attraction of the observer is a ball in the state space with a radius proportional to  $\mathfrak{r}$ . In hardware, this observer can be implemented using a numerical integration technique like Euler's method [88].

An energy regulation controller can be formed by basing the energy function off the estimated velocity. Following the same derivation from Section 3.2, define a storage function

$$S = \frac{1}{2}(\hat{E} - E_{\text{ref}})^2 \quad (5.18)$$

$$\hat{E} = \frac{1}{2}\dot{\hat{q}}^\top M(q)\dot{\hat{q}} + \mathcal{P}(q). \quad (5.19)$$

Its time derivative is then

$$\dot{S} = (\dot{\hat{E}})(\hat{E} - E_{\text{ref}}) \quad (5.20)$$

$$= \dot{\hat{q}}^\top \left( M(\hat{q})\ddot{\hat{q}} + \frac{1}{2}\dot{M}(\hat{q})\dot{\hat{q}} + G(\hat{q}) \right) (\hat{E} - E_{\text{ref}}). \quad (5.21)$$

From equation (5.16),  $\ddot{\hat{q}} = \dot{z} + \mathfrak{L}_d(z + \mathfrak{L}_d\hat{q})$ , and by some substitution

$$\dot{S} = \dot{\hat{q}}^\top \left( M(\hat{q})M(q)^{-1}Bu + R \right) (\hat{E} - E_{\text{ref}}) \quad (5.22)$$

$$R = M(\hat{q}) \left( M(q)^{-1}(J^\top F - C(q, \dot{q}_0)\dot{q}_0 - G(q)) + \mathfrak{L}_d(z + \mathfrak{L}_d\hat{q}) \right) \quad (5.23)$$

$$+ \frac{1}{2}\dot{M}(\hat{q})\dot{\hat{q}} + G(\hat{q}). \quad (5.24)$$

Consider the case where  $B$  is full rank. In the prosthesis application, this can be achieved by modeling the system so that the knee and ankle joint angles are the only state variables and using the force sensor to estimate the effect of the unmodeled dynamics. Again, since this is theory, I omit the details of this model. An energy regulation controller can be chosen as

$$u_r = (M(\hat{q})M(q)^{-1}B)^{-1}(-R) - \kappa (M(\hat{q})M(q)^{-1}B)^\top \dot{\hat{q}}(\hat{E} - E_{\text{ref}}), \quad (5.25)$$

which ensures

$$\dot{S} = -2\kappa \|\dot{\hat{q}}\|^2 S, \quad (5.26)$$

so the observer energy converges to the reference energy. If the observer state is also converging to the true state, then the true system energy is guaranteed to converge to the reference energy.

### 5.3 Experiments

This section covers a proof-of-concept experiment of using the proposed embedded virtual spring with an energy regulation controller on a powered prosthetic leg. Here, I use the prosthesis using a bypass that folds my leg back and a platform sole on the other foot (see Figure 5.1), so this example is somewhat removed from the target use case of amputee locomotion. To clarify, the controller during stance is a combination of the COP-to-hip embedded virtual spring from equation (5.10), with the energy oscillator from equation (5.11) and associated smoothing and saturation. The control parameters,  $k_s = 16000N \cdot m^{-1}$ ,  $L_o = 0.440m$ ,  $m_s = 1kg$ ,  $\kappa = 0.1$  were found via heuristically testing for comfort, stability, and safety. The energy oscillator control rate of change is saturated at  $50N \cdot m \cdot s^{-1}$ , and the weight  $\beta = 0.5$  for the exponential smoothing filters. The COP estimation is saturated to fit in between the heel and toe of the prosthetic foot,  $[-0.04m, 0.06m]$ , and is not allowed to go backwards. During swing, a PD controller from [81] was used to track joint trajectories

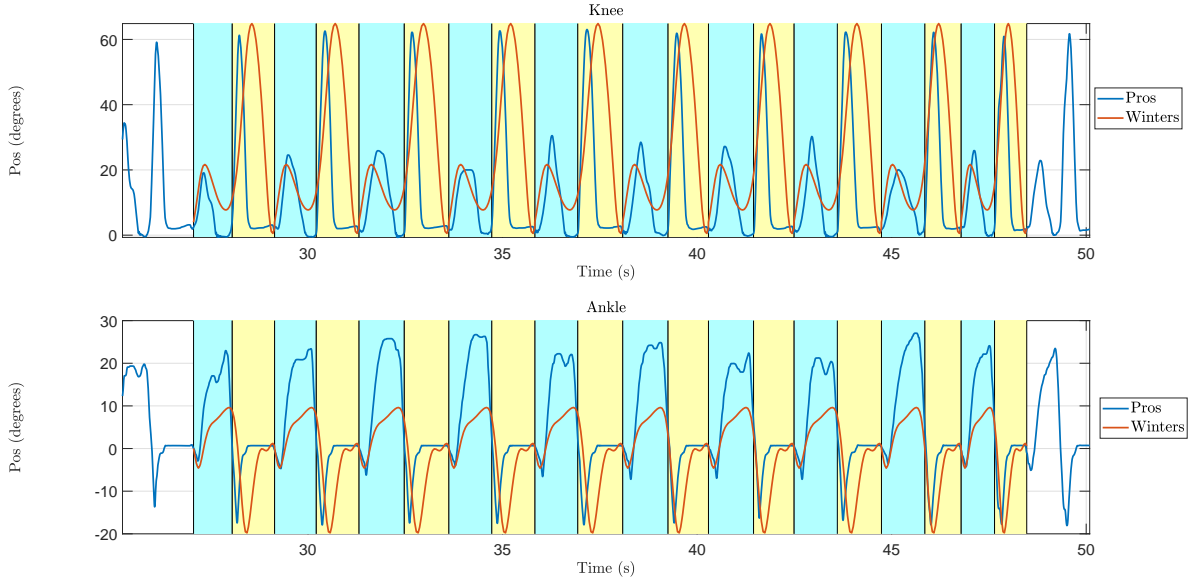


Figure 5.4: Knee and ankle positions versus time of the prosthesis and reference biological data from [1]. The blue highlighted area is stance, the yellow is swing.

parameterized by the hip position of the user, with  $K_p = K_d = 7$ . The transition from stance-to-swing and vice versa is facilitated by sensing the magnitude of the force applied foot-shank force sensor, with a transition threshold of  $100N$  and a hold time of  $0.1s$  to prevent high frequency switching. During the switch, the stance and swing controllers are interpolated with a time varying weighting over the hold time to ensure smooth transitions between control phases. The data presented in the figures in this section is from treadmill walking at  $2.2$  mph on level ground for 8 steps.

Figure 5.4 is a plot of the joint angles of the prosthesis over time during the experiment compared to the biological reference data [1] used to generate the trajectories for the swing controller. During swing, the joints follow Winter's data quite closely which makes sense because the control is specifically designed to accomplish this. The interesting feature is that the knee joint during stance also strongly resembles Winter's data as well, which is an emergent behavior from the closed-loop dynamics. The ankle trajectory of the prosthesis at the beginning of stance also strongly follows the biological trajectory then overshoots the

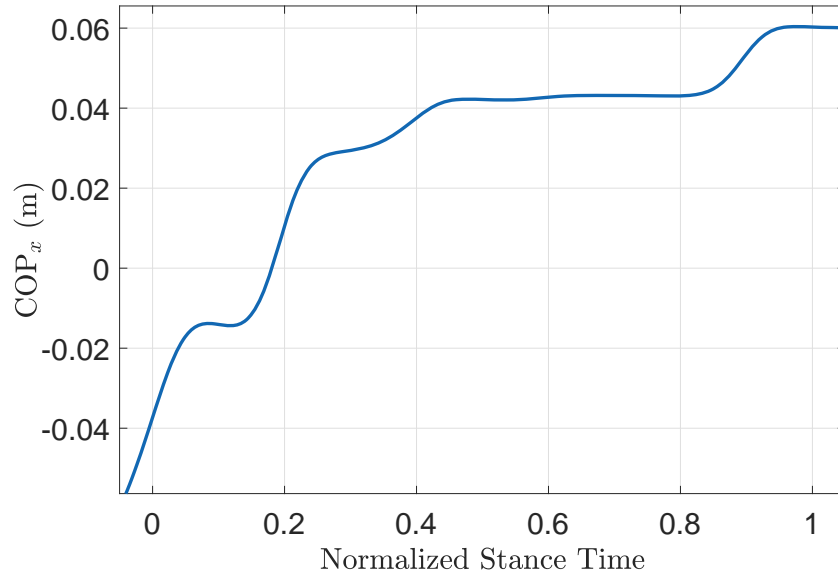


Figure 5.5: A smoothing spline fit to the COP-virtual spring contact point over normalized stance time. The COP is measured relative to the heel, with the positive direction being the way the user is facing.

peak value of Winter’s data. These results indicate that the virtual spring embedding does result in behavior similar to the biological system (the human leg). The increased ankle motion at the end of stance could be viewed as an beneficial outcome because this correlates to an increased distance over which to perform positive work during push-off. It could also be a result of asymmetry in the relative location of the prosthesis knee versus the sound side knee in the experimental setup and the use of the platform sole.

Figure 5.5 plots a fit of the average COP trajectory vs time over stance. Here, we can see that the user quickly rolls the heel and the virtual spring contact point spends the majority of stance close to the toe. The commanded net torque at the knee and ankle over time is shown in Figure 5.6, while the torques for the virtual spring and energy oscillator are shown in Figures 5.7 and 5.8. Again, the stance control output is calculated all the time but applied with a weighting that depends on phase. During the yellow shaded region in swing, these torques are basically not applied. The takeaway from these results is that

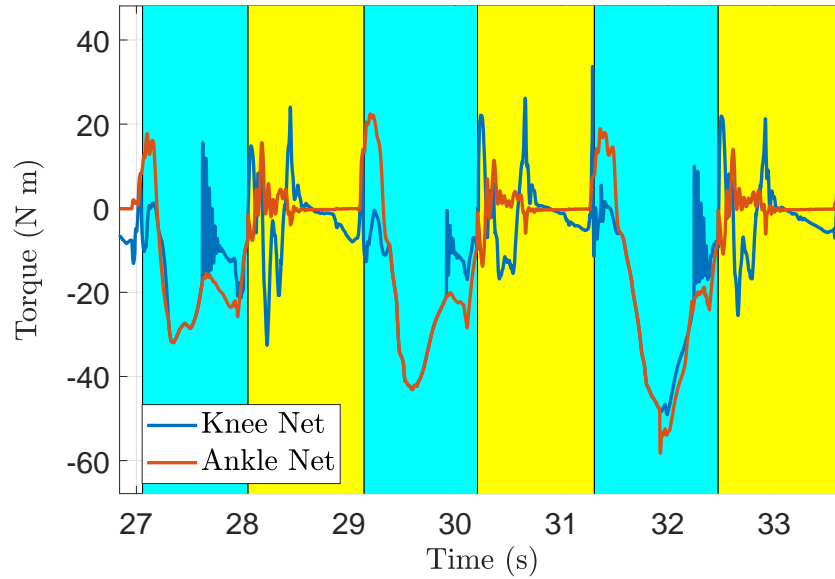


Figure 5.6: Net torques.

the nonlinear embedding of a virtual spring with an energy oscillator is a viable method of enabling biomimetic locomotion using a powered prosthetic leg. However, the efficacy in terms of improvement over a passive device or other methods of controlling a powered device is still undetermined and is a subject for future work.

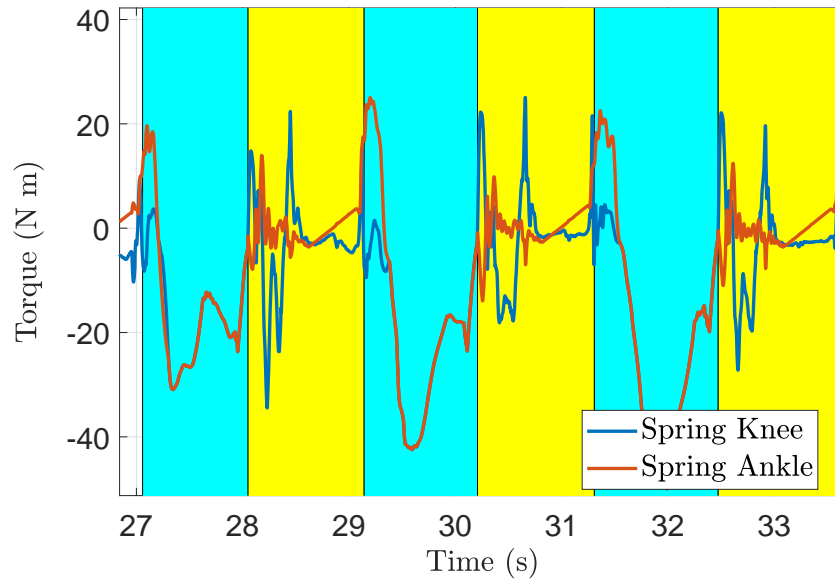


Figure 5.7: Spring torques.

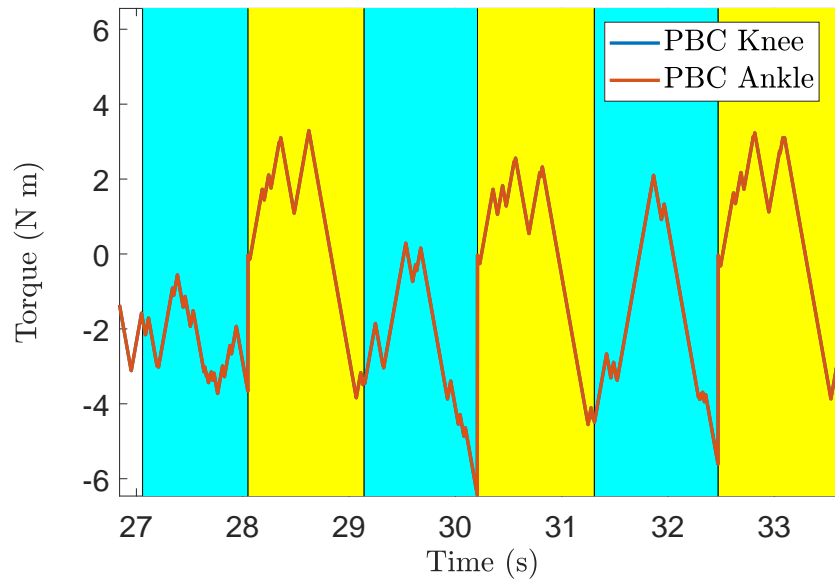


Figure 5.8: Energy oscillator torques.

## CHAPTER 6

### CONCLUSIONS

This dissertation contributes to both the fields of biped locomotion and wearable assistive/rehabilitation devices by improving the understanding of how to embed simple models of locomotion into complex systems and how to put energy at the forefront of the design process.

In Chapter 3, I introduce a passivity based framework for energy regulation in arbitrarily underactuated mechanical systems. I also consider a framework for regulating a time-varying reference energy and show how this can be used to regulate a work based energy function for dissipative hybrid systems with passive limit cycles. I also introduce a scheme for updating the reference energy online based on the output of the impact dynamics which allows implementation without a priori knowledge of the precise energy associated with a passive limit cycle.

In Chapter 4, I go over ways to use energy shaping and regulation to generate and stabilize limit cycles in: the Spring Loaded Inverted Pendulum, the Compass Gait Biped, the RABBIT model, and the Flat Foot Biped model. In the SLIP model, I show how energy regulation is necessary to stabilize the model's natural periodic orbits and that a large range of running behaviors can be achieved through parameter total energy regulation and through an energy based oscillator. For the compass gait model, I show how the virtual mass ratio can be changed to generate new walking speeds and that the impact based reference energy update scheme is effective in this scenario. I also demonstrate that energy regulation can stabilize natural limit cycles that are unstable for the passive system through a simulation that substitutes stairs for a shallow slope. For the RABBIT model, I show how to embed the SLIP model with energy regulation to achieve a walking gait. Using the Flat Foot Model, I develop a new decentralized formulation that provides a theoretical framework to address both uncertainty in the biped model and a lack of sensing, by allowing the designer

to ignore arbitrary states and model parameters in the system. This scheme is desirable in the control of biped locomotion because it can allow for a reduction of sensing components in the hardware, compensate for uncertainties in the dynamic model of the biped, and reduce the computational complexity of the control. The decentralized PBC retains useful qualities of the centralized approach, such as arbitrary underactuation, synergy with inner-loop controllers, and improved robustness and convergence rate of the limit cycle.

In Chapter 5, I demonstrate that the ideas developed in Chapter 4 for energy shaping and regulation control for biped locomotion can be translated into the prosthesis control application. Here, I embed a virtual spring between the user's hip and the local center of pressure of the prosthetic foot, based on the SLIP model. On top of this, an energy based oscillator is introduced to perform positive work against the system. This system is demonstrated to effectively achieve a biomimetic walking behavior. Finally, I introduce a proof of stability for a rigid robot system with a passivity based observer and energy regulation controller.

## **Future Work**

There are several avenues for future work in the area of energy shaping and regulation control for both biped locomotion and wearable assistive devices. In the area of biped locomotion, there are tasks beyond simply changing walking speed and slopes; there is obstacle avoidance, slipping, walk-run transitions, fall recovery, and others. I think it would be worthwhile to perhaps find a template model capable of negotiating a wider range of tasks or switching between target systems designed to deal with specific tasks. Many of the methods I describe in Chapter 4 have also yet to be implemented in a real autonomous biped system like ATLAS [89] or Valkyrie [90]. There are also interesting implications for power regeneration based on energy shaping control, since under this method the closed-loop energy along the limit cycle should be conserved.



In the domain of assistive devices, the application of energy regulation has yet to be explored for exoskeletons. However, the torques induced by passivity based energy regulation method in Chapter 3 can spike very quickly, so perhaps some modification of the technique is required when actuators are collocated with a user's joints. For both exoskeletons and prosthetic devices, it could be interesting to construct higher DOF data driven Lagrangian dynamics to match through energy shaping, rather than analytical simple models like the SLIP. Finally, the obvious extension of my work in Chapter 5 is to perform testing with the target population the device and control is meant to help, people with trans-femoral amputation.

## REFERENCES

- [1] D. A. Winter, *Biomechanics and motor control of human movement*. Hoboken, NJ: John Wiley & Sons, 2009.
- [2] K. Lechler, B. Frossard, L. Whelan, D. Langlois, R. Müller, and K. Kristjansson, “Motorized biomechatronic upper and lower limb prostheses—clinically relevant outcomes,” *PM&R*, vol. 10, no. 9, pp. S207–S219, 2018.
- [3] A. S. Voloshina and S. H. Collins, “Lower limb active prosthetic systems—overview,” in *Wearable Robotics*. Elsevier, 2020, pp. 469–486.
- [4] D. Quintero, “Virtual constraint control of powered prosthetic legs: Unifying the gait cycle,” Ph.D. dissertation, 2018.
- [5] D. Quintero, D. J. Villarreal, and R. D. Gregg, “Preliminary experiments with a unified controller for a powered knee-ankle prosthetic leg across walking speeds,” in *2016 IEEE/RSJ International Conference on Intelligent Robots and Systems (IROS)*. Daejeon, Korea: IEEE, 2016, pp. 5427–5433.
- [6] T. Elery, S. Rezazadeh, C. Nesler, J. Doan, H. Zhu, and R. D. Gregg, “Design and benchtop validation of a powered knee-ankle prosthesis with high-torque, low-impedance actuators,” in *IEEE Int. Conf. Robotics & Automation*, 2018.
- [7] A. Calanca, R. Muradore, and P. Fiorini, “A review of algorithms for compliant control of stiff and fixed-compliance robots,” *IEEE/ASME Transactions on Mechatronics*, vol. 21, no. 2, pp. 613–624, 2015.
- [8] M. Goldfarb, “Control for a self-contained microcomputer-controlled above-knee prosthesis,” Ph.D. dissertation, Massachusetts Institute of Technology, 1992.
- [9] F. Sup, A. Bohara, and M. Goldfarb, “Design and control of a powered transfemoral prosthesis,” *The International journal of robotics research*, vol. 27, no. 2, pp. 263–273, 2008.
- [10] M. F. Eilenberg, H. Geyer, and H. Herr, “Control of a powered ankle-foot prosthesis based on a neuromuscular model,” *IEEE transactions on neural systems and rehabilitation engineering*, vol. 18, no. 2, pp. 164–173, 2010.
- [11] D. Quintero, D. J. Villarreal, D. J. Lambert, S. Kapp, and R. D. Gregg, “Continuous-phase control of a powered knee-ankle prosthesis: Amputee experiments across speeds and inclines,” *IEEE Transactions on Robotics*, vol. 34, no. 3, pp. 686–701, 2018.
- [12] E. R. Westervelt, J. W. Grizzle, C. Chevallereau, J. H. Choi, and B. Morris, “Feedback Control of Dynamic Bipedal Robot Locomotion,” *Crc Press*, p. 528, 2007.

- [13] K. R. Embry, D. J. Villarreal, R. L. Macaluso, and R. D. Gregg, “Modeling the kinematics of human locomotion over continuously varying speeds and inclines,” *IEEE transactions on neural systems and rehabilitation engineering*, vol. 26, no. 12, pp. 2342–2350, 2018.
- [14] A. M. Bloch, N. E. Leonard, and J. E. Marsden, “Controlled Lagrangians and the stabilization of Euler-Poincare mechanical systems,” *International Journal of Robust and Nonlinear Control*, vol. 11, no. 3, pp. 191–214, 2001.
- [15] M. Spong, J. Holm, and D. Lee, “Passivity-Based Control of Bipedal Locomotion,” *IEEE Rob. Autom. Mag.*, vol. 14, no. June, pp. 30–40, 2007.
- [16] J. K. Holm and M. W. Spong, “Kinetic energy shaping for gait regulation of underactuated bipeds,” *Proceedings of the IEEE International Conference on Control Applications*, no. 1, pp. 1232–1238, 2008.
- [17] G. Lv and R. D. Gregg, “Underactuated potential energy shaping with contact constraints: Application to a powered knee-ankle orthosis,” *IEEE Transactions on Control Systems Technology*, vol. 26, no. 1, pp. 181–193, 2018.
- [18] G. Lv, H. Zhu, and R. D. Gregg, “On the design and control of highly backdrivable lower-limb exoskeletons: A discussion of past and ongoing work,” *IEEE Control Systems Magazine*, vol. 38, no. 6, pp. 88–113, 2018.
- [19] B. Yi, R. Ortega, D. Wu, and W. Zhang, “Orbital stabilization of nonlinear systems via mexican sombrero energy shaping and pumping-and-damping injection,” *arXiv preprint arXiv:1903.04070*, 2019.
- [20] M. Yeatman, G. Lv, and R. D. Gregg, “Decentralized passivity-based control with a generalized energy storage function for robust biped locomotion,” *Journal of Dynamic Systems, Measurement, and Control*, vol. 141, no. 10, p. 101007, 2019.
- [21] S. Kajita, F. Kanehiro, K. Kaneko, K. Yokoi, and H. Hirukawa, “The 3d linear inverted pendulum mode: A simple modeling for a biped walking pattern generation,” in *Proceedings 2001 IEEE/RSJ International Conference on Intelligent Robots and Systems. Expanding the Societal Role of Robotics in the the Next Millennium (Cat. No. 01CH37180)*, vol. 1. IEEE, 2001, pp. 239–246.
- [22] A. Rajagopal, C. L. Dembia, M. S. DeMers, D. D. Delp, J. L. Hicks, and S. L. Delp, “Full-body musculoskeletal model for muscle-driven simulation of human gait,” *IEEE transactions on biomedical engineering*, vol. 63, no. 10, pp. 2068–2079, 2016.
- [23] H. Geyer, A. Seyfarth, and R. Blickhan, “Compliant leg behaviour explains basic dynamics of walking and running,” *Proceedings of the Royal Society B: Biological Sciences*, vol. 273, no. 1603, pp. 2861–2867, 2006.

- [24] A. Goswami, B. Thuilot, and B. Espiau, “Compass-like biped robot part i: Stability and bifurcation of passive gaits,” Ph.D. dissertation, INRIA, 1996.
- [25] P. M. Wensing and D. E. Orin, “High-speed humanoid running through control with a 3d-slip model,” in *2013 IEEE/RSJ International Conference on Intelligent Robots and Systems*. IEEE, 2013, pp. 5134–5140.
- [26] R. D. Gregg and M. W. Spong, “Bringing the compass-gait bipedal walker to three dimensions,” in *2009 IEEE/RSJ International Conference on Intelligent Robots and Systems*. IEEE, 2009, pp. 4469–4474.
- [27] M. McGrath, D. Howard, and R. Baker, “The strengths and weaknesses of inverted pendulum models of human walking,” *Gait & posture*, vol. 41, no. 2, pp. 389–394, 2015.
- [28] N. Hogan, “The mechanics of multi-joint posture and movement control,” *Biological cybernetics*, vol. 52, no. 5, pp. 315–331, 1985.
- [29] G. Agarwal and C. Gottlieb, “Compliance of the human ankle joint,” 1977.
- [30] K. T. Bates, D. Collins, R. Savage, J. McClymont, E. Webster, T. C. Pataky, K. D’Aout, W. I. Sellers, M. R. Bennett, and R. H. Crompton, “The evolution of compliance in the human lateral mid-foot,” *Proceedings of the Royal Society B: Biological Sciences*, vol. 280, no. 1769, p. 20131818, 2013.
- [31] D. Quintero, A. E. Martin, and R. D. Gregg, “Toward unified control of a powered prosthetic leg: A simulation study,” *IEEE Transactions on Control Systems Technology*, vol. 26, no. 1, pp. 305–312, 2017.
- [32] A. H. Hansen, D. S. Childress, and S. C. Miff, “Roll-over characteristics of human walking on inclined surfaces,” *Human movement science*, vol. 23, no. 6, pp. 807–821, 2004.
- [33] M. Kwan and M. Hubbard, “Optimal foot shape for a passive dynamic biped,” *Journal of theoretical biology*, vol. 248, no. 2, pp. 331–339, 2007.
- [34] K. Z. Takahashi, M. T. Gross, H. Van Werkhoven, S. J. Piazza, and G. S. Sawicki, “Adding stiffness to the foot modulates soleus force-velocity behaviour during human walking,” *Scientific reports*, vol. 6, no. 1, pp. 1–11, 2016.
- [35] A. E. Martin and J. P. Schmiedeler, “Predicting human walking gaits with a simple planar model,” *Journal of biomechanics*, vol. 47, no. 6, pp. 1416–1421, 2014.
- [36] D. D. Holm, T. Schmäh, and C. Stoica, *Geometric mechanics and symmetry: from finite to infinite dimensions*. Oxford University Press, 2009, vol. 12.

- [37] R. M. Murray, Z. Li, S. S. Sastry, and S. S. Sastry, *A mathematical introduction to robotic manipulation*. Boca Raton, Florida: CRC press, 1994.
- [38] G. Lv and R. D. Gregg, “Underactuated potential energy shaping with contact constraints: Application to a powered knee-ankle orthosis,” *IEEE Transactions on Control Systems Technology*, vol. 26, no. 1, pp. 181–193, 2018.
- [39] X. Liu, “On differential geometric approach to nonlinear systems affine in control,” *arXiv preprint arXiv:1707.04684*, 2017.
- [40] E. R. Westervelt, J. W. Grizzle, and D. E. Koditschek, “Hybrid zero dynamics of planar biped walkers,” *IEEE Trans. Autom. Control*, vol. 48, no. 1, pp. 42–56, 2003.
- [41] R. D. Gregg and M. W. Spong, “Reduction-based control of three-dimensional bipedal walking robots,” *Int. J. Rob. Res.*, vol. 29, no. 6, pp. 680–702, 2010.
- [42] R. W. Sinnet, “Energy shaping of mechanical systems via control lyapunov functions with applications to bipedal locomotion,” Ph.D. dissertation, Texas A & M University, College Station Texas, 2015.
- [43] R. Sepulchre, M. Jankovic, and P. V. Kokotovic, *Constructive nonlinear control*. Berlin, Germany: Springer Science & Business Media, 2012.
- [44] R. D. Gregg IV, “Geometric control and motion planning for three-dimensional bipedal locomotion,” Ph.D. dissertation, University of Illinois at Urbana-Champaign, 2011.
- [45] M. W. Spong, S. Hutchinson, M. Vidyasagar *et al.*, *Robot modeling and control*. Wiley New York, 2006, vol. 3.
- [46] G. Garofalo, C. Ott, and A. Albu-Schäffer, “Walking control of fully actuated robots based on the bipedal slip model,” in *2012 IEEE International Conference on Robotics and Automation*. IEEE, 2012, pp. 1456–1463.
- [47] M. R. Yeatman, G. Lv, and R. D. Gregg, “Passivity-based control with a generalized energy storage function for robust walking of biped robots,” in *American Control Conference*, Milwaukee, Wisconsin, June 2018, pp. 2958–2963.
- [48] G. Blankenstein, R. Ortega, and A. J. Van Der Schaft, “The matching conditions of controlled lagrangians and ida-passivity based control,” *International Journal of Control*, vol. 75, no. 9, pp. 645–665, 2002.
- [49] G. Lv and R. D. Gregg, “Towards total energy shaping control of lower-limb exoskeletons,” in *American Control Conference*, Seattle, Washington, 2017, pp. 4851–4857.

- [50] R. D. Gregg, A. K. Tilton, S. Candido, T. Bretl, and M. W. Spong, “Control and planning of 3-d dynamic walking with asymptotically stable gait primitives,” *IEEE Transactions on Robotics*, vol. 28, no. 6, pp. 1415–1423, 2012.
- [51] P. A. Bhounsule, A. Zamani, and J. Pusey, “Switching between limit cycles in a model of running using exponentially stabilizing discrete control lyapunov function,” in *2018 Annual American Control Conference (ACC)*. IEEE, 2018, pp. 3714–3719.
- [52] M. W. Spong and F. Bullo, “Controlled symmetries and passive walking,” *IEEE Trans. Autom. Control*, vol. 50, no. 7, pp. 1025–1031, 2005.
- [53] T. McGeer *et al.*, “Passive dynamic walking,” *Int. J. Robotic Res.*, vol. 9, no. 2, pp. 62–82, 1990.
- [54] R. Naldi and R. G. Sanfelice, “Passivity-based control for hybrid systems with applications to mechanical systems exhibiting impacts,” *Automatica*, vol. 49, no. 5, pp. 1104–1116, 2013.
- [55] G. Garofalo and C. Ott, “Repetitive jumping control for biped robots via force distribution and energy regulation,” in *Human Friendly Robotics*. Springer, 2019, pp. 29–45.
- [56] M. J. Coleman, A. Chatterjee, and A. Ruina, “Motions of a rimless spoked wheel: a simple three-dimensional system with impacts,” *Dynamics and stability of systems*, vol. 12, no. 3, pp. 139–159, 1997.
- [57] A. Nathan, “The rayleigh-van der pol harmonic oscillator,” *International Journal of Electronics Theoretical and Experimental*, vol. 43, no. 6, pp. 609–614, 1977.
- [58] M. A. Khamsi and W. A. Kirk, *An introduction to metric spaces and fixed point theory*. John Wiley & Sons, 2011, vol. 53.
- [59] C. A. Desoer and M. Vidyasagar, *Feedback systems: input-output properties*. SIAM, 2009.
- [60] R. J. Full and D. E. Koditschek, “Templates and anchors: neuromechanical hypotheses of legged locomotion on land,” *Journal of experimental biology*, vol. 202, no. 23, pp. 3325–3332, 1999.
- [61] S. Heim and A. Spröwitz, “Beyond basins of attraction: Quantifying robustness of natural dynamics,” *IEEE Transactions on Robotics*, 2019.
- [62] Wikipedia contributors, “Compass (drawing tool) — Wikipedia, the free encyclopedia,” 2020, [Online; accessed 18-May-2020]. [Online]. Available: [https://en.wikipedia.org/wiki/Compass\\_\(drawing\\_tool\)](https://en.wikipedia.org/wiki/Compass_(drawing_tool))

- [63] M. Garcia, A. Chatterjee, A. Ruina, and M. Coleman, “The simplest walking model: stability, complexity, and scaling,” 1998.
- [64] K. Byl and R. Tedrake, “Metastable walking on stochastically rough terrain,” *Proceedings of robotics: science and systems IV*, pp. 6490–6495.
- [65] A. T. Safa, M. G. Saadat, and M. Naraghi, “Passive dynamic of the simplest walking model: Replacing ramps with stairs,” *Mechanism and Machine Theory*, vol. 42, no. 10, pp. 1314–1325, 2007.
- [66] A. Goswami, B. Espiau, and A. Keramane, “Limit cycles in a passive compass gait biped and passivity-mimicking control laws,” *Autonomous Robots*, vol. 4, no. 3, pp. 273–286, 1997.
- [67] S. N. Whittlesey, R. E. van Emmerik, and J. Hamill, “The swing phase of human walking is not a passive movement,” *Motor control*, vol. 4, no. 3, pp. 273–292, 2000.
- [68] C. Xu, A. Ming, and Q. Chen, “Characteristic equations and gravity effects on virtual passive bipedal walking,” in *2014 IEEE International Conference on Robotics and Biomimetics (ROBIO 2014)*. IEEE, 2014, pp. 1296–1301.
- [69] E. Westervelt, G. Buche, and J. Grizzle, “Inducing dynamically stable walking in an underactuated prototype planar biped,” in *IEEE International Conference on Robotics and Automation, 2004. Proceedings. ICRA’04. 2004*, vol. 4. IEEE, 2004, pp. 4234–4239.
- [70] M. Zefran, F. Bullo, and M. Stein, “A notion of passivity for hybrid systems,” in *Decision and Control, IEEE Conference on*, vol. 1, Orlando, Florida, 2001, pp. 768–773.
- [71] F. Asano, Z.-W. Luo, and M. Yamakita, “Biped gait generation and control based on a unified property of passive dynamic walking,” *IEEE Transactions on Robotics*, vol. 21, no. 4, pp. 754–762, 2005.
- [72] M.-Y. Cheng and C.-S. Lin, “Measurement of robustness for biped locomotion using a linearized poincaré map,” *Robotica*, vol. 14, no. 3, pp. 253–259, 1996.
- [73] T. Koolen, T. De Boer, J. Rebula, A. Goswami, and J. Pratt, “Capturability-based analysis and control of legged locomotion, part 1: Theory and application to three simple gait models,” *The International Journal of Robotics Research*, vol. 31, no. 9, pp. 1094–1113, 2012.
- [74] D. G. Hobbelen and M. Wisse, “A disturbance rejection measure for limit cycle walkers: The gait sensitivity norm,” *IEEE Transactions on robotics*, vol. 23, no. 6, pp. 1213–1224, 2007.

- [75] M. Wisse, D. G. Hobbelen, R. J. Rotteveel, S. O. Anderson, and G. J. Zeglin, “Ankle springs instead of arc-shaped feet for passive dynamic walkers,” in *Humanoid Robots, IEEE-RAS International Conference on*. Genova, Italy: IEEE, 2006, pp. 110–116.
- [76] S. N. M. Thangal, M. Talaty, and S. Balasubramanian, “Assessment of gait sensitivity norm as a predictor of risk of falling during walking in a neuromusculoskeletal model,” *Medical engineering & physics*, vol. 35, no. 10, pp. 1483–1489, 2013.
- [77] D. G. Hobbelen and M. Wisse, “Swing-leg retraction for limit cycle walkers improves disturbance rejection,” *IEEE Transactions on Robotics*, vol. 24, no. 2, pp. 377–389, 2008.
- [78] D. J. Block, K. J. Åström, and M. W. Spong, “The reaction wheel pendulum,” *Synthesis Lectures on Control and Mechatronics*, vol. 1, no. 1, pp. 1–105, 2007.
- [79] A. E. Martin and R. D. Gregg, “Stable, robust hybrid zero dynamics control of powered lower-limb prostheses,” *IEEE Trans. Autom. Control*, vol. 62, no. 8, pp. 3930–3942, 2017.
- [80] R. D. Gregg, T. Lenzi, L. J. Hargrove, and J. W. Sensinger, “Virtual constraint control of a powered prosthetic leg: From simulation to experiments with transfemoral amputees,” *IEEE Trans. Rob.*, vol. 30, no. 6, pp. 1455–1471, 2014.
- [81] T. Elery, S. Rezazadeh, C. Nesler, and R. D. Gregg, “Design and validation of a powered knee–ankle prosthesis with high-torque, low-impedance actuators,” *IEEE Transactions on Robotics*, 2020.
- [82] G. Stewart, *The skeletal and muscular systems*. Philadelphia: Chelsea House Publishers, 2004.
- [83] D. J. Farris and G. S. Sawicki, “The mechanics and energetics of human walking and running: a joint level perspective,” *Journal of The Royal Society Interface*, vol. 9, no. 66, pp. 110–118, 2011.
- [84] J. M. Donelan, R. Kram, and A. D. Kuo, “Simultaneous positive and negative external mechanical work in human walking,” *Journal of biomechanics*, vol. 35, no. 1, pp. 117–124, 2002.
- [85] S. W. Lipfert, M. Günther, D. Renjewski, and A. Seyfarth, “Impulsive ankle push-off powers leg swing in human walking,” *Journal of experimental biology*, vol. 217, no. 8, pp. 1218–1228, 2014.
- [86] H. Berghuis and H. Nijmeijer, “A passivity approach to controller-observer design for robots,” *IEEE Transactions on robotics and automation*, vol. 9, no. 6, pp. 740–754, 1993.



- [87] J. J. LaViola, “Double exponential smoothing: an alternative to kalman filter-based predictive tracking,” in *Proceedings of the workshop on Virtual environments 2003*, 2003, pp. 199–206.
- [88] T. I. Lakoba, “Simple euler method and its modifications,” *Lecture Notes for MATH334*, 2012.
- [89] G. Nelson, A. Saunders, and R. Playter, “The petman and atlas robots at boston dynamics,” *Humanoid Robotics: A Reference*, pp. 169–186, 2019.
- [90] N. A. Radford, P. Strawser, K. Hambuchen, J. S. Mehling, W. K. Verdeyen, A. S. Donnan, J. Holley, J. Sanchez, V. Nguyen, L. Bridgwater *et al.*, “Valkyrie: Nasa’s first bipedal humanoid robot,” *Journal of Field Robotics*, vol. 32, no. 3, pp. 397–419, 2015.

## **BIOGRAPHICAL SKETCH**

Mark was born in Macon, Georgia, and after moving all over the country, ended up at The University of Texas at Dallas with a full-ride scholarship for undergrad in 2011. There, he met his future advisor and mentor, Dr. Robert Gregg, who solidified his interest in robotics and control through undergrad research. Mark graduated in 2015 with a double degree in Mechanical Engineering and Computer Science, then moved to Los Angeles, California for an internship at Hyperloop Technologies and work for Haas Automation. This experience in industry convinced him that if he wanted to lead the development of interesting, cutting edge technology, he needed a PhD. Thus, he came back to UTD to work in the Locomotor Control System Laboratory from 2016-2020. Mark hopes to continue to innovate at the intersection of robotics, autonomy, and human-machine interaction.

## CURRICULUM VITAE

mark.x.yeatman@gmail.com

www.mark-yeatman.net

Phone: +1 (469) 263-6520

**Education**      **University of Texas at Dallas**  
Ph.D. Mechanical Engineering, 2020 (Expected)  
Fields: Dynamics and Control Systems

**University of Texas at Dallas**  
B.S. Mechanical Engineering, 2015  
B.S. Computer Science, 2015

**Domain**  
**Expertise**      Nonlinear Control, Robotics, Optimization, Biomechanics

**Technology**  
**Expertise**      Matlab/Simulink, Python, C/C++, Labview,  
Git/SVN, Linux, Embedded Systems Programming, Motor Control

**Dissertation**    **“Energy and Passivity Based Control for Bipedes and Assistive Walking Devices”**  
The primary outcome of this work is a control method for a powered lower-limb prosthesis that explicitly injects energy into the combined human-prosthesis system to assist amputee locomotion. The method accounts for the human energy input which allows the prosthesis to work with the user rather than fighting them. It was implemented on UTD Leg 2 and tested using a bypass adapter.

**Teaching**      **Feedback Systems — University of Texas at Dallas**  
Fall 2017, Fall 2018  
Title: *Teaching Assistant*

**Robotics Team Coach — ACE High School, Camarillo CA**  
Spring 2016  
Title: *Programming Coach*

## Industry Experience

### **Haas Automation — Oxnard, CA**

Sept 2015 - May 2016

Title: *Software QA Engineer*

Performed software and hardware tests of CNC mills and lathes to ensure correct implementation of features, requirements, and specifications. Wrote scripts using custom software and G-Code, provided bug reports for development team.

### **Hyperloop Technologies — Los Angeles, CA**

Summer 2015

Title: *Systems, Controls, and Dynamics Intern*

Analyzed structural, thermal, and dynamic constraints to design an experimental and novel rotor component in a linear induction motor. Integrated the convex optimization framework CVX into systems level optimization of power system design and route planning.

## Journal Publications

**M. Yeatman**, G. Lv, and R. Gregg, “Decentralized Passivity-Based Control with a Generalized Energy Storage Function for Robust Biped Locomotion,” *ASME Journal of Dynamic Systems, Measurement, and Control*, 141(10): 101007, 2019.

**M. Yeatman** and R. Gregg, “Using Energy Shaping and Tracking to Generate Natural Limit Cycles in Mechanical Systems with Impacts,” *ASME Journal & of Computational and Nonlinear Dynamics*, under review.

## Conference Publications

**M. Yeatman**, G. Lv, and R. Gregg, “Passivity-Based Control with a Generalized Energy Storage Function for Robust Bipedal Walking,” in *American Control Conference*, Milwaukee, WI, 2018.

## Poster Presentations

**M. Yeatman** and R. Gregg, “Energy and Passivity Based Control of Biped Locomotion”, *Texas Systems Day*, College Station, TX, 2019

**M. Yeatman**, S. Rezazadeh, and R. Gregg, “Energy Shaping and Tracking for Natural Limit Cycles in Hybrid Systems”, *Dynamic Walking*, Online, 2020